Accepted Manuscript

A first order hyperbolic framework for large strain computational solid dynamics. Part II: Total Lagrangian compressible, nearly incompressible and truly incompressible elasticity

Antonio J. Gil, Chun Hean Lee, Javier Bonet, Rogelio Ortigosa

PII: S0045-7825(15)00363-1
DOI: http://dx.doi.org/10.1016/j.cma.2015.11.010
Reference: CMA 10754

To appear in: *Comput. Methods Appl. Mech. Engrg.*

Received date: 12 June 2015
Revised date: 12 October 2015
Accepted date: 2 November 2015

Please cite this article as: A.J. Gil, C.H. Lee, J. Bonet, R. Ortigosa, A first order hyperbolic framework for large strain computational solid dynamics. Part II: Total Lagrangian compressible, nearly incompressible and truly incompressible elasticity, *Comput. Methods Appl. Mech. Engrg.* (2015), http://dx.doi.org/10.1016/j.cma.2015.11.010

A first order hyperbolic framework for large strain computational solid dynamics. Part II: Total Lagrangian compressible, nearly incompressible and truly incompressible elasticity

Antonio J. Gil[1], Chun Hean Lee[2], Javier Bonet[3], Rogelio Ortigosa

Zienkiewicz Centre for Computational Engineering, College of Engineering
Swansea University, Bay Campus, SA1 8EN, United Kingdom

Abstract

In Part I of this series, Bonet *et al*. [1] introduced a new computational framework for the analysis of large strain isothermal fast solid dynamics, where a mixed set of Total Lagrangian conservation laws was presented in terms of the linear momentum and an extended set of strain measures, namely the deformation gradient, its co-factor and its Jacobian. The main aim of this paper is to expand this formulation to the case of nearly incompressible and truly incompressible materials. The paper is further enhanced with three key novelties. First, the use of polyconvex nearly incompressible strain energy functionals enables the definition of generalised convex entropy functions and associated entropy fluxes. Two variants of the same formulation can then be obtained, namely, conservation-based and entropy-based, depending on the unknowns of the system. Crucially, the study of the eigenvalue structure of the system is carried out in order to demonstrate its hyperbolicity and, thus, obtain the correct time step bounds for explicit time integrators. Second, the development of a stabilised Petrov-Galerkin framework is presented for both systems of hyperbolic equations, that is, when expressed in terms of either conservation or entropy variables. Third, an adapted fractional step method, built upon the work presented in Gil *et al*. [2], is presented to extend the

[1]Corresponding author: a.j.gil@swansea.ac.uk
[2]Corresponding author: c.h.lee@swansea.ac.uk
[3]Corresponding author: j.bonet@swansea.ac.uk

range of applications towards the incompressibility limit. Finally, a series of numerical examples are presented in order to assess the applicability and robustness of the proposed formulation. The overall scheme shows excellent behaviour in compressible, nearly incompressible and truly incompressible scenarios, yielding equal order of convergence for velocities and stresses.

Keywords: Entropy variables, Conservation laws, Fast dynamics, Petrov-Galerkin, Incompressibility, Fractional step

1. Introduction

Traditional displacement-based finite element formulations [3, 4], in conjunction with Newmark-type time integrators, are typically employed when simulating large strain complex engineering problems. However, this approach presents a number of well-known shortcomings, namely, a reduced order of convergence for strains and stresses, inefficiency in nearly and truly incompressible bending dominated scenarios [5–7], numerical instabilities in the form of shear and volumetric locking, non-physical hydrostatic pressure fluctuations [8] and high frequency noise [9] in the vicinity of sharp spatial gradients.

For nearly and truly incompressible materials, selective reduced integration techniques, such as the B-bar [10, 11] or the mean dilatation approach [12], have been proven to be very effective for computational simulations [10, 11], despite not circumventing the inf-sup Ladyzhenskaya-Babuška-Brezzi (LBB) condition [13] and resulting in a reduced order of convergence for the stresses. In addition, these techniques are primarily developed for hexahedral elements, for which robust and cost effective three-dimensional unstructured mesh generators are not as well as established as unstructured tetrahedral mesh generators [14].

In the context of linear tetrahedral elements, some of the numerical difficulties mentioned above can be partially addressed with the use of high order schemes [15–17], mixed velocity/pressure stabilised formulations [8, 18–20] or nodally integrated linear tetrahedral elements [21–25]. The latter resort to some form of projection in reducing the volumetric constraints. Notably, the very first family of nodal pressure elements was proposed by Bonet and Burton [24] and its resulting methodology performed extremely well in nearly incompressible impact problems. This class of methods was, however, found to behave poorly in bending dominated problems. Numerous attempts have

been reported at improving the robustness of the formulation [6–8], but these enhanced methodologies still suffer from artificial mechanisms similar to hourglassing [8, 26–28].

In a very recent work, Scovazzi and co-authors [14] proposed an effective alternative tetrahedral velocity/pressure Updated Lagrangian mixed methodology. The authors introduced stabilising mechanisms through the use of the Variational Multi-Scale (VMS) method, widely used in the context of Computational Fluid Dynamics (CFD) [29–36].

Over the last few years, the authors of this paper have introduced a new mixed conservation-based methodology, where the linear momentum $\boldsymbol{p}$ and the deformation gradient $\boldsymbol{F}$ are treated as primary variables of a system of first order conservation laws. Both velocities, deviatoric stresses and volumetric stresses display the same rate of convergence, which proves ideal in the case of linear finite elements. This approach has been thoroughly analysed by the authors using a wide variety of spatial second order discretisation techniques, namely cell centred upwind Finite Volume Method (FVM) [37], vertex centred Jameson-Schmidt-Turkel (JST) FVM [38], two step Taylor Galerkin Finite Element Method (FEM) [39] and Petrov-Galerkin (PG) FEM [5]. Crucially, all of these approaches render equal order of convergence for velocities and stresses (both deviatoric and volumetric). A similar scheme has also been developed by Kluth and Després [40], opting in their case for a first order cell centred FVM.

In subsequent papers, the two-field $\boldsymbol{p}$-$\boldsymbol{F}$ formulation was then augmented by incorporating a new conservation law for the Jacobian of the deformation J [41, 42] to effectively solve nearly incompressible deformations [2, 43, 44]. Moreover, the $\boldsymbol{p}$-$\boldsymbol{F}$-J formulation was also extended to account for truly incompressible materials utilising a tailor-made fractional step approach [45].

Further enhancement of this framework has recently been reported by the authors [1] in Part I of this series, when considering compressible materials governed by a polyconvex constitutive law [46] where the co-factor $\boldsymbol{H}$ of the deformation plays a dominant role. It is worthwhile to emphasise that polyconvexity [46, 47] is a well accepted mathematical requirement that guarantees both stability and the existence of real wave speeds. The extended set of unknowns $\boldsymbol{p}$-$\boldsymbol{F}$-$\boldsymbol{H}$-J yields an elegant system of conservation laws, where the existence of a generalised convex entropy function enables the derivation of a symmetric system [48] of hyperbolic equations, dual of that expressed in terms of conservation variables, namely $\boldsymbol{v}$-$\boldsymbol{\Sigma}_{\boldsymbol{F}}$-$\boldsymbol{\Sigma}_{\boldsymbol{F}}$-$\Sigma_J$.

In this paper, both the conservation-based $\boldsymbol{p}$-$\boldsymbol{F}$-$\boldsymbol{H}$-J system and its en-

tropy (dual) $\boldsymbol{v}$-$\boldsymbol{\Sigma_F}$-$\boldsymbol{\Sigma_F}$-Σ_J counterpart are revisited, with specific emphasis on materials governed by a polyconvex nearly incompressible constitutive law (i.e. Mooney-Rivlin and neo-Hookean). The polyconvex nature of the nearly incompressible constitutive model, a guarantor of physical stability, leads to a Hessian operator with non-zero off-diagonal terms, in contrast to the simpler expression for the case of the compressible model reported in Part I of this series [1]. This extra complexity leads to a more elaborate variational formulation, one of the objectives of this Part II paper.

To maintain the consistency with the previous paper of the series, a Petrov-Galerkin computational framework, formerly presented in [2], is employed for the spatial discretisation of both the set of conservation-based $\boldsymbol{p}$-$\boldsymbol{F}$-$\boldsymbol{H}$-J and entropy-based $\boldsymbol{v}$-$\boldsymbol{\Sigma_F}$-$\boldsymbol{\Sigma_F}$-Σ_J variables. From the time discretisation standpoint, four discretisations are implemented in conjunction with an explicit time integrator, where the time step size is controlled through the Courant-Friedrichs-Lewy number by the volumetric wave speed. In the incompressibility limit, this wave can reach very high values leading to a very inefficient algorithm. In this case, the paper introduces an adapted Petrov-Galerkin type fractional step method [2], taking inspiration from the work of Gil *et al*. [2], where the time step size is limited by the shear wave speed. A series of numerical examples will be examined to assess the robustness and capabilities of the mixed algorithm. Although the formulation is not restricted to a specific finite element technology, in this paper linear tetrahedral elements will be used and compared against other well established techniques.

The outline of the present paper is as follows. Section 2 presents the set of mixed conservation linear momentum/geometry equations for large strain isothermal fast dynamics. Compressible and nearly incompressible polyconvex constitutive laws are then presented in Section 3. Subsequently, Section 4 introduces a new set of entropy-based velocity/stresses variables for solid dynamics, dual of the original conservation set of linear momentum/strains variables. This section ends with the study of the eigenstructure of the entropy system, critical in order to demonstrate its hyperbolicity and, hence, obtain the correct time step bounds for explicit time integrators. Sections 5 and 6 introduce the numerical methodology of a stabilised Petrov-Galerkin finite element framework for conservation- and entropy-based systems, respectively. For truly and nearly incompressible materials, both conservation- and entropy-based fractional step approaches are also presented. Section 7 describes briefly the Newton-Raphson iterative technique necessary to com-

pute the corresponding strains from given stresses (in the case of using the entropy-based approach). In Section 8, an extensive set of numerical examples is presented to assess the performance of the proposed method and to draw some comparisons against previous results published by the authors [1, 2, 20]. Finally, Section 9 summarises some concluding remarks and current directions of research.

2. Total Lagrangian conservation laws

Let us consider the motion of a continuum which in its material (or initial) configuration is defined by a domain $V \subset \mathbb{R}^3$ of boundary ∂V with unit outward normal vector $\boldsymbol{N}$. After the motion, the continuum occupies a spatial (or current) configuration defined by a domain $v \subset \mathbb{R}^3$ of boundary ∂v with outward unit normal $\boldsymbol{n}$. The motion is described by a t time-dependent mapping field $\boldsymbol{\phi}$ which links a material particle from material configuration $\boldsymbol{X} \in V$ to spatial configuration $\boldsymbol{x} \in v$ according to $\boldsymbol{x} = \boldsymbol{\phi}(\boldsymbol{X}, t)$. The motion can be described by a system of first order conservation laws expressed in a Total Lagrangian setting as follows [1]:

$$\begin{aligned}
&\frac{\partial \boldsymbol{p}}{\partial t} - \mathrm{DIV}\boldsymbol{P} = \boldsymbol{f}_0; \\
&\frac{\partial \boldsymbol{F}}{\partial t} - \mathrm{DIV}\left(\frac{1}{\rho_0}\boldsymbol{p} \otimes \boldsymbol{I}\right) = \boldsymbol{0}; \\
&\frac{\partial \boldsymbol{H}}{\partial t} - \mathrm{CURL}\left(\frac{1}{\rho_0}\boldsymbol{p} \times \boldsymbol{F}\right) = \boldsymbol{0}; \\
&\frac{\partial J}{\partial t} - \mathrm{DIV}\left(\frac{1}{\rho_0}\boldsymbol{H}^T\boldsymbol{p}\right) = 0,
\end{aligned} \tag{1}$$

where $\boldsymbol{p}$ represents the linear momentum per unit of undeformed volume, ρ_0 is the initial density, $\boldsymbol{f}_0$ is the body force per unit of undeformed volume, $\boldsymbol{F}$ is the deformation gradient tensor (or fibre map), $\boldsymbol{H}$ is the cofactor of the deformation gradient tensor (or area map), J is the Jacobian of the deformation gradient tensor (or volume map), $\boldsymbol{P}$ represents the first Piola-Kirchhoff stress tensor, DIV and CURL represent the material divergence and curl operators [1] and $\times$ is used to represent the cross product between vectors and/or second order tensors in the sense of [1, 20, 49, 50]. Above system (1) can alternatively be written in a compact manner as:

$$\frac{\partial \boldsymbol{\mathcal{U}}}{\partial t} + \frac{\partial \boldsymbol{\mathcal{F}}_I}{\partial X_I} = \boldsymbol{\mathcal{S}}; \qquad \forall I = 1, 2, 3, \tag{2}$$

where $\boldsymbol{\mathcal{U}}$ denotes the set of conservation variables, $\boldsymbol{\mathcal{S}}$ the source terms and $\boldsymbol{\mathcal{F}}_I$ the flux vector in the Cartesian direction I, as follows:

$$\boldsymbol{\mathcal{U}} = \begin{bmatrix} \boldsymbol{p} \\ \boldsymbol{F} \\ \boldsymbol{H} \\ J \end{bmatrix}; \qquad \boldsymbol{\mathcal{F}}_I = - \begin{bmatrix} \boldsymbol{P}\boldsymbol{E}_I \\ \frac{1}{\rho_0}\boldsymbol{p} \otimes \boldsymbol{E}_I \\ \boldsymbol{F} \times \left(\frac{1}{\rho_0}\boldsymbol{p} \otimes \boldsymbol{E}_I\right) \\ \boldsymbol{H} : \left(\frac{1}{\rho_0}\boldsymbol{p} \otimes \boldsymbol{E}_I\right) \end{bmatrix}; \qquad \boldsymbol{\mathcal{S}} = \begin{bmatrix} \boldsymbol{f}_0 \\ \boldsymbol{0} \\ \boldsymbol{0} \\ 0 \end{bmatrix}, \tag{3}$$

with $\boldsymbol{E}_I$ is the I-th unit vector of the Cartesian basis defined as:

$$\boldsymbol{E}_1 = \begin{bmatrix} 1 \\ 0 \\ 0 \end{bmatrix}; \qquad \boldsymbol{E}_2 = \begin{bmatrix} 0 \\ 1 \\ 0 \end{bmatrix}; \qquad \boldsymbol{E}_3 = \begin{bmatrix} 0 \\ 0 \\ 1 \end{bmatrix}. \tag{4}$$

For completeness, the flux Jacobian matrix is defined as $\boldsymbol{\mathcal{A}}_I = \frac{\partial \boldsymbol{\mathcal{F}}_I}{\partial \boldsymbol{\mathcal{U}}}$ [1]. Notice that in the presence of non-smooth solutions, above system (1) of local conservation laws is accompanied by suitable jump conditions as described in [1]. It is clear from (1) that the material divergence of $\boldsymbol{H}$ vanishes, as does the material CURL of $\boldsymbol{F}$:

$$\mathrm{DIV}\boldsymbol{H} = \boldsymbol{0}; \qquad \mathrm{CURL}\boldsymbol{F} = \boldsymbol{0}, \tag{5}$$

representing the so-called involutions of the system [1, 37]. For closure of system (1), an appropriate constitutive law satisfying both the principle of objectivity (frame invariance) and the second law of Thermodynamics (Coleman-Noll procedure) [12] must be established. In this paper, compressible and nearly incompressible hyperelastic polyconvex constitutive models will be employed and presented in the following section. Finally, for the complete definition of the Initial Boundary Value Problem (IBVP), initial and boundary (essential and natural) conditions must be specified.

The IBVP defined by a simplified version of the above conservation-based $\boldsymbol{\mathcal{U}}$ system (3) has been thoroughly studied by the authors using a wide variety of spatial discretisation techniques, namely cell centred upwind Finite Volume Method (FVM) [37], vertex centred Jameson-Schmidt-Turkel (JST) FVM [38], upwind FVM [44], two step Taylor Galerkin Finite Element Method (FEM) [39] and Petrov-Galerkin (PG) FEM [5].

3. Constitutive law: Polyconvex elasticity

Polyconvexity is a well accepted mathematical requirement for admissible strain energy functionals to be satisfied in order to describe elastic materials in the large strain regime [1, 46, 51]. Essentially, the strain energy Ψ per unit of undeformed volume must be a function of $\boldsymbol{\nabla}_0\boldsymbol{x}$[4] via a convex multi-variable function W as:

$$\Psi(\boldsymbol{\nabla}_0\boldsymbol{x}) = W(\boldsymbol{F}, \boldsymbol{H}, J), \tag{6}$$

where W is convex with respect to its 19 variables, namely, J and the 3×3 components of $\boldsymbol{F}$ and $\boldsymbol{H}$. Frame invariance implies that W must be independent of the rotational components of $\boldsymbol{F}$ and $\boldsymbol{H}$ via the symmetric tensors $\boldsymbol{C} = \boldsymbol{F}^T\boldsymbol{F}$ and $\boldsymbol{G} = \boldsymbol{H}^T\boldsymbol{H}$, respectively. In addition, for isotropic materials, this dependency can be further simplified through the use of the invariants $\{I_1, I_2, I_3\}$ of $\boldsymbol{C}$ defined as:

$$I_1 = \boldsymbol{F} : \boldsymbol{F}; \qquad I_2 = \boldsymbol{H} : \boldsymbol{H}; \qquad I_3 = J^2. \tag{7}$$

The three strain measures $\boldsymbol{F}$, $\boldsymbol{H}$ and J have corresponding work conjugate stresses $\boldsymbol{\Sigma}_{\boldsymbol{F}}$, $\boldsymbol{\Sigma}_{\boldsymbol{H}}$ and Σ_J defined by [20, 51]:

$$\boldsymbol{\Sigma}_{\boldsymbol{F}}(\boldsymbol{F}, \boldsymbol{H}, J) = \frac{\partial W}{\partial \boldsymbol{F}}; \qquad \boldsymbol{\Sigma}_{\boldsymbol{H}}(\boldsymbol{F}, \boldsymbol{H}, J) = \frac{\partial W}{\partial \boldsymbol{H}}; \qquad \Sigma_J(\boldsymbol{F}, \boldsymbol{H}, J) = \frac{\partial W}{\partial J}. \tag{8}$$

Crucially, the convexity of W ensures that the above set of constitutive relationships can be inverted, that is, the relationship between $\{\boldsymbol{\Sigma}_{\boldsymbol{F}}, \boldsymbol{\Sigma}_{\boldsymbol{H}}, \Sigma_J\}$ and $\{\boldsymbol{F}, \boldsymbol{H}, J\}$ is one to one[5].

Following References [1, 20], it is then possible to express the first Piola Kirchhoff stress tensor $\boldsymbol{P}$ in terms of the extended set of strains $\{\boldsymbol{F}, \boldsymbol{H}, J\}$ and conjugate stresses $\{\boldsymbol{\Sigma}_{\boldsymbol{F}}, \boldsymbol{\Sigma}_{\boldsymbol{H}}, \Sigma_J\}$ as:

$$\boldsymbol{P} = \boldsymbol{\Sigma}_{\boldsymbol{F}} + \boldsymbol{\Sigma}_{\boldsymbol{H}} \boldsymbol{\times} \boldsymbol{F} + \Sigma_J \boldsymbol{H}. \tag{9}$$

Furthermore, the symmetric positive semidefinite Hessian operator $[\mathbb{H}_W]$ of the strain energy functional W (6) is introduced by computing the second

[4] The symbol $\boldsymbol{\nabla}_0$ represents material gradient in undeformed space: $[\boldsymbol{\nabla}_0]_I \equiv \frac{\partial}{\partial X_I}$.

[5] The reversed constitutive law can be written as: $\boldsymbol{F}_{\boldsymbol{\Sigma}} = \boldsymbol{F}(\boldsymbol{\Sigma}_{\boldsymbol{F}}, \boldsymbol{\Sigma}_{\boldsymbol{H}}, \Sigma_J)$, $\boldsymbol{H}_{\boldsymbol{\Sigma}} = \boldsymbol{H}(\boldsymbol{\Sigma}_{\boldsymbol{F}}, \boldsymbol{\Sigma}_{\boldsymbol{H}}, \Sigma_J)$ and $J_{\boldsymbol{\Sigma}} = J(\boldsymbol{\Sigma}_{\boldsymbol{F}}, \boldsymbol{\Sigma}_{\boldsymbol{H}}, \Sigma_J)$.

derivatives of W with respect to the strain set $\{\boldsymbol{F}, \boldsymbol{H}, J\}$ [1, 20], to give:

$$[\mathbb{H}_W] = \begin{bmatrix} W_{\boldsymbol{FF}} & W_{\boldsymbol{FH}} & W_{\boldsymbol{F}J} \\ W_{\boldsymbol{HF}} & W_{\boldsymbol{HH}} & W_{\boldsymbol{H}J} \\ W_{J\boldsymbol{F}} & W_{J\boldsymbol{H}} & W_{JJ} \end{bmatrix} = \begin{bmatrix} \frac{\partial^2 W}{\partial \boldsymbol{F} \partial \boldsymbol{F}} & \frac{\partial^2 W}{\partial \boldsymbol{F} \partial \boldsymbol{H}} & \frac{\partial^2 W}{\partial \boldsymbol{F} \partial J} \\ \frac{\partial^2 W}{\partial \boldsymbol{H} \partial \boldsymbol{F}} & \frac{\partial^2 W}{\partial \boldsymbol{H} \partial \boldsymbol{H}} & \frac{\partial^2 W}{\partial \boldsymbol{H} \partial J} \\ \frac{\partial^2 W}{\partial J \partial \boldsymbol{F}} & \frac{\partial^2 W}{\partial J \partial \boldsymbol{H}} & \frac{\partial^2 W}{\partial J \partial J} \end{bmatrix}. \tag{10}$$

3.1. Compressible polyconvex model

In the case of a compressible Mooney-Rivlin model, an admissible polyconvex strain energy can be defined as [1, 20, 44]:

$$W = \alpha I_1 + \beta I_2 + f(J), \tag{11}$$

where α and β are positive material parameters and f is a convex function of the Jacobian J defined by:

$$f(J) = -4\beta J - 2\alpha \ln J + \frac{\lambda}{2}(J-1)^2, \tag{12}$$

with λ another positive material parameter. With the aid of expressions (7), (8), (11) and (12), the conjugate stresses become:

$$\boldsymbol{\Sigma}_{\boldsymbol{F}} = 2\alpha \boldsymbol{F}; \quad \boldsymbol{\Sigma}_{\boldsymbol{H}} = 2\beta \boldsymbol{H}; \quad \Sigma_J = f'(J), \tag{13}$$

and the Hessian operator $[\mathbb{H}_W]$ (10) adopts the following simple expression

$$[\mathbb{H}_W] = \begin{bmatrix} W_{\boldsymbol{FF}} & \boldsymbol{0} & \boldsymbol{0} \\ \boldsymbol{0} & W_{\boldsymbol{HH}} & \boldsymbol{0} \\ \boldsymbol{0} & \boldsymbol{0} & W_{JJ} \end{bmatrix}, \tag{14}$$

with diagonal components

$$W_{\boldsymbol{FF}} = 2\alpha \boldsymbol{\mathcal{I}}; \quad W_{\boldsymbol{HH}} = 2\beta \boldsymbol{\mathcal{I}}; \quad W_{JJ} = \lambda + 2\alpha J^{-2}. \tag{15}$$

Here, $\boldsymbol{\mathcal{I}}$ represents the fourth order identity tensor defined in indicial notation as $[\boldsymbol{\mathcal{I}}]_{iIjJ} = \delta_{ij}\delta_{IJ}$[6]. It is easy to prove that the Hessian operator (14) is

[6]Capital letters are used to identify Cartesian directions in the initial undeformed configuration and lower case letters are used to identify Cartesian directions in the final configuration [12].

positive definite for parameters $\{\alpha, \beta, \lambda\} > 0$. For $\beta = 0$, the Mooney-Rivlin model degenerates in the so-called neo-Hookean model. Following [20], appropriate values for the material parameters α, β and λ can be selected by ensuring that the tangent elasticity operator at the initial undeformed configuration coincides with the classic linearised elasticity operator expressed in terms of the Lamé coefficients λ and μ. Specifically, $\alpha + \beta = \frac{\mu}{2}$, expressed in terms of the shear modulus μ.

3.2. Nearly incompressible polyconvex model

For a polyconvex nearly incompressible Mooney-Rivlin material, the strain energy W can be additively decomposed into deviatoric $\hat{W}(\boldsymbol{F}, \boldsymbol{H}, J)$ and volumetric $U(J)$ contributions as [20]:

$$W = \hat{W} + U; \qquad \hat{W} = \varsigma J^{-2/3} I_1 + \xi J^{-2} I_2^{3/2}; \qquad U = \frac{\kappa}{2}(J-1)^2, \tag{16}$$

where ς, ξ and κ are positive material parameters of a similar nature to the parameters α, β and λ defined above for the compressible Mooney-Rivlin model (11)-(12). It is worthwhile to notice how the deviatoric component $\hat{W}$ of the strain energy depends explicitly on the Jacobian J. As already stated in [20], this arises as a consequence of the polyconvex requirement imposed on the constitutive model. Using the above energy functional W (16), the conjugate stresses (8) yield:

$$\boldsymbol{\Sigma}_{\boldsymbol{F}} = \frac{\partial \hat{W}}{\partial \boldsymbol{F}} = 2\varsigma J^{-2/3} \boldsymbol{F}; \qquad \boldsymbol{\Sigma}_{\boldsymbol{H}} = \frac{\partial \hat{W}}{\partial \boldsymbol{H}} = 3\xi J^{-2} I_2^{1/2} \boldsymbol{H}, \tag{17}$$

and

$$\Sigma_J = \hat{\Sigma}_J + p; \qquad \hat{\Sigma}_J = \frac{\partial \hat{W}}{\partial J} = -\frac{2\varsigma}{3} J^{-5/3} I_1 - 2\xi J^{-3} I_2^{3/2}, \tag{18}$$

where p represents the pressure field defined by

$$p = \frac{dU}{dJ} = \kappa(J-1). \tag{19}$$

Note that the conjugate stress associated with the Jacobian, namely Σ_J, consists of both a deviatoric contribution $\hat{\Sigma}_J$ and a volumetric (or pressure) contribution p. Thus, the first Piola-Kirchhoff stress tensor (9) can be formulated as:

$$\boldsymbol{P} = \hat{\boldsymbol{P}} + p\boldsymbol{H}; \qquad \hat{\boldsymbol{P}} = \boldsymbol{\Sigma}_{\boldsymbol{F}} + \boldsymbol{\Sigma}_{\boldsymbol{H}} \times \boldsymbol{F} + \hat{\Sigma}_J \boldsymbol{H}. \tag{20}$$

The Hessian operator $[\mathbb{H}_W]$ (10) adopts the following expression

$$[\mathbb{H}_W] = \begin{bmatrix} W_{\boldsymbol{FF}} & \mathbf{0} & W_{\boldsymbol{FJ}} \\ \mathbf{0} & W_{\boldsymbol{HH}} & W_{\boldsymbol{HJ}} \\ W_{J\boldsymbol{F}} & W_{J\boldsymbol{H}} & W_{JJ} \end{bmatrix}, \tag{21}$$

with components

$$\begin{aligned} &W_{\boldsymbol{FF}} = 2\varsigma J^{-2/3}\boldsymbol{\mathcal{I}}; \quad W_{\boldsymbol{HH}} = 3\xi J^{-2} I_2^{1/2}\left[I_2^{-1}\boldsymbol{H}\otimes\boldsymbol{H} + \boldsymbol{\mathcal{I}}\right]; \quad W_{JJ} = \gamma + \kappa; \\ &W_{\boldsymbol{FJ}} = -\frac{4\varsigma}{3} J^{-5/3}\boldsymbol{F}; \quad W_{\boldsymbol{HJ}} = -6\xi J^{-3} I_2^{1/2}\boldsymbol{H}; \quad W_{J\boldsymbol{F}} = W_{\boldsymbol{FJ}}; \quad W_{J\boldsymbol{H}} = W_{\boldsymbol{HJ}}; \end{aligned} \tag{22}$$

with

$$\gamma = \frac{\partial^2 \hat{W}}{\partial J \partial J} = \frac{10\varsigma}{9} J^{-8/3} I_1 + 6\xi J^{-4} I_2^{3/2}. \tag{23}$$

Positive definiteness of the above Hessian operator $[\mathbb{H}_W]$ has been shown in Reference [20] when $\{\varsigma, \xi, \kappa\} > 0$. As can be observed, the polyconvex nature of the nearly incompressible constitutive model leads to a Hessian operator with non-zero off-diagonal terms (22), in contrast to the simpler expression (14) for the case of the compressible model. This extra complexity leads to a more elaborate computational formulation as will be presented in subsequent sections of this paper.

Analogously to that stated in the above subsection, for $\xi = 0$, this nearly incompressible Mooney-Rivlin model degenerates in the so-called nearly incompressible neo-Hookean model. By comparison of the tangent elasticity operator at the initial undeformed configuration with that of the classic linearised elasticity operator, appropriate values for the material parameters ς and ξ can be defined in terms of the shear modulus μ, that is, $2\varsigma + 3\sqrt{3}\xi = \mu$.

Finally, it is worth pointing out that the classical (non-polyconvex) nearly incompressible neo-Hookean model used in [2] can be simply recovered by taking $\varsigma = \frac{\mu}{2}$ and $\xi = 0$ into (16) and replacing J in $\hat{W}$ (16) with $J_{\boldsymbol{F}}$ ($J_{\boldsymbol{F}} \equiv \det \boldsymbol{F}$). However, this type of model is not suitable for the formulation presented in this paper due to its non-polyconvex nature [20].

4. Entropy-based conservation laws

In order to derive an appropriate entropy-based system, consider the following convex entropy function $S_{\boldsymbol{\mathcal{U}}}$ defined as [1]:

$$S_{\boldsymbol{\mathcal{U}}}(\boldsymbol{p},\boldsymbol{F},\boldsymbol{H},J) = \underbrace{\frac{1}{2\rho_0}\boldsymbol{p}\cdot\boldsymbol{p}}_{\text{Kinetic energy}} + \underbrace{W(\boldsymbol{F},\boldsymbol{H},J)}_{\text{Elastic strain energy}}, \tag{24}$$

which clearly represents the kinetic and elastic energy contributions per unit of undeformed volume. A conjugate set of entropy variables $\boldsymbol{\mathcal{V}}$ (of the original set of conservation variables $\boldsymbol{\mathcal{U}}$) is obtained through the derivatives of $S_{\boldsymbol{\mathcal{U}}}$ as

$$\boldsymbol{\mathcal{V}} = \frac{\partial S_{\boldsymbol{\mathcal{U}}}}{\partial \boldsymbol{\mathcal{U}}} = \begin{bmatrix} \boldsymbol{v} \\ \boldsymbol{\Sigma}_{\boldsymbol{F}} \\ \boldsymbol{\Sigma}_{\boldsymbol{H}} \\ \Sigma_J \end{bmatrix}, \tag{25}$$

where the conjugate stresses $\{\boldsymbol{\Sigma}_{\boldsymbol{F}}, \boldsymbol{\Sigma}_{\boldsymbol{H}}, \Sigma_J\}$ are already defined in (8) and $\boldsymbol{v}$ represents the velocity of the system (i.e. $\boldsymbol{p} = \rho_0 \boldsymbol{v}$).

Remark 1:

Alternatively, it is also possible to derive the set of conservation variables $\boldsymbol{\mathcal{U}}$ as the conjugate set of variables associated with the above set of entropy variables $\boldsymbol{\mathcal{V}}$. For this, we must consider the following convex function $S_{\boldsymbol{\mathcal{V}}}$ obtained via a Legendre transform as:

$$S_{\boldsymbol{\mathcal{V}}}(\boldsymbol{v},\boldsymbol{\Sigma}_{\boldsymbol{F}},\boldsymbol{\Sigma}_{\boldsymbol{H}},\Sigma_J) = \frac{\rho_0}{2}(\boldsymbol{v}\cdot\boldsymbol{v}) + \max_{\{\boldsymbol{F},\boldsymbol{H},J\}} \left\{\boldsymbol{\Sigma}_{\boldsymbol{F}} : \boldsymbol{F} + \boldsymbol{\Sigma}_{\boldsymbol{H}} : \boldsymbol{H} + \Sigma_J J - W(\boldsymbol{F},\boldsymbol{H},J)\right\}. \tag{26}$$

Differentiating the above expression $S_{\boldsymbol{\mathcal{V}}}$ yields the set of conservation variables defined as:

$$\boldsymbol{\mathcal{U}} = \frac{\partial S_{\boldsymbol{\mathcal{V}}}}{\partial \boldsymbol{\mathcal{V}}} = \begin{bmatrix} \boldsymbol{p} \\ \boldsymbol{F} \\ \boldsymbol{H} \\ J \end{bmatrix}. \tag{27}$$

Using expressions (10) and (25), the Hessian operator associated with the convex entropy function $S_{\boldsymbol{\mathcal{U}}}$ is obtained as:

$$[\mathbb{H}_{S_{\boldsymbol{\mathcal{U}}}}] = \frac{\partial \boldsymbol{\mathcal{V}}}{\partial \boldsymbol{\mathcal{U}}} = \frac{\partial^2 S_{\boldsymbol{\mathcal{U}}}}{\partial \boldsymbol{\mathcal{U}} \partial \boldsymbol{\mathcal{U}}} = \left[\begin{array}{c|c} \frac{1}{\rho_0}\boldsymbol{I} & \mathbf{0} \\ \hline \mathbf{0} & [\mathbb{H}_W] \end{array}\right] = \left[\begin{array}{c|ccc} \frac{1}{\rho_0}\boldsymbol{I} & \multicolumn{3}{c}{\mathbf{0}} \\ \hline & W_{\boldsymbol{FF}} & W_{\boldsymbol{FH}} & W_{\boldsymbol{FJ}} \\ \mathbf{0} & W_{\boldsymbol{HF}} & W_{\boldsymbol{HH}} & W_{\boldsymbol{HJ}} \\ & W_{\boldsymbol{JF}} & W_{\boldsymbol{JH}} & W_{JJ} \end{array}\right]. \tag{28}$$

where $\boldsymbol{I}$ symbolises the second order identity tensor. Pre-multiplication of system (2) with the Hessian $[\mathbb{H}_{S_{\boldsymbol{\mathcal{U}}}}]$ (28), leads to a new set of conjugate entropy based laws as:

$$\frac{\partial \boldsymbol{\mathcal{V}}}{\partial t} = -[\mathbb{H}_{S_{\boldsymbol{\mathcal{U}}}}] \frac{\partial \boldsymbol{\mathcal{F}}_I}{\partial X_I} + [\mathbb{H}_{S_{\boldsymbol{\mathcal{U}}}}] \boldsymbol{\mathcal{S}}. \tag{29}$$

In particular, the equation associated with the conjugate entropy variable $\boldsymbol{v}$ reads:

$$\frac{\partial \boldsymbol{v}}{\partial t} = \frac{1}{\rho_0} \mathrm{DIV} \boldsymbol{P} + \frac{1}{\rho_0} \boldsymbol{f}_0, \tag{30}$$

and the equations associated with the conjugate stresses $\{\boldsymbol{\Sigma_F}, \boldsymbol{\Sigma_H}, \Sigma_J\}$ (i.e. stress rate equations) can be formulated as:

$$\frac{\partial \boldsymbol{\Sigma_F}}{\partial t} = (W_{\boldsymbol{FF}} + W_{\boldsymbol{FH}} \boldsymbol{\times} \boldsymbol{F_\Sigma} + W_{\boldsymbol{FJ}} \otimes \boldsymbol{H_\Sigma}) : \boldsymbol{\nabla}_0 \boldsymbol{v}; \tag{31a}$$

$$\frac{\partial \boldsymbol{\Sigma_H}}{\partial t} = (W_{\boldsymbol{HF}} + W_{\boldsymbol{HH}} \boldsymbol{\times} \boldsymbol{F_\Sigma} + W_{\boldsymbol{HJ}} \otimes \boldsymbol{H_\Sigma}) : \boldsymbol{\nabla}_0 \boldsymbol{v}; \tag{31b}$$

$$\frac{\partial \Sigma_J}{\partial t} = (W_{\boldsymbol{JF}} + W_{\boldsymbol{JH}} \boldsymbol{\times} \boldsymbol{F_\Sigma} + W_{JJ} \boldsymbol{H_\Sigma}) : \boldsymbol{\nabla}_0 \boldsymbol{v}. \tag{31c}$$

In above equations (31), $\{\boldsymbol{F_\Sigma}, \boldsymbol{H_\Sigma}, J_\Sigma\}$ symbolise the set of strain measures obtained in terms of the conjugate stresses $\{\boldsymbol{\Sigma_F}, \boldsymbol{\Sigma_H}, \Sigma_J\}$ via a reversed constitutive law (which will be later presented in Section 7 of the paper). The above general expression for the conjugate stresses' update can be particularised for the compressible and nearly incompressible polyconvex Mooney-Rivlin material models defined above, which is the objective of the following subsections.

4.1. Compressible entropy formulation

The conjugate stresses' updates for the case of the compressible Mooney-Rivlin constitutive model (see Section 3.1) can be simply derived by substituting the diagonal Hessian operator (10) and its components (15) into system (31) to yield:

$$\frac{\partial \boldsymbol{\Sigma}_{\boldsymbol{F}}}{\partial t} = 2\alpha \boldsymbol{\nabla}_0 \boldsymbol{v}; \tag{32a}$$

$$\frac{\partial \boldsymbol{\Sigma}_{\boldsymbol{H}}}{\partial t} = 2\beta \left(\boldsymbol{F}_{\boldsymbol{\Sigma}} \boldsymbol{\times} \boldsymbol{\nabla}_0 \boldsymbol{v} \right); \tag{32b}$$

$$\frac{\partial \Sigma_J}{\partial t} = \chi \left(\boldsymbol{H}_{\boldsymbol{\Sigma}} : \boldsymbol{\nabla}_0 \boldsymbol{v} \right), \tag{32c}$$

where $\chi = \lambda + 2\alpha J_{\boldsymbol{\Sigma}}^{-2}$. In the case of the neo-Hookean model ($\beta = 0$), the above system (32) can be further simplified by removing redundant equation (32b) (as the conjugate stress $\boldsymbol{\Sigma}_{\boldsymbol{H}} \equiv \boldsymbol{0}$). The area map tensor $\boldsymbol{H}_{\boldsymbol{\Sigma}}$ used in equation (32c) is thus defined by $\boldsymbol{H}_{\boldsymbol{\Sigma}} = \frac{1}{2} \boldsymbol{F}_{\boldsymbol{\Sigma}} \boldsymbol{\times} \boldsymbol{F}_{\boldsymbol{\Sigma}}$.

4.2. Nearly incompressible entropy formulation

For a nearly incompressible Mooney-Rivlin material (see Section 3.2) and with the help of equation (21), the conjugate stresses' updates can be obtained as:

$$\frac{\partial \boldsymbol{\Sigma}_{\boldsymbol{F}}}{\partial t} = (W_{\boldsymbol{FF}} + W_{\boldsymbol{F}J} \otimes \boldsymbol{H}_{\boldsymbol{\Sigma}}) : \boldsymbol{\nabla}_0 \boldsymbol{v}; \tag{33a}$$

$$\frac{\partial \boldsymbol{\Sigma}_{\boldsymbol{H}}}{\partial t} = (W_{\boldsymbol{HH}} \boldsymbol{\times} \boldsymbol{F}_{\boldsymbol{\Sigma}} + W_{\boldsymbol{H}J} \otimes \boldsymbol{H}_{\boldsymbol{\Sigma}}) : \boldsymbol{\nabla}_0 \boldsymbol{v}; \tag{33b}$$

$$\frac{\partial \Sigma_J}{\partial t} = (W_{J\boldsymbol{F}} + W_{J\boldsymbol{H}} \boldsymbol{\times} \boldsymbol{F}_{\boldsymbol{\Sigma}} + (\gamma + \kappa) \boldsymbol{H}_{\boldsymbol{\Sigma}}) : \boldsymbol{\nabla}_0 \boldsymbol{v}, \tag{33c}$$

where the components $W_{\boldsymbol{FF}}$, $W_{\boldsymbol{F}J}$, $W_{\boldsymbol{HH}}$, $W_{\boldsymbol{H}J}$, $W_{J\boldsymbol{F}}$, $W_{J\boldsymbol{H}}$ and γ have already been defined in (22) and (23). Using equation (18) for $\Sigma_J = \hat{\Sigma}_J + p$, it is interesting to split expression (33c) into two evolution updates for $\hat{\Sigma}_J$ and p, to yield:

$$\frac{\partial \hat{\Sigma}_J}{\partial t} = (W_{J\boldsymbol{F}} + W_{J\boldsymbol{H}} \boldsymbol{\times} \boldsymbol{F}_{\boldsymbol{\Sigma}} + \gamma \boldsymbol{H}_{\boldsymbol{\Sigma}}) : \boldsymbol{\nabla}_0 \boldsymbol{v}; \qquad \frac{\partial p}{\partial t} = \kappa \left(\boldsymbol{H}_{\boldsymbol{\Sigma}} : \boldsymbol{\nabla}_0 \boldsymbol{v} \right). \tag{34}$$

The splitting separates the above stress rates (33) into deviatoric $\{\boldsymbol{\Sigma}_{\boldsymbol{F}}, \boldsymbol{\Sigma}_{\boldsymbol{H}}, \hat{\Sigma}_J\}$ and volumetric p contributions. The unknowns of the problem now become $\{\boldsymbol{v}, \boldsymbol{\Sigma}_{\boldsymbol{F}}, \boldsymbol{\Sigma}_{\boldsymbol{H}}, \hat{\Sigma}_J, p\}$. As stated in the previous section, $\boldsymbol{\Sigma}_{\boldsymbol{H}} \equiv \boldsymbol{0}$ for the degenerate neo-Hookean model with $\boldsymbol{H}_{\boldsymbol{\Sigma}} = \frac{1}{2} \boldsymbol{F}_{\boldsymbol{\Sigma}} \boldsymbol{\times} \boldsymbol{F}_{\boldsymbol{\Sigma}}$.

4.3. Eigenvalue structure

As it is well known, the study of the eigenvalue structure of the system (33) is crucial in order to guarantee its hyperbolicity. In Reference [1], the authors verified the hyperbolic nature of the problem for the case of a compressible polyconvex Mooney-Rivlin model. In References [2, 44], the authors repeated the same exercise, but in the case of a nearly incompressible non-polyconvex neo-Hookean model. In this paper, the same methodology is extended to the case of a nearly incompressible polyconvex Mooney-Rivlin (and neo-Hookean) constitutive model. The eigenvalues (or wave speeds) and the corresponding eigenvectors for the system (33) can be determined by identifying possible plane wave solutions (in the absence of source terms) of the type [1]:

$$\boldsymbol{\mathcal{V}} = \phi(\boldsymbol{X}\cdot\boldsymbol{N} - c_\alpha t)\bar{\boldsymbol{\mathcal{V}}}_\alpha = \phi(\boldsymbol{X}\cdot\boldsymbol{N} - c_\alpha t)\begin{bmatrix} \bar{\boldsymbol{v}}_\alpha \\ \bar{\boldsymbol{\Sigma}}^\alpha_{\boldsymbol{F}} \\ \bar{\boldsymbol{\Sigma}}^\alpha_{\boldsymbol{H}} \\ \bar{\Sigma}^\alpha_J \end{bmatrix}, \tag{35}$$

where ϕ denotes a scalar real valued function, c_α is the wave speed corresponding to the eigenmode $\bar{\boldsymbol{\mathcal{V}}}_\alpha$ and $\boldsymbol{N}$ is the direction of propagation. It is easy to show that the above expression for entropy variables leads to an eigenvalue problem (refer to equation (29)) given by[7]

$$\boldsymbol{\mathcal{A}}^T_{\boldsymbol{N}}\bar{\boldsymbol{\mathcal{V}}}_\alpha = c_\alpha\bar{\boldsymbol{\mathcal{V}}}_\alpha; \qquad\qquad \boldsymbol{\mathcal{A}}^T_{\boldsymbol{N}} = \boldsymbol{\mathcal{A}}^T_I N_I. \tag{37}$$

It is far simpler to deal with the resulting eigenproblem by considering each individual component of the system. For this purpose, note first that the time derivative, material gradient, material divergence and material curl

[7] An alternative representation of the eigenvalue problem for conservation variables is described as follows [2]:

$$\boldsymbol{\mathcal{A}}_{\boldsymbol{N}}\bar{\boldsymbol{\mathcal{U}}}_\alpha = c_\alpha\bar{\boldsymbol{\mathcal{U}}}_\alpha; \qquad \boldsymbol{\mathcal{A}}_{\boldsymbol{N}} = \boldsymbol{\mathcal{A}}_I N_I; \qquad \bar{\boldsymbol{\mathcal{V}}}_\alpha = [\mathbb{H}_{S_{\boldsymbol{\mathcal{U}}}}]\bar{\boldsymbol{\mathcal{U}}}_\alpha. \tag{36}$$

operators for the proposed plane wave solution become,

$$\begin{aligned}
\frac{\partial \boldsymbol{\mathcal{V}}}{\partial t} &= -c_\alpha \bar{\boldsymbol{\mathcal{V}}}_\alpha \phi'; \\
\boldsymbol{\nabla}_0 \boldsymbol{v} &= (\bar{\boldsymbol{v}}_\alpha \otimes \boldsymbol{N})\, \phi'; \\
\boldsymbol{\nabla}_0 \Sigma_J &= \left(\bar{\Sigma}_J^\alpha \boldsymbol{N}\right) \phi'; \\
\mathrm{DIV}\boldsymbol{\Sigma}_{\boldsymbol{F}} &= \left(\bar{\boldsymbol{\Sigma}}_{\boldsymbol{F}}^\alpha \boldsymbol{N}\right) \phi'; \\
\mathrm{CURL}\boldsymbol{\Sigma}_{\boldsymbol{H}} &= -\left(\bar{\boldsymbol{\Sigma}}_{\boldsymbol{H}}^\alpha \times \boldsymbol{N}\right) \phi'.
\end{aligned} \tag{38}$$

Using these expressions, together with the aid of expressions (5), (30) and (33), and the properties associated with the vector and tensor cross products given in [20], leads after some simple algebra to:

$$\begin{aligned}
-\left(\bar{\boldsymbol{\Sigma}}_{\boldsymbol{F}}^\alpha + \boldsymbol{F}_{\boldsymbol{\Sigma}} \times \bar{\boldsymbol{\Sigma}}_{\boldsymbol{H}}^\alpha + \bar{\Sigma}_J^\alpha \boldsymbol{H}_{\boldsymbol{\Sigma}}\right) \boldsymbol{N} &= \rho_0 c_\alpha \bar{\boldsymbol{v}}_\alpha \\
-\left(W_{\boldsymbol{FF}} + W_{\boldsymbol{F}J} \otimes \boldsymbol{H}_{\boldsymbol{\Sigma}}\right) : (\bar{\boldsymbol{v}}_\alpha \otimes \boldsymbol{N}) &= c_\alpha \bar{\boldsymbol{\Sigma}}_{\boldsymbol{F}}^\alpha \\
-\left(W_{\boldsymbol{HH}} \times \boldsymbol{F}_{\boldsymbol{\Sigma}} + W_{\boldsymbol{H}J} \otimes \boldsymbol{H}_{\boldsymbol{\Sigma}}\right) : (\bar{\boldsymbol{v}}_\alpha \otimes \boldsymbol{N}) &= c_\alpha \bar{\boldsymbol{\Sigma}}_{\boldsymbol{H}}^\alpha \\
-\left(W_{J\boldsymbol{F}} + W_{J\boldsymbol{H}} \times \boldsymbol{F}_{\boldsymbol{\Sigma}} + W_{JJ} \boldsymbol{H}_{\boldsymbol{\Sigma}}\right) : (\bar{\boldsymbol{v}}_\alpha \otimes \boldsymbol{N}) &= c_\alpha \bar{\Sigma}_J^\alpha.
\end{aligned} \tag{39}$$

As a consequence of the high level of redundancy in the system of equations being considered, only 6 wave speeds are different from zero. These can be readily identified by substituting the last three equations for the stresses into the first one to give an eigenvalue problem for the velocity component alone as

$$2\varsigma J_\Sigma^{-2/3} \bar{\boldsymbol{v}}_\alpha + K\left(\Lambda_T^2 - \boldsymbol{\Lambda}_T\right) \bar{\boldsymbol{v}}_\alpha + L\boldsymbol{n}(\bar{\boldsymbol{v}}_\alpha \cdot \boldsymbol{n}) = \rho_0 c_\alpha^2 \bar{\boldsymbol{v}}_\alpha, \tag{40}$$

where

$$\begin{aligned}
\boldsymbol{\Lambda}_T &= \boldsymbol{F}\boldsymbol{T}_1 \otimes \boldsymbol{F}\boldsymbol{T}_1 + \boldsymbol{F}\boldsymbol{T}_2 \otimes \boldsymbol{F}\boldsymbol{T}_2; \\
\Lambda_T^2 &= \boldsymbol{F}\boldsymbol{T}_1 \cdot \boldsymbol{F}\boldsymbol{T}_1 + \boldsymbol{F}\boldsymbol{T}_2 \cdot \boldsymbol{F}\boldsymbol{T}_2 = \mathrm{tr}\boldsymbol{\Lambda}_T, \\
K &= 3\xi J_\Sigma^{-2} I_2^{1/2}; \\
L &= W_{JJ}\Lambda_A^2 - \frac{8\varsigma}{3} J_\Sigma^{-5/3} \Lambda_A \Lambda_N + \Xi K \left(\Xi I_2^{-1} - \frac{4}{J_\Sigma}\Lambda_A\right); \\
\Lambda_A \boldsymbol{n} &= \boldsymbol{H}\boldsymbol{N}; \\
\Lambda_N \boldsymbol{n} &= \boldsymbol{F}\boldsymbol{N}; \\
\Lambda_A^2 &= \boldsymbol{H}\boldsymbol{N} \cdot \boldsymbol{H}\boldsymbol{N}; \\
\Xi &= \Lambda_N \left[(\boldsymbol{F}_{\boldsymbol{\Sigma}} : \boldsymbol{F}_{\boldsymbol{\Sigma}}) - \Lambda_N^2\right].
\end{aligned} \tag{41}$$

Note that by construction $\boldsymbol{n}$ is a unit vector orthogonal to the vectors $\boldsymbol{FT}_{1,2}$ which lie on the propagation surface. The first set of eigenvectors/eigenvalues corresponding to p-waves is obtained by taking $\bar{\boldsymbol{v}} = \boldsymbol{n}$ to give,

$$c_{1,2} = \pm\sqrt{\frac{2\varsigma J_\Sigma^{-2/3} + K\Lambda_T^2 + W_{JJ}\Lambda_A^2 - \frac{8\varsigma}{3}J_\Sigma^{-5/3}\Lambda_A\Lambda_N + \Xi K\left[\Xi I_2^{-1} - \frac{4}{J_\Sigma}\Lambda_A\right]}{\rho_0}}. \tag{42}$$

The associated eigenvectors are obtained from equation (39) to give:

$$\bar{\boldsymbol{\mathcal{V}}}_{1,2} = \begin{bmatrix} \boldsymbol{n} \\ -\frac{1}{c_{1,2}}\left(W_{\boldsymbol{FF}} + W_{\boldsymbol{FJ}} \otimes \boldsymbol{H}_{\boldsymbol{\Sigma}}\right) : (\boldsymbol{n} \otimes \boldsymbol{N}) \\ -\frac{1}{c_{1,2}}\left(W_{\boldsymbol{HH}} \times \boldsymbol{F}_{\boldsymbol{\Sigma}} + W_{\boldsymbol{HJ}} \otimes \boldsymbol{H}_{\boldsymbol{\Sigma}}\right) : (\boldsymbol{n} \otimes \boldsymbol{N}) \\ -\frac{1}{c_{1,2}}\left(W_{\boldsymbol{JF}} + W_{\boldsymbol{JH}} \times \boldsymbol{F}_{\boldsymbol{\Sigma}} + W_{JJ}\boldsymbol{H}_{\boldsymbol{\Sigma}}\right) : (\boldsymbol{n} \otimes \boldsymbol{N}) \end{bmatrix}. \tag{43}$$

The next four eigenvalues correspond to shear waves where the vibration takes place on the propagation plane. The corresponding velocity vectors are orthogonal to $\boldsymbol{n}$ and in the directions of the unit eigenvectors $\{\boldsymbol{t}_1, \boldsymbol{t}_2\}$ of the rank two tensor $\boldsymbol{\Lambda}_T$. The wave speeds are given by:

$$\begin{aligned} c_{3,4} &= \pm\sqrt{\frac{2\varsigma J_\Sigma^{-2/3} + K\left(\Lambda_T^2 - \lambda_1^2\right)}{\rho_0}}; \\ c_{5,6} &= \pm\sqrt{\frac{2\varsigma J_\Sigma^{-2/3} + K\left(\Lambda_T^2 - \lambda_2^2\right)}{\rho_0}}, \end{aligned} \tag{44}$$

where $\lambda_{1,2}^2$ are the eigenvalues of $\boldsymbol{\Lambda}_T$, that is:

$$\boldsymbol{\Lambda}_T = \lambda_1^2 \boldsymbol{t}_1 \otimes \boldsymbol{t}_1 + \lambda_2^2 \boldsymbol{t}_2 \otimes \boldsymbol{t}_2. \tag{45}$$

The corresponding eigenvectors are given by:

$$\bar{\boldsymbol{\mathcal{V}}}_{3,4} = \begin{bmatrix} \boldsymbol{t}_1 \\ -\frac{W_{\boldsymbol{FF}}}{c_{3,4}} : (\boldsymbol{t}_1 \otimes \boldsymbol{N}) \\ -\frac{W_{\boldsymbol{HH}}}{c_{3,4}} : [\boldsymbol{F} \times (\boldsymbol{t}_1 \otimes \boldsymbol{N})] \\ -\frac{W_{\boldsymbol{JH}}}{c_{3,4}} : [\boldsymbol{F} \times (\boldsymbol{t}_1 \otimes \boldsymbol{N})] \end{bmatrix}; \qquad \bar{\boldsymbol{\mathcal{V}}}_{5,6} = \begin{bmatrix} \boldsymbol{t}_2 \\ -\frac{W_{\boldsymbol{FF}}}{c_{5,6}} : (\boldsymbol{t}_2 \otimes \boldsymbol{N}) \\ -\frac{W_{\boldsymbol{HH}}}{c_{5,6}} : [\boldsymbol{F} \times (\boldsymbol{t}_2 \otimes \boldsymbol{N})] \\ -\frac{W_{\boldsymbol{JH}}}{c_{5,6}} : [\boldsymbol{F} \times (\boldsymbol{t}_2 \otimes \boldsymbol{N})] \end{bmatrix}. \tag{46}$$

For a fully incompressible material, the conservation equation for volume map evolution $\dot{J}$ in spatial (or current) configuration is replaced by the constraint $\operatorname{div} \boldsymbol{v} = 0$, and thus leads to $\bar{\boldsymbol{v}}_\alpha \cdot \boldsymbol{n} = 0$. This constraint, once substituted into equation (40) yields

$$\rho_0 c_\alpha^2 \boldsymbol{v}_\alpha = 2\varsigma J_{\boldsymbol{\Sigma}}^{-2/3} \bar{\boldsymbol{v}}_\alpha + K \left(\Lambda_T^2 - \boldsymbol{\Lambda}_T\right) \bar{\boldsymbol{v}}_\alpha, \tag{47}$$

leading to only two pairs of non-zero eigenvalues corresponding to the shear waves $c_{3,4} = c_{5,6} = \pm c_s$ (44) with eigenvectors $\bar{\boldsymbol{\mathcal{V}}}_{3,4}$ and $\bar{\boldsymbol{\mathcal{V}}}_{5,6}$.

5. Petrov-Galerkin (PG) conservation-based variational formulation

In this Section, expanding the work of the authors in previous Reference [1], two variationally consistent PG computational frameworks are presented for the conservation-based system $\boldsymbol{p}$-$\boldsymbol{F}$-$\boldsymbol{H}$-J, namely, an explicit compressible and nearly incompressible scheme (Section 5.1) and a tailor-made PG fractional step algorithm (Section 5.2).

5.1. Nearly incompressible $\boldsymbol{p}$-$\boldsymbol{F}$-$\boldsymbol{H}$-J formulation

The stabilised variational statement for the set of conservation laws (3) can be derived through the use of suitable work conjugates [5]. To achieve this, we first need to define appropriate stabilised conjugate variables $\delta\boldsymbol{\mathcal{V}}^{st} = \left[\delta\boldsymbol{v}^{st}, \delta\boldsymbol{\Sigma}_{\boldsymbol{F}}^{st}, \delta\boldsymbol{\Sigma}_{\boldsymbol{H}}^{st}, \delta\Sigma_J^{st}\right]^T$ via augmented weighting functions [48] as $\delta\boldsymbol{\mathcal{V}}^{st} = \delta\boldsymbol{\mathcal{V}} + \boldsymbol{\tau}^T \boldsymbol{\mathcal{A}}_I^T \frac{\partial \delta\boldsymbol{\mathcal{V}}}{\partial X_I}$. Use of expressions (29), (30), (33) and consideration of the involution equations (5) for the deformation gradient and its cofactor, yields

$$\delta\boldsymbol{v}^{st} = \delta\boldsymbol{v} - \frac{\tau_{\boldsymbol{p}}}{\rho_0}\left(\mathrm{DIV}\delta\boldsymbol{\Sigma}_{\boldsymbol{F}} - \boldsymbol{F} \times \mathrm{CURL}\delta\boldsymbol{\Sigma}_{\boldsymbol{H}} + \boldsymbol{H}\boldsymbol{\nabla}_0\delta\Sigma_J\right); \tag{48a}$$

$$\delta\boldsymbol{\Sigma}_{\boldsymbol{F}}^{st} = \delta\boldsymbol{\Sigma}_{\boldsymbol{F}} - \tau_{\boldsymbol{F}}\left(W_{\boldsymbol{FF}} + W_{\boldsymbol{F}J} \otimes \boldsymbol{H}\right) : \boldsymbol{\nabla}_0\delta\boldsymbol{v}; \tag{48b}$$

$$\delta\boldsymbol{\Sigma}_{\boldsymbol{H}}^{st} = \delta\boldsymbol{\Sigma}_{\boldsymbol{H}} - \tau_{\boldsymbol{H}}\left(W_{\boldsymbol{HH}} \times \boldsymbol{F} + W_{\boldsymbol{H}J} \otimes \boldsymbol{H}\right) : \boldsymbol{\nabla}_0\delta\boldsymbol{v}; \tag{48c}$$

$$\delta\Sigma_J^{st} = \delta\Sigma_J - \tau_J\left(W_{J\boldsymbol{F}} + W_{J\boldsymbol{H}} \times \boldsymbol{F} + W_{JJ}\boldsymbol{H}\right) : \boldsymbol{\nabla}_0\delta\boldsymbol{v}. \tag{48d}$$

The residuals $\boldsymbol{\mathcal{R}}_{\boldsymbol{\mathcal{U}}} = [\boldsymbol{\mathcal{R}}_{\boldsymbol{p}}, \boldsymbol{\mathcal{R}}_{\boldsymbol{F}}, \boldsymbol{\mathcal{R}}_{\boldsymbol{H}}, \mathcal{R}_J]^T$ of the conservation laws (3) are defined by

$$\boldsymbol{\mathcal{R}}_{\boldsymbol{\mathcal{U}}} = \begin{bmatrix} \boldsymbol{\mathcal{R}}_{\boldsymbol{p}} \\ \boldsymbol{\mathcal{R}}_{\boldsymbol{F}} \\ \boldsymbol{\mathcal{R}}_{\boldsymbol{H}} \\ \mathcal{R}_J \end{bmatrix} = \begin{bmatrix} \mathrm{DIV}\boldsymbol{P} + \boldsymbol{f}_0 - \dot{\boldsymbol{p}} \\ \boldsymbol{\nabla}_0 \boldsymbol{v} - \dot{\boldsymbol{F}} \\ \boldsymbol{F} \times \boldsymbol{\nabla}_0 \boldsymbol{v} - \dot{\boldsymbol{H}} \\ \boldsymbol{H} : \boldsymbol{\nabla}_0 \boldsymbol{v} - \dot{J} \end{bmatrix} \tag{49}$$

where the dot over a variable is used to denote differentiation in time. Using expressions in (48a-48d) and (49), it is now possible to derive a stabilised weak statement by multiplying appropriate conjugate virtual fields $\delta\boldsymbol{\mathcal{V}}^{st}$ with the corresponding residuals $\boldsymbol{\mathcal{R}}_{\boldsymbol{\mathcal{U}}}$, and integrating over the initial volume V, to give

$$0 = \int_V \left(\delta \boldsymbol{v}^{st} \cdot \boldsymbol{\mathcal{R}}_{\boldsymbol{p}} + \delta \boldsymbol{\Sigma}^{st}_{\boldsymbol{F}} : \boldsymbol{\mathcal{R}}_{\boldsymbol{F}} + \delta \boldsymbol{\Sigma}^{st}_{\boldsymbol{H}} : \boldsymbol{\mathcal{R}}_{\boldsymbol{H}} + \delta \Sigma^{st}_J \mathcal{R}_J \right) dV. \tag{50}$$

By re-grouping expression (50) according to each virtual conjugate variable, it is possible to extract first the terms containing the virtual velocity $\delta\boldsymbol{v}$ as:

$$\begin{aligned} 0 = & \int_V \left(\delta \boldsymbol{v} \cdot \boldsymbol{\mathcal{R}}_{\boldsymbol{p}} - \tau_{\boldsymbol{F}} \boldsymbol{\mathcal{R}}_{\boldsymbol{F}} : (W_{\boldsymbol{FF}} + W_{\boldsymbol{FJ}} \otimes \boldsymbol{H}) : \boldsymbol{\nabla}_0 \delta \boldsymbol{v} \right) dV \\ & - \int_V \left(\tau_{\boldsymbol{H}} \boldsymbol{\mathcal{R}}_{\boldsymbol{H}} : (W_{\boldsymbol{HH}} \times \boldsymbol{F} + W_{\boldsymbol{HJ}} \otimes \boldsymbol{H}) : \boldsymbol{\nabla}_0 \delta \boldsymbol{v} \right) dV \\ & - \int_V \left(\tau_J \mathcal{R}_J \left(W_{\boldsymbol{JF}} + W_{\boldsymbol{JH}} \times \boldsymbol{F} + W_{JJ} \boldsymbol{H} \right) : \boldsymbol{\nabla}_0 \delta \boldsymbol{v} \right) dV. \end{aligned} \tag{51}$$

Integrating by parts the first term on the right hand side of (51) and expanding the resulting equation yields:

$$\int_V \delta \boldsymbol{v} \cdot \frac{\partial \boldsymbol{p}}{\partial t} \, dV = \int_V \delta \boldsymbol{v} \cdot \boldsymbol{f}_0 \, dV + \int_{\partial V} \delta \boldsymbol{v} \cdot \boldsymbol{t}_B \, dA - \int_V \boldsymbol{P}^{st} : \boldsymbol{\nabla}_0 \delta \boldsymbol{v} \, dV, \tag{52}$$

where the stabilised first Piola-Kirchhoff stress $\boldsymbol{P}^{st}$ is:

$$\boldsymbol{P}^{st} = \boldsymbol{\Sigma}^{st}_{\boldsymbol{F}} + \boldsymbol{\Sigma}^{st}_{\boldsymbol{H}} \times \boldsymbol{F} + \Sigma^{st}_J \boldsymbol{H}, \tag{53}$$

with corresponding stabilised conjugate stresses as

$$\begin{aligned}\boldsymbol{\Sigma}_{\boldsymbol{F}}^{st} &= \boldsymbol{\Sigma}_{\boldsymbol{F}} + \tau_{\boldsymbol{F}} W_{\boldsymbol{FF}} : \boldsymbol{\mathcal{R}}_{\boldsymbol{F}} + \tau_J W_{J\boldsymbol{F}} \mathcal{R}_J;\\ \boldsymbol{\Sigma}_{\boldsymbol{H}}^{st} &= \boldsymbol{\Sigma}_{\boldsymbol{H}} + \tau_{\boldsymbol{H}} W_{\boldsymbol{HH}} : \boldsymbol{\mathcal{R}}_{\boldsymbol{H}} + \tau_J W_{J\boldsymbol{H}} \mathcal{R}_J;\\ \Sigma_J^{st} &= \Sigma_J + \tau_{\boldsymbol{F}} W_{\boldsymbol{F}J} : \boldsymbol{\mathcal{R}}_{\boldsymbol{F}} + \tau_{\boldsymbol{H}} W_{\boldsymbol{H}J} : \boldsymbol{\mathcal{R}}_{\boldsymbol{H}} + \tau_J W_{JJ} \mathcal{R}_J.\end{aligned} \tag{54}$$

Following a Variational Multi-Scale (VMS) stabilisation procedure [29–36, 52], these stresses (54) can be alternatively expressed in terms of stabilised strains as:

$$\boldsymbol{\Sigma}_{\boldsymbol{F}}^{st} \approx \boldsymbol{\Sigma}_{\boldsymbol{F}}(\boldsymbol{F}^{st}, J^{st}); \quad \boldsymbol{\Sigma}_{\boldsymbol{H}}^{st} \approx \boldsymbol{\Sigma}_{\boldsymbol{H}}(\boldsymbol{H}^{st}, J^{st}); \quad \Sigma_J^{st} \approx \Sigma_J(\boldsymbol{F}^{st}, \boldsymbol{H}^{st}, J^{st}), \tag{55}$$

where

$$\boldsymbol{F}^{st} = \boldsymbol{F} + \tau_{\boldsymbol{F}} \boldsymbol{\mathcal{R}}_{\boldsymbol{F}}; \quad \boldsymbol{H}^{st} = \boldsymbol{H} + \tau_{\boldsymbol{H}} \boldsymbol{\mathcal{R}}_{\boldsymbol{H}}; \quad J^{st} = J + \tau_J \mathcal{R}_J. \tag{56}$$

In the above expressions (55) and (56), the residual terms $\{\boldsymbol{\mathcal{R}}_{\boldsymbol{F}}, \boldsymbol{\mathcal{R}}_{\boldsymbol{H}}, \mathcal{R}_J\}$ represent the difference between the time rate of the corresponding strain variable and its evaluation in terms of the material gradient of the velocities. To reduce the implicitness of the formulation, a simple procedure has been proposed in references [1, 2, 5] whereby the above time residuals are replaced by their time integrated geometric equivalents $\{\boldsymbol{\mathcal{R}}_{\boldsymbol{F}}^{\boldsymbol{x}}, \boldsymbol{\mathcal{R}}_{\boldsymbol{H}}^{\boldsymbol{x}}, \mathcal{R}_J^{\boldsymbol{x}}\}$, to give:

$$\begin{aligned}\boldsymbol{F}^{st} &= \boldsymbol{F} + \underbrace{\tau_{\boldsymbol{F}} \boldsymbol{\mathcal{R}}_{\boldsymbol{F}} + \zeta_{\boldsymbol{F}} \boldsymbol{\mathcal{R}}_{\boldsymbol{F}}^{\boldsymbol{x}}}_{\boldsymbol{F}^{sub}}; \quad \boldsymbol{\mathcal{R}}_{\boldsymbol{F}}^{\boldsymbol{x}} = \boldsymbol{F}_{\boldsymbol{x}} - \boldsymbol{F}; \quad \boldsymbol{F}_{\boldsymbol{x}} = \boldsymbol{\nabla}_0 \boldsymbol{x}\\ \boldsymbol{H}^{st} &= \boldsymbol{H} + \underbrace{\tau_{\boldsymbol{H}} \boldsymbol{\mathcal{R}}_{\boldsymbol{H}} + \zeta_{\boldsymbol{H}} \boldsymbol{\mathcal{R}}_{\boldsymbol{H}}^{\boldsymbol{x}}}_{\boldsymbol{H}^{sub}}; \quad \boldsymbol{\mathcal{R}}_{\boldsymbol{H}}^{\boldsymbol{x}} = \boldsymbol{H}_{\boldsymbol{x}} - \boldsymbol{H}; \quad \boldsymbol{H}_{\boldsymbol{x}} = \frac{1}{2} \boldsymbol{\nabla}_0 \boldsymbol{x} \times \boldsymbol{\nabla}_0 \boldsymbol{x}\\ J^{st} &= J + \underbrace{\tau_J \mathcal{R}_J + \zeta_J \mathcal{R}_J^{\boldsymbol{x}}}_{J^{sub}}; \quad \mathcal{R}_J^{\boldsymbol{x}} = J_{\boldsymbol{x}} - J; \quad J_{\boldsymbol{x}} = \det(\boldsymbol{\nabla}_0 \boldsymbol{x}),\end{aligned} \tag{57}$$

where $\zeta_{\boldsymbol{F}}$, $\zeta_{\boldsymbol{H}}$ and ζ_J are dimensionless stabilisation parameters, in the range of $[0, 0.5]$. Note that subgrid-scale terms $\{\boldsymbol{F}^{sub}, \boldsymbol{H}^{sub}, J^{sub}\}$ are considered small with respect to coarse-scale terms $\{\boldsymbol{F}, \boldsymbol{H}, J\}$.

Remark 2:

In this paper, we restrict ourselves to the local linearisation of a residual-based stabilisation, neglecting the products of subgrid-scale terms (being

these higher-order corrections). Thus, it is interesting to derive the following simplified version of (55) as:

$$\boldsymbol{\Sigma}_{\boldsymbol{F}}^{st} \approx \boldsymbol{\Sigma}_{\boldsymbol{F}}(\boldsymbol{F}^{st}, J); \quad \boldsymbol{\Sigma}_{\boldsymbol{H}}^{st} \approx \boldsymbol{\Sigma}_{\boldsymbol{H}}(\boldsymbol{H}^{st}, J); \quad \hat{\Sigma}_{J}^{st} \approx \hat{\Sigma}_{J}(\boldsymbol{F}, \boldsymbol{H}, J^{st}). \tag{58}$$

Consideration of C_0 linear shape functions N_a for both the conservation variables and the stabilised virtual fields, leads to the following semi-discretised linear momentum rate equation at each node a:

$$\sum_b M_{ab}\dot{\boldsymbol{p}}_b = \int_V N_a \boldsymbol{f}_0 \, dV + \int_{\partial V} N_a \boldsymbol{t}_B \, dA - \int_V \boldsymbol{P}^{st} \boldsymbol{\nabla}_0 N_a \, dV, \tag{59}$$

where the consistent mass contribution $M_{ab} = \int_V N_a N_b dV$. Finally, the enhanced conjugate stress measures defined in equations (48b), (48c) and (48d) can be introduced into the weighted residual equation (50). This gives a set of strain update equations as:

$$\sum_b M_{ab}\dot{\boldsymbol{F}}_b = -\int_V \frac{1}{\rho_0} \boldsymbol{p}^{st} \otimes \boldsymbol{\nabla}_0 N_a \, dV + \int_{\partial V} N_a \left(\boldsymbol{v}_B \otimes \boldsymbol{N}\right) \, dA; \tag{60a}$$

$$\sum_b M_{ab}\dot{\boldsymbol{H}}_b = \int_V \frac{1}{\rho_0} \boldsymbol{p}^{st} \boldsymbol{\times} \boldsymbol{F} \boldsymbol{\times} \boldsymbol{\nabla}_0 N_a \, dV - \int_{\partial V} N_a \left(\boldsymbol{v}_B \boldsymbol{\times} \boldsymbol{F} \boldsymbol{\times} \boldsymbol{N}\right) \, dA; \tag{60b}$$

$$\sum_b M_{ab}\dot{J}_b = -\int_V \frac{1}{\rho_0} \boldsymbol{p}^{st} \cdot \boldsymbol{H} \boldsymbol{\nabla}_0 N_a \, dV + \int_{\partial V} N_a (\boldsymbol{v}_B \cdot \boldsymbol{H}\boldsymbol{N}) dA, \tag{60c}$$

where $\boldsymbol{p}^{st} = \boldsymbol{p} + \tau_{\boldsymbol{p}} \boldsymbol{\mathcal{R}}_{\boldsymbol{p}}$. In addition, traction and linear momentum vectors at the boundary, denoted as $\boldsymbol{t}_B$ (59) and $\boldsymbol{v}_B$ (60a-60c), are directly computed from prescribed (i.e. natural and essential) boundary conditions. In order to speed up the algorithm, the consistent mass matrix contributions are replaced by lumped mass matrix contributions without affecting the order of convergence [5].

However, as discussed in Reference [1], the involutions described by equation (5) are no longer enforced by applying correction to the linear momentum $\boldsymbol{p}$, namely $\boldsymbol{p}^{st}$, in (60a) and (60b). For this reason, the stabilisation of the momentum field should only be applied to the third equation above (60c).

Moreover, by setting $\tau_J = 0$, and by assigning $\tau_{\boldsymbol{F}} = \tau_{\boldsymbol{H}} = \tau$ and $\zeta_{\boldsymbol{F}} = \zeta_{\boldsymbol{H}} = \zeta$, equations (59), (60a), (60b) and (60c) are fully decoupled and

can be solved in a sequential manner. Equations (60a) and (60b) are first solved to obtain $\dot{\boldsymbol{F}}$ and $\dot{\boldsymbol{H}}$ which can then be substituted into (59) to deduce $\dot{\boldsymbol{p}}$. Once $\dot{\boldsymbol{p}}$ is determined, $\dot{J}$ can finally be obtained from (60c). Thus, the time discrete version of the four-field $\boldsymbol{p}$-$\boldsymbol{F}$-$\boldsymbol{H}$-J conservation formulation (see equations (59), (60a), (60b) and (60c)) for polyconvex elasticity is reduced to the consideration of four stabilising parameters, namely $\{\tau, \tau_{\boldsymbol{p}}, \zeta, \zeta_J\}$.

Finally, the set of stabilised semidiscrete nodal equations which have been produced can then be explicitly integrated from time step t^n to t^{n+1}. In this case, the explicit one-step two-stage Total Variation Diminishing RungeKutta (TVD-RK) time integrator [53] is preferred due to its excellent TVD properties (refer to Section 4 in [5] for further discussion). The scheme is suitably modified to guarantee the conservation of angular momentum, as described in [5]. The evaluation of the maximum time increment is intimately related to the minimum size of element h_{min} and the maximum (volumetric) wave speed c_{max} (42) via the Courant-Friedrichs-Lewy number α_{CFL}.

5.2. Truly incompressible $\boldsymbol{p}$-$\boldsymbol{F}$-$\boldsymbol{H}$-J formulation: Fractional step approach

In the case of nearly or truly incompressible materials, the volumetric wave speed (42) can reach very high values leading to prohibitively small time steps. This can have a very negative effect in the computational efficiency of the algorithm. In Gil *et al.* [2], a tailor-made PG fractional step algorithm was introduced for the three-field $\boldsymbol{p}$-$\boldsymbol{F}$-J mixed formulation. Extension of this variational PG fractional step method to include the new conservation law for the area map $\boldsymbol{H}$ under the consideration of a polyconvex constitutive law is presented below.

Following Reference [2], a predictor-corrector algorithm is designed to advance the problem unknowns from t^n to t^{n+1}. It is typical to first advance in time and then discretise in space using a suitable PG stabilisation [5]. To achieve this, note first that the predictor (or intermediate) step of the

algorithm is defined as:

$$\frac{\boldsymbol{p}^{int}-\boldsymbol{p}^{n}}{\Delta t}-\mathrm{DIV}\boldsymbol{P}^{n}-\boldsymbol{f}_{0}^{n}=\boldsymbol{0}; \tag{61a}$$

$$\frac{\boldsymbol{F}^{n+1}-\boldsymbol{F}^{n}}{\Delta t}-\boldsymbol{\nabla}_{0}\boldsymbol{v}^{n}=\boldsymbol{0}; \tag{61b}$$

$$\frac{\boldsymbol{H}^{n+1}-\boldsymbol{H}^{n}}{\Delta t}-\boldsymbol{F}^{n}\times\boldsymbol{\nabla}_{0}\boldsymbol{v}^{n}=\boldsymbol{0}; \tag{61c}$$

$$\frac{J^{int}-J^{n}}{\Delta t}-\boldsymbol{H}^{n}:\boldsymbol{\nabla}_{0}\boldsymbol{v}^{n}=0, \tag{61d}$$

and the corrector step

$$\frac{\boldsymbol{p}^{n+1}-\boldsymbol{p}^{int}}{\Delta t}-\mathrm{DIV}\left[\Delta p\boldsymbol{H}^{n}\right]=\boldsymbol{0}; \tag{62a}$$

$$\frac{J^{n+1}-J^{int}}{\Delta t}-\boldsymbol{H}^{n}:\boldsymbol{\nabla}_{0}\Delta\boldsymbol{v}=0. \tag{62b}$$

Here, the pressure and velocity increments are

$$\Delta p=p^{n+1}-p^{n};\qquad \Delta\boldsymbol{v}=\boldsymbol{v}^{n+1}-\boldsymbol{v}^{n}, \tag{63}$$

respectively. Observe that the summation of (61) and (62) recovers the original assumption that the pressure p and the velocity $\boldsymbol{v}$ used for the Jacobian (volumetric) evolution (61d) are computed implicitly in t^{n+1}, assuming the deformation gradient $\boldsymbol{F}$ and its cofactor $\boldsymbol{H}$ to be frozen at time t^{n} [2].

Application of the operator $\boldsymbol{H}^{n}:\boldsymbol{\nabla}_{0}(\cdot)$ to above expression (62a) gives:

$$\boldsymbol{H}^{n}:\boldsymbol{\nabla}_{0}\boldsymbol{v}^{n+1}-\boldsymbol{H}^{n}:\boldsymbol{\nabla}_{0}\boldsymbol{v}^{int}-\frac{\Delta t}{\rho_{0}}\boldsymbol{H}^{n}:\boldsymbol{\nabla}_{0}\left[\mathrm{DIV}\left(\Delta p\boldsymbol{H}^{n}\right)\right]=0. \tag{64}$$

For simplicity and without loss of generality, the material density ρ_0 has been assumed to be constant across the entire domain. To allow for the case of a nearly incompressible material, we can replace the first term on the left hand side of (64) by employing an appropriate volumetric constitutive law:

$$\boldsymbol{H}^{n}:\boldsymbol{\nabla}_{0}\boldsymbol{v}^{n+1}=\frac{1}{\kappa}\frac{\Delta p}{\Delta t}. \tag{65}$$

Using this relationship on the first term of (64), it yields

$$\frac{1}{\kappa}\frac{\Delta p}{\Delta t}-\boldsymbol{H}^{n}:\boldsymbol{\nabla}_{0}\boldsymbol{v}^{int}-\frac{\Delta t}{\rho_{0}}\boldsymbol{H}^{n}:\boldsymbol{\nabla}_{0}\left[\mathrm{DIV}\left(\Delta p\boldsymbol{H}^{n}\right)\right]=0. \tag{66}$$

For a truly incompressible material $\kappa = \infty$ and the right hand side of (65) vanishes resulting in the incompressibility constraint. Moreover, combining equations (61d), (62b) and (65), the Jacobian is constrained to be always a constant value, namely $J^{n+1} = J^n$, throughout the entire deformation process.

5.2.1. Variational fractional step conservation-based formulation

To obtain a single variational statement of the system (61), (62) and (66), we first define the residuals of these equations as:

$$\boldsymbol{\mathcal{R}}_{\mathcal{U}} = \begin{bmatrix} \boldsymbol{\mathcal{R}}_{\boldsymbol{p}^{int}} \\ \boldsymbol{\mathcal{R}}_{\boldsymbol{F}} \\ \boldsymbol{\mathcal{R}}_{\boldsymbol{H}} \\ \mathcal{R}_{J^{int}} \\ \mathcal{R}_{p} \\ \boldsymbol{\mathcal{R}}_{\boldsymbol{p}} \\ \mathcal{R}_{J} \end{bmatrix} = \begin{bmatrix} \mathrm{DIV}\boldsymbol{P}^n + \boldsymbol{f}_0^n - \frac{\left(\boldsymbol{p}^{int} - \boldsymbol{p}^n\right)}{\Delta t} \\ \boldsymbol{\nabla}_0 \boldsymbol{v}^n - \frac{\left(\boldsymbol{F}^{n+1} - \boldsymbol{F}^n\right)}{\Delta t} \\ \boldsymbol{F}^n \boldsymbol{\times} \boldsymbol{\nabla}_0 \boldsymbol{v}^n - \frac{\left(\boldsymbol{H}^{n+1} - \boldsymbol{H}^n\right)}{\Delta t} \\ \boldsymbol{H}^n : \boldsymbol{\nabla}_0 \boldsymbol{v}^n - \frac{\left(J^{int} - J^n\right)}{\Delta t} \\ \boldsymbol{H}^n : \boldsymbol{\nabla}_0 \boldsymbol{v}^{int} + \frac{\Delta t}{\rho_0} \boldsymbol{H}^n : \boldsymbol{\nabla}_0 \left[\mathrm{DIV}\left(\Delta p \boldsymbol{H}^n\right)\right] - \frac{1}{\kappa}\frac{\Delta p}{\Delta t} \\ \mathrm{DIV}\left[\Delta p \boldsymbol{H}^n\right] - \frac{\left(\boldsymbol{p}^{n+1} - \boldsymbol{p}^{int}\right)}{\Delta t} \\ \boldsymbol{H}^n : \boldsymbol{\nabla}_0 \Delta \boldsymbol{v} - \frac{\left(J^{n+1} - J^{int}\right)}{\Delta t} \end{bmatrix}. \tag{67}$$

Using appropriate stabilised conjugate virtual fields $\delta\boldsymbol{\mathcal{V}}^{st}$ defined in (48), the underlying weak statement is defined by:

$$0 = \int_V \left(\delta \boldsymbol{v}^{st} \cdot \boldsymbol{\mathcal{R}}_{\boldsymbol{p}^{int}} + \delta \boldsymbol{\Sigma}_{\boldsymbol{F}}^{st} : \boldsymbol{\mathcal{R}}_{\boldsymbol{F}} + \delta \boldsymbol{\Sigma}_{\boldsymbol{H}}^{st} : \boldsymbol{\mathcal{R}}_{\boldsymbol{H}} + \delta \Sigma_J^{st} (\mathcal{R}_p + \mathcal{R}_{J^{int}})\right) \, dV. \tag{68}$$

Following a similar finite element spatial discretisation as that presented in Section 5.1, where $\delta\boldsymbol{\mathcal{V}}^{st}$ and $\boldsymbol{\mathcal{U}}$ are expanded in terms of C_0 linear shape functions, the resulting predictor system satisfying involutions (5) in a weak

sense (as discussed in equations (60a) and (60b)) yields:

$$\sum_b M_{ab}\frac{(\boldsymbol{p}_b^{int}-\boldsymbol{p}_b^n)}{\Delta t}=\int_V N_a\boldsymbol{f}_0^n\,dV+\int_{\partial V}N_a\boldsymbol{t}_B^n\,dA-\int_V\boldsymbol{P}^{st}\boldsymbol{\nabla}_0N_a\,dV; \tag{69a}$$

$$\sum_b M_{ab}\frac{(\boldsymbol{F}_b^{n+1}-\boldsymbol{F}_b^n)}{\Delta t}=-\int_V\frac{1}{\rho_0}\boldsymbol{p}^n\otimes\boldsymbol{\nabla}_0N_a\,dV+\int_{\partial V}N_a\left(\boldsymbol{v}_B\otimes\boldsymbol{N}\right)\,dA; \tag{69b}$$

$$\sum_b M_{ab}\frac{(\boldsymbol{H}_b^{n+1}-\boldsymbol{H}_b^n)}{\Delta t}=\int_V\frac{1}{\rho_0}\boldsymbol{p}^n\times\boldsymbol{F}^n\times\boldsymbol{\nabla}_0N_a\,dV-\int_{\partial V}N_a\left(\boldsymbol{v}_B\times\boldsymbol{F}^n\times\boldsymbol{N}\right)\,dA; \tag{69c}$$

$$\sum_b M_{ab}\frac{(J_b^{int}-J_b^n)}{\Delta t}=-\int_V\frac{1}{\rho_0}\boldsymbol{p}^{st}\cdot\boldsymbol{H}^n\boldsymbol{\nabla}_0N_a\,dV+\int_{\partial V}N_a(\boldsymbol{v}_B\cdot\boldsymbol{H}^n\boldsymbol{N})dA, \tag{69d}$$

where $\boldsymbol{p}^{st}=\boldsymbol{p}+\tau_{\boldsymbol{p}}\boldsymbol{\mathcal{R}}_{\boldsymbol{p}^{int}}$. By setting $\tau_{\boldsymbol{p}}=0$, the above formulation can then be solved in a sequential manner. Equations (69b), (69c) and (69d) are first solved to obtain $\boldsymbol{F}^{n+1}$, $\boldsymbol{H}^{n+1}$ and J^{int}, which can then be substituted into (69a) to deduce $\boldsymbol{p}^{int}$.

Moreover, from expression (68), the corrector step of this two-stage fractional step algorithm is formulated as:

$$\sum_b\left[M_{ab}^{vol}+\frac{\Delta t^2}{\rho_0}\mathcal{K}_{ab}\right]\left(\frac{\Delta p}{\Delta t}\right)=\int_{\partial V}N_a\boldsymbol{v}^B\cdot\boldsymbol{H}^n\boldsymbol{N}\,dA-\int_V\frac{\boldsymbol{p}^{st}}{\rho_0}\cdot\left(\boldsymbol{H}^n\boldsymbol{\nabla}_0N_a\right)\,dV, \tag{70}$$

where the mass matrix contribution M_{ab}^{vol}, the viscosity matrix contribution $\mathcal{K}_{ab}$ and the stabilised linear momentum $\boldsymbol{p}^{st}$ are defined as

$$M_{ab}^{vol}:=\int_V\frac{1}{\kappa}N_aN_b\,dV; \tag{71a}$$

$$\mathcal{K}_{ab}:=\int_V\left(\boldsymbol{H}^n\boldsymbol{\nabla}_0N_a\right)\cdot\left(\boldsymbol{H}^n\boldsymbol{\nabla}_0N_b\right)\,dV; \tag{71b}$$

$$\boldsymbol{p}^{st}:=\boldsymbol{p}^{int}+\tau_{\boldsymbol{p}}\boldsymbol{\mathcal{R}}_{\boldsymbol{p}^{int}}, \tag{71c}$$

respectively.

It is now possible to update the linear momentum and Jacobian of the deformation via a standard Bubnov-Galerkin formulation, together with the

use of the incompressibility constraint (65), to give

$$\sum_b M_{ab}\frac{\left(\boldsymbol{p}_b^{n+1}-\boldsymbol{p}_b^{int}\right)}{\Delta t}=\int_V N_a\mathrm{DIV}(\Delta p\boldsymbol{H}^n)\,dV; \tag{72a}$$

$$\sum_b M_{ab}\frac{\left(J^{n+1}-J^{int}\right)}{\Delta t}=\int_V\left(\frac{N_a}{\kappa}\frac{\Delta p}{\Delta t}-N_a\boldsymbol{H}^n:\boldsymbol{\nabla}_0\boldsymbol{v}^n\right)dV. \tag{72b}$$

As mentioned at the end of Section 5.1, the algorithm is finally evolved in time via a Total Variation Diminishing Runge-Kutta time integrator with a time step limit controlled, in this case, by the shear wave speed c_s (47).

6. Petrov-Galerkin (PG) entropy-based variational formulation

Taking advantage of the properties of polyconvexity (see Section 3), this section introduces two new variationally consistent PG computational frameworks for the entropy-based systems defined above. Specifically, a nearly incompressible $\boldsymbol{v}$-$\boldsymbol{\Sigma_F}$-$\boldsymbol{\Sigma_H}$-$\hat{\Sigma}_J$-p entropy formulation and its compressible $\boldsymbol{v}$-$\boldsymbol{\Sigma_F}$-$\boldsymbol{\Sigma_H}$-Σ_J counterpart (Section 6.1). In addition, as these explicit schemes can be computationally expensive in the case of large values of the bulk modulus, a tailor-made fractional step PG algorithm is also presented (Section 6.2).

6.1. Nearly incompressible $\boldsymbol{v}$-$\boldsymbol{\Sigma_F}$-$\boldsymbol{\Sigma_H}$-$\hat{\Sigma}_J$-p entropy formulation

As stated above, the standard Bubnov-Galerkin variational formulation requires extra numerical stabilisation, which can be introduced by means of a Petrov-Galerkin approach [54], whereby the conjugate weighting functions $\delta\boldsymbol{\mathcal{U}}$ are augmented as $\delta\boldsymbol{\mathcal{U}}^{st}=\delta\boldsymbol{\mathcal{U}}+\boldsymbol{\tau}\boldsymbol{\mathcal{A}}_I\frac{\partial\delta\boldsymbol{\mathcal{U}}}{\partial X_I}$. In the case of a diagonal stabilisation matrix $\boldsymbol{\tau}$, the individual components of $\delta\boldsymbol{\mathcal{U}}^{st}$ are easily obtained with the help of equations (3) and (5), to give:

$$\delta\boldsymbol{p}^{st}=\delta\boldsymbol{p}-\tau_{\boldsymbol{v}}\left([\boldsymbol{\mathcal{C}}_{\boldsymbol{F}}]_I:\frac{\partial\delta\boldsymbol{F}}{\partial X_I}+[\boldsymbol{\mathcal{C}}_{\boldsymbol{H}}]_I:\frac{\partial\delta\boldsymbol{H}}{\partial X_I}+(\hat{\boldsymbol{\mathcal{C}}}_J+\kappa\boldsymbol{H}_{\boldsymbol{\Sigma}})\boldsymbol{\nabla}_0\delta J\right); \tag{73a}$$

$$\delta\boldsymbol{F}^{st}=\delta\boldsymbol{F}-\frac{\tau_{\boldsymbol{F}}}{\rho_0}\left(\boldsymbol{\nabla}_0\delta\boldsymbol{p}\right); \tag{73b}$$

$$\delta\boldsymbol{H}^{st}=\delta\boldsymbol{H}-\frac{\tau_{\boldsymbol{H}}}{\rho_0}\left(\boldsymbol{F}_{\boldsymbol{\Sigma}}\boldsymbol{\times}\boldsymbol{\nabla}_0\delta\boldsymbol{p}\right); \tag{73c}$$

$$\delta J^{st}=\delta J-\frac{\tau_J}{\rho_0}\left(\boldsymbol{H}_{\boldsymbol{\Sigma}}:\boldsymbol{\nabla}_0\delta\boldsymbol{p}\right), \tag{73d}$$

where

$$[\boldsymbol{\mathcal{C}}_{\boldsymbol{F}}]_I := \frac{\partial\left(\boldsymbol{P}\boldsymbol{E}_I\right)}{\partial \boldsymbol{F}}; \quad [\boldsymbol{\mathcal{C}}_{\boldsymbol{H}}]_I := \frac{\partial\left(\boldsymbol{P}\boldsymbol{E}_I\right)}{\partial \boldsymbol{H}}; \quad \hat{\boldsymbol{\mathcal{C}}}_J := \frac{\partial \hat{\boldsymbol{P}}}{\partial J}. \tag{74}$$

Observe that $\tau_{\boldsymbol{v}}$, $\tau_{\boldsymbol{F}}$, $\tau_{\boldsymbol{H}}$ and τ_J are appropriate numerical stabilisation parameters. Their units are those of time and are usually chosen as a fraction of the time step for explicit integration schemes [32, 54]. Moreover, the residual $\boldsymbol{\mathcal{R}}_{\boldsymbol{\mathcal{V}}}$ of the entropy system (30), (33a,b) and (34) can be expressed as:

$$\boldsymbol{\mathcal{R}}_{\boldsymbol{\mathcal{V}}} = \begin{bmatrix} \boldsymbol{\mathcal{R}}_{\boldsymbol{v}} \\ \boldsymbol{\mathcal{R}}_{\boldsymbol{\Sigma}_{\boldsymbol{F}}} \\ \boldsymbol{\mathcal{R}}_{\boldsymbol{\Sigma}_{\boldsymbol{H}}} \\ \mathcal{R}_{\hat{\Sigma}_J} \\ \mathcal{R}_p \end{bmatrix} = \begin{bmatrix} \frac{1}{\rho_0}\mathrm{DIV}\boldsymbol{P} + \frac{1}{\rho_0}\boldsymbol{f}_0 - \dot{\boldsymbol{v}} \\ (W_{\boldsymbol{F}\boldsymbol{F}} + W_{\boldsymbol{F}J} \otimes \boldsymbol{H}_{\boldsymbol{\Sigma}}) : \boldsymbol{\nabla}_0 \boldsymbol{v} - \dot{\boldsymbol{\Sigma}}_{\boldsymbol{F}} \\ (W_{\boldsymbol{H}\boldsymbol{H}} \times \boldsymbol{F}_{\boldsymbol{\Sigma}} + W_{\boldsymbol{H}J} \otimes \boldsymbol{H}_{\boldsymbol{\Sigma}}) : \boldsymbol{\nabla}_0 \boldsymbol{v} - \dot{\boldsymbol{\Sigma}}_{\boldsymbol{H}} \\ (W_{J\boldsymbol{F}} + W_{J\boldsymbol{H}} \times \boldsymbol{F}_{\boldsymbol{\Sigma}} + \gamma \boldsymbol{H}_{\boldsymbol{\Sigma}}) : \boldsymbol{\nabla}_0 \boldsymbol{v} - \dot{\hat{\Sigma}}_J \\ \kappa\left(\boldsymbol{H}_{\boldsymbol{\Sigma}} : \boldsymbol{\nabla}_0 \boldsymbol{v}\right) - \dot{p} \end{bmatrix}. \tag{75}$$

It is now possible to derive a stabilised weak form for the entropy formulation by multiplying the conjugate virtual fields $\delta \boldsymbol{\mathcal{U}}^{st}$ (73) with the corresponding residuals $\boldsymbol{\mathcal{R}}_{\boldsymbol{\mathcal{V}}}$ (75) and integrating over the material volume V, to give

$$0 = \int_V \left(\delta \boldsymbol{p}^{st} \cdot \boldsymbol{\mathcal{R}}_{\boldsymbol{v}} + \delta \boldsymbol{F}^{st} : \boldsymbol{\mathcal{R}}_{\boldsymbol{\Sigma}_{\boldsymbol{F}}} + \delta \boldsymbol{H}^{st} : \boldsymbol{\mathcal{R}}_{\boldsymbol{\Sigma}_{\boldsymbol{H}}} + \delta J^{st}\left(\mathcal{R}_{\hat{\Sigma}_J} + \mathcal{R}_p\right)\right) dV. \tag{76}$$

Following a similar C_0 linear finite element spatial discretisation strategy as that presented in previous Section 5, the velocity evolution at each node a is given as:

$$\sum_b M_{ab} \dot{\boldsymbol{v}}_b = \int_V \frac{N_a}{\rho_0} \boldsymbol{f}_0 \, dV + \int_{\partial V} \frac{N_a}{\rho_0} \boldsymbol{t}_B \, dA - \int_V \frac{1}{\rho_0} \boldsymbol{P}^{st} \boldsymbol{\nabla}_0 N_a \, dV, \tag{77}$$

where the stabilised first Piola-Kirchhoff stress $\boldsymbol{P}^{st}$ has already been defined in (53). For the evaluation of (53), $\boldsymbol{F}$ and $\boldsymbol{H}$ are obtained by using reversed constitutive laws, namely, $\boldsymbol{F}$ is evaluated as $\boldsymbol{F}_{\boldsymbol{\Sigma}}$ and $\boldsymbol{H}$ is evaluated as $\boldsymbol{H}_{\boldsymbol{\Sigma}}$.

In addition, the deviatoric stabilised stresses $\{\boldsymbol{\Sigma}_{\boldsymbol{F}}^{st}, \boldsymbol{\Sigma}_{\boldsymbol{H}}^{st}, \hat{\Sigma}_J^{st}\}$ are formulated as

$$\boldsymbol{\Sigma}_{\boldsymbol{F}}^{st} = \boldsymbol{\Sigma}_{\boldsymbol{F}} + \tau_{\boldsymbol{F}} \boldsymbol{\mathcal{R}}_{\boldsymbol{\Sigma}_{\boldsymbol{F}}}; \quad \boldsymbol{\Sigma}_{\boldsymbol{H}}^{st} = \boldsymbol{\Sigma}_{\boldsymbol{H}} + \tau_{\boldsymbol{H}} \boldsymbol{\mathcal{R}}_{\boldsymbol{\Sigma}_{\boldsymbol{H}}}; \quad \hat{\Sigma}_J^{st} = \hat{\Sigma}_J + \tau_J \mathcal{R}_{\hat{\Sigma}_J}, \tag{78}$$

and the stabilised pressure as

$$p^{st} = p + \tau_p \mathcal{R}_p. \tag{79}$$

As in the conservation-based system approach reported in the previous Section, the traction at the boundary $\boldsymbol{t}_B$ in (77) can be directly obtained from prescribed boundary conditions.

For consistency with the stabilised stresses presented in (58), the time integrated geometric equivalent stabilisations can be incorporated with the use of a Taylor series expansion for the linear approximation of the relevant stabilised variables:

$$\boldsymbol{\Sigma}_{\boldsymbol{F}}^{st} = \boldsymbol{\Sigma}_{\boldsymbol{F}} + \tau_{\boldsymbol{F}} \boldsymbol{\mathcal{R}}_{\boldsymbol{\Sigma}_{\boldsymbol{F}}} + \zeta_{\boldsymbol{F}} (W_{\boldsymbol{FF}} : \boldsymbol{\mathcal{R}}_{\boldsymbol{F}}^{\boldsymbol{x}}); \tag{80a}$$

$$\boldsymbol{\Sigma}_{\boldsymbol{H}}^{st} = \boldsymbol{\Sigma}_{\boldsymbol{H}} + \tau_{\boldsymbol{H}} \boldsymbol{\mathcal{R}}_{\boldsymbol{\Sigma}_{\boldsymbol{H}}} + \zeta_{\boldsymbol{H}} (W_{\boldsymbol{HH}} : \boldsymbol{\mathcal{R}}_{\boldsymbol{H}}^{\boldsymbol{x}}); \tag{80b}$$

$$\hat{\Sigma}_J^{st} = \hat{\Sigma}_J + \tau_J \mathcal{R}_{\hat{\Sigma}_J} + \zeta_J (\gamma \mathcal{R}_J^{\boldsymbol{x}}); \tag{80c}$$

$$p^{st} = p + \tau_p \mathcal{R}_p + \mu \zeta_p \mathcal{R}_p^{\boldsymbol{x}}; \quad \mathcal{R}_p^{\boldsymbol{x}} = J_{\boldsymbol{x}} - 1 - \frac{p}{\kappa}. \tag{80d}$$

Here, $\zeta_{\boldsymbol{F}}$, $\zeta_{\boldsymbol{H}}$, ζ_J and ζ_p are dimensionless stabilisation parameters. In addition, $\{\boldsymbol{\mathcal{R}}_{\boldsymbol{F}}^{\boldsymbol{x}}, \boldsymbol{\mathcal{R}}_{\boldsymbol{H}}^{\boldsymbol{x}}, \mathcal{R}_J^{\boldsymbol{x}}\}$ are the time integrated geometric residuals already defined in (57) and $\{W_{\boldsymbol{FF}}, W_{\boldsymbol{HH}}, \gamma\}$ are components of the Hessian operator already presented in (22) and (23). The inclusion of the material parameter μ in $\mathcal{R}_p^{\boldsymbol{x}}$ ensures the consistency of the physical units.

Finally, introducing the C_0 linear interpolation for the stress variables and their conjugate strains gives a full set of equations for the nodal stress values:

$$\sum_b M_{ab} \dot{\boldsymbol{\Sigma}}_{\boldsymbol{F}}^b = \int_V N_a \left(W_{\boldsymbol{FF}} + W_{\boldsymbol{F}J} \otimes \boldsymbol{H}_{\boldsymbol{\Sigma}} \right) : \boldsymbol{\nabla}_0 \boldsymbol{v} \, dV; \tag{81a}$$

$$\sum_b M_{ab} \dot{\boldsymbol{\Sigma}}_{\boldsymbol{H}}^b = \int_V N_a \left(W_{\boldsymbol{HH}} \boldsymbol{\times} \boldsymbol{F}_{\boldsymbol{\Sigma}} + W_{\boldsymbol{H}J} \otimes \boldsymbol{H}_{\boldsymbol{\Sigma}} \right) : \boldsymbol{\nabla}_0 \boldsymbol{v} \, dV; \tag{81b}$$

$$\sum_b M_{ab} \dot{\hat{\Sigma}}_J^b = \int_V N_a \left(W_{J\boldsymbol{F}} + W_{J\boldsymbol{H}} \boldsymbol{\times} \boldsymbol{F}_{\boldsymbol{\Sigma}} + \gamma \boldsymbol{H}_{\boldsymbol{\Sigma}} \right) : \boldsymbol{\nabla}_0 \boldsymbol{v} \, dV; \tag{81c}$$

$$\sum_b M_{ab} \dot{p}^b = \int_{\partial V} N_a \, \kappa \, \boldsymbol{v}_B \cdot (\boldsymbol{H}_{\boldsymbol{\Sigma}} \boldsymbol{N}) \, dA - \int_V \kappa \, \boldsymbol{v}^{st} \cdot (\boldsymbol{H}_{\boldsymbol{\Sigma}} \boldsymbol{\nabla}_0 N_a) \, dV, \tag{81d}$$

where the stabilised velocity $\boldsymbol{v}^{st} = \boldsymbol{v} + \tau_{\boldsymbol{v}} \boldsymbol{\mathcal{R}}_{\boldsymbol{v}}$. As discussed in Section 5, to ensure the satisfaction of the involutions described by equation (5), stabilisation is only included for the velocity field used in the stress update (81d). Equations (77) and (81) represent a stabilised system of differential equations in time for the entropy variables $\{\boldsymbol{v}, \boldsymbol{\Sigma}_{\boldsymbol{F}}, \boldsymbol{\Sigma}_{\boldsymbol{H}}, \hat{\Sigma}_J, p\}$.

To derive a complete explicit scheme, we set $\tau_p = 0$ (80d) and choose appropriate non-dimensional values of $\{\zeta_{\boldsymbol{F}}, \zeta_{\boldsymbol{H}}, \zeta_J, \zeta_p\}$ in (77), typically in the range of $[0, 0.5]$. In practice, it is crucial to establish a computational framework with the minimum number of stabilisation parameters. For this reason, we collapse three stabilisation parameters appearing in (78) into a single parameter $\tau_{\boldsymbol{F}} = \tau_{\boldsymbol{H}} = \tau_J = \tau$, and set $\zeta_{\boldsymbol{F}} = \zeta_{\boldsymbol{H}} = \zeta$ and $\zeta_J = \zeta_p$, reducing the number of stabilisation parameters to $\{\tau, \tau_{\boldsymbol{v}}, \zeta, \zeta_J\}$.

The entropy-based system for a compressible material can also be obtained as a degenerate case of the above system (77)-(81), in terms of the reduced set of unknowns $\boldsymbol{v}$-$\boldsymbol{\Sigma}_{\boldsymbol{F}}$-$\boldsymbol{\Sigma}_{\boldsymbol{H}}$-$\Sigma_J$. This formulation is the conjugate version of that presented by the authors in [1] and included here for the sake of completeness. Indeed, following a similar C_0 linear finite element spatial discretisation procedure for the entropy variables $\boldsymbol{\mathcal{V}}$ and their conjugates $\delta\boldsymbol{\mathcal{U}}$, the time rate of a full stabilised compressible entropy system (see Section 4.1) can be written as:

$$\sum_b M_{ab} \dot{\boldsymbol{v}}_b = \int_V \frac{N_a}{\rho_0} \boldsymbol{f}_0 \, dV + \int_{\partial V} \frac{N_a}{\rho_0} \boldsymbol{t}_B \, dA - \int_V \frac{1}{\rho_0} \boldsymbol{P}^{st} \boldsymbol{\nabla}_0 N_a \, dV; \tag{82a}$$

$$\sum_b M_{ab} \dot{\boldsymbol{\Sigma}}^b_{\boldsymbol{F}} = \int_V N_a (2\alpha \boldsymbol{\nabla}_0 \boldsymbol{v}) \, dV; \tag{82b}$$

$$\sum_b M_{ab} \dot{\boldsymbol{\Sigma}}^b_{\boldsymbol{H}} = \int_V N_a (2\beta \boldsymbol{F}_{\boldsymbol{\Sigma}} \boldsymbol{\times} \boldsymbol{\nabla}_0 \boldsymbol{v}) \, dV; \tag{82c}$$

$$\sum_b M_{ab} \dot{\Sigma}^b_J = \int_V N_a \chi \boldsymbol{H}_{\boldsymbol{\Sigma}} : \boldsymbol{\nabla}_0 \boldsymbol{v} \, dV - \int_V \chi \boldsymbol{H}_{\boldsymbol{\Sigma}} \boldsymbol{\nabla}_0 N_a \cdot \tau_{\boldsymbol{p}} \boldsymbol{\mathcal{R}}_{\boldsymbol{v}} \, dV, \tag{82d}$$

with $\chi = \lambda + 2\alpha J_{\boldsymbol{\Sigma}}^{-2}$ already defined in Section 4.1.

As mentioned at the end of Section 5.1, the algorithm is finally evolved in time via a Total Variation Diminishing Runge-Kutta time integrator with a time step limit controlled, in this case, by the volumetric wave speed (42).

6.2. Truly incompressible $\boldsymbol{v}$-$\boldsymbol{\Sigma_F}$-$\boldsymbol{\Sigma_H}$-$\hat{\Sigma}_J$-p entropy formulation: Fractional step approach

The explicit $\boldsymbol{v}$-$\boldsymbol{\Sigma_F}$-$\boldsymbol{\Sigma_H}$-$\hat{\Sigma}_J$-p PG formulation presented above is not computationally suitable to simulate nearly (or truly) incompressible materials, as the volumetric wave speed can be significantly high. In these situations, it is preferred to resolve the incompressibility constraint in an implicit manner. In this section, we present an adapted fractional step method tailor-made to deal with truly incompressible materials.

The time update of the set of entropy variables from $\boldsymbol{\mathcal{V}}^n$ to $\boldsymbol{\mathcal{V}}^{n+1}$ over a time step Δt is split in two stages, with the pressure field p and the velocity field $\boldsymbol{v}$ solved implicitly at time t^{n+1}. Firstly, the algorithm is advanced explicitly yielding an intermediate set of entropy variables $\boldsymbol{\mathcal{V}}^{int}$, which is then projected after implicitly solving a Poisson-like equation [2] for the pressure increment.

Thus, the first (predictor or intermediate) step of the two-stage fractional step algorithm is defined as

$$\frac{\boldsymbol{v}^{int}-\boldsymbol{v}^n}{\Delta t}-\frac{1}{\rho_0}\mathrm{DIV}\boldsymbol{P}^n-\frac{1}{\rho_0}\boldsymbol{f}_0^n=\boldsymbol{0}; \tag{83a}$$

$$\frac{\boldsymbol{\Sigma}_{\boldsymbol{F}}^{int}-\boldsymbol{\Sigma}_{\boldsymbol{F}}^n}{\Delta t}-(W_{\boldsymbol{FF}}^n+W_{\boldsymbol{F}J}^n\otimes\boldsymbol{H}_{\boldsymbol{\Sigma}}^n):\boldsymbol{\nabla}_0\boldsymbol{v}^n=\boldsymbol{0}; \tag{83b}$$

$$\frac{\boldsymbol{\Sigma}_{\boldsymbol{H}}^{int}-\boldsymbol{\Sigma}_{\boldsymbol{H}}^n}{\Delta t}-(W_{\boldsymbol{HH}}^n\boldsymbol{\times}\boldsymbol{F}_{\boldsymbol{\Sigma}}^n+W_{\boldsymbol{H}J}^n\otimes\boldsymbol{H}_{\boldsymbol{\Sigma}}^n):\boldsymbol{\nabla}_0\boldsymbol{v}^n=\boldsymbol{0}; \tag{83c}$$

$$\frac{\hat{\Sigma}_J^{int}-\hat{\Sigma}_J^n}{\Delta t}-(W_{J\boldsymbol{F}}^n+W_{J\boldsymbol{H}}^n\boldsymbol{\times}\boldsymbol{F}_{\boldsymbol{\Sigma}}^n+\gamma^n\boldsymbol{H}_{\boldsymbol{\Sigma}}^n):\boldsymbol{\nabla}_0\boldsymbol{v}^n=0, \tag{83d}$$

and the second (corrector) step:

$$\frac{\boldsymbol{v}^{n+1}-\boldsymbol{v}^{int}}{\Delta t}-\frac{1}{\rho_0}\mathrm{DIV}\left[\Delta p\boldsymbol{H}_{\boldsymbol{\Sigma}}^n\right]=\boldsymbol{0}; \tag{84a}$$

$$\frac{\boldsymbol{\Sigma}_{\boldsymbol{F}}^{n+1}-\boldsymbol{\Sigma}_{\boldsymbol{F}}^{int}}{\Delta t}-W_{\boldsymbol{F}J}^n\left[\boldsymbol{H}_{\boldsymbol{\Sigma}}^n:\boldsymbol{\nabla}_0\Delta\boldsymbol{v}\right]=\boldsymbol{0}; \tag{84b}$$

$$\frac{\boldsymbol{\Sigma}_{\boldsymbol{H}}^{n+1}-\boldsymbol{\Sigma}_{\boldsymbol{H}}^{int}}{\Delta t}-W_{\boldsymbol{H}J}^n\left[\boldsymbol{H}_{\boldsymbol{\Sigma}}^n:\boldsymbol{\nabla}_0\Delta\boldsymbol{v}\right]=\boldsymbol{0}; \tag{84c}$$

$$\frac{\hat{\Sigma}_J^{n+1}-\hat{\Sigma}_J^{int}}{\Delta t}-(W_{J\boldsymbol{F}}^n+W_{J\boldsymbol{H}}^n\boldsymbol{\times}\boldsymbol{F}_{\boldsymbol{\Sigma}}^n+\gamma^n\boldsymbol{H}_{\boldsymbol{\Sigma}}^n):\boldsymbol{\nabla}_0\Delta\boldsymbol{v}=0. \tag{84d}$$

Here, the pressure and velocity increments are defined as in (63). Notice that the deformation gradient $\boldsymbol{F}_{\boldsymbol{\Sigma}}$ and its cofactor $\boldsymbol{H}_{\boldsymbol{\Sigma}}$ are frozen at time t^n [2] to reduce the implicitness of the formulation.

Application of the operator $\boldsymbol{H}^n_{\boldsymbol{\Sigma}} : \boldsymbol{\nabla}_0(\cdot)$ to above equation (84a) and the use of (65) gives the exact same expression for the Poisson-like equation (66), but this time replacing $\boldsymbol{H}^n$ with $\boldsymbol{H}^n_{\boldsymbol{\Sigma}}$:

$$\frac{1}{\kappa}\frac{\Delta p}{\Delta t} - \boldsymbol{H}^n_{\boldsymbol{\Sigma}} : \boldsymbol{\nabla}_0 \boldsymbol{v}^{int} - \frac{\Delta t}{\rho_0}\boldsymbol{H}^n_{\boldsymbol{\Sigma}} : \boldsymbol{\nabla}_0 \left[\mathrm{DIV}\left(\Delta p \boldsymbol{H}^n_{\boldsymbol{\Sigma}}\right)\right] = 0. \tag{85}$$

6.2.1. Variational nonlinear fractional step entropy formulation

The residual $\boldsymbol{\mathcal{R}}_{\boldsymbol{\mathcal{V}}}$ of each time-discrete expressions, namely (83), (84) and (66), can be expressed as:

$$\boldsymbol{\mathcal{R}}_{\boldsymbol{\mathcal{V}}} = \begin{bmatrix} \boldsymbol{\mathcal{R}}_{\boldsymbol{v}^{int}} \\ \boldsymbol{\mathcal{R}}_{\boldsymbol{\Sigma}^{int}_{\boldsymbol{F}}} \\ \boldsymbol{\mathcal{R}}_{\boldsymbol{\Sigma}^{int}_{\boldsymbol{H}}} \\ \mathcal{R}_{\hat{\Sigma}^{int}_J} \\ \mathcal{R}_p \\ \boldsymbol{\mathcal{R}}_{\boldsymbol{v}} \\ \boldsymbol{\mathcal{R}}_{\boldsymbol{\Sigma}_{\boldsymbol{F}}} \\ \boldsymbol{\mathcal{R}}_{\boldsymbol{\Sigma}_{\boldsymbol{H}}} \\ \mathcal{R}_{\hat{\Sigma}_J} \end{bmatrix} = \begin{bmatrix} \frac{1}{\rho_0}\mathrm{DIV}\boldsymbol{P}^n + \frac{1}{\rho_0}\boldsymbol{f}^n_0 - \frac{\left(\boldsymbol{v}^{int} - \boldsymbol{v}^n\right)}{\Delta t} \\ (W^n_{\boldsymbol{FF}} + W^n_{\boldsymbol{FJ}} \otimes \boldsymbol{H}^n_{\boldsymbol{\Sigma}}) : \boldsymbol{\nabla}_0 \boldsymbol{v}^n - \frac{\left(\boldsymbol{\Sigma}^{int}_{\boldsymbol{F}} - \boldsymbol{\Sigma}^n_{\boldsymbol{F}}\right)}{\Delta t} \\ (W^n_{\boldsymbol{HH}} \boldsymbol{\times} \boldsymbol{F}^n_{\boldsymbol{\Sigma}} + W^n_{\boldsymbol{HJ}} \otimes \boldsymbol{H}^n_{\boldsymbol{\Sigma}}) : \boldsymbol{\nabla}_0 \boldsymbol{v}^n - \frac{\left(\boldsymbol{\Sigma}^{int}_{\boldsymbol{H}} - \boldsymbol{\Sigma}^n_{\boldsymbol{H}}\right)}{\Delta t} \\ (W^n_{\boldsymbol{JF}} + W^n_{\boldsymbol{JH}} \boldsymbol{\times} \boldsymbol{F}^n_{\boldsymbol{\Sigma}} + \gamma \boldsymbol{H}^n_{\boldsymbol{\Sigma}}) : \boldsymbol{\nabla}_0 \boldsymbol{v}^n - \frac{\left(\hat{\Sigma}^{int}_J - \hat{\Sigma}^n_J\right)}{\Delta t} \\ \mu \boldsymbol{H}^n_{\boldsymbol{\Sigma}} : \boldsymbol{\nabla}_0 \boldsymbol{v}^{int} + \frac{\mu \Delta t}{\rho_0}\boldsymbol{H}^n_{\boldsymbol{\Sigma}} : \boldsymbol{\nabla}_0 \left[\mathrm{DIV}\left(\Delta p \boldsymbol{H}^n_{\boldsymbol{\Sigma}}\right)\right] - \frac{\mu}{\kappa}\frac{\Delta p}{\Delta t} \\ \frac{1}{\rho_0}\mathrm{DIV}\left[\Delta p \boldsymbol{H}^n_{\boldsymbol{\Sigma}}\right] - \frac{\left(\boldsymbol{v}^{n+1} - \boldsymbol{v}^{int}\right)}{\Delta t} \\ W^n_{\boldsymbol{FJ}}\left[\boldsymbol{H}^n_{\boldsymbol{\Sigma}} : \boldsymbol{\nabla}_0 \Delta \boldsymbol{v}\right] - \frac{\left(\boldsymbol{\Sigma}^{n+1}_{\boldsymbol{F}} - \boldsymbol{\Sigma}^{int}_{\boldsymbol{F}}\right)}{\Delta t} \\ W^n_{\boldsymbol{HJ}}\left[\boldsymbol{H}^n_{\boldsymbol{\Sigma}} : \boldsymbol{\nabla}_0 \Delta \boldsymbol{v}\right] - \frac{\left(\boldsymbol{\Sigma}^{n+1}_{\boldsymbol{H}} - \boldsymbol{\Sigma}^{int}_{\boldsymbol{H}}\right)}{\Delta t} \\ (W^n_{\boldsymbol{JF}} + W^n_{\boldsymbol{JH}} \boldsymbol{\times} \boldsymbol{F}^n_{\boldsymbol{\Sigma}} + \gamma^n \boldsymbol{H}^n_{\boldsymbol{\Sigma}}) : \boldsymbol{\nabla}_0 \Delta \boldsymbol{v} - \frac{\left(\hat{\Sigma}^{n+1}_J - \hat{\Sigma}^{int}_J\right)}{\Delta t} \end{bmatrix}. \tag{86}$$

Using appropriate stabilised conjugate virtual fields $\delta \boldsymbol{\mathcal{U}}^{st}$ already defined in (73a-73d), the stabilised variational statements for predictor step and pressure correction can be obtained. Following a similar finite element spatial

discretisation as that presented in Section 6 (where $\boldsymbol{\mathcal{V}}$ and $\delta\boldsymbol{\mathcal{U}}$ are expanded in terms of C_0 linear shape functions) and grouping the expression according to each virtual conjugate variable, the resulting predictor system of equations yields

$$\sum_b M_{ab}\frac{(\boldsymbol{v}_b^{int}-\boldsymbol{v}_b^n)}{\Delta t} = \int_{\partial V}\frac{N_a}{\rho_0}\boldsymbol{t}_B^n\,dA + \int_V \frac{N_a}{\rho_0}\boldsymbol{f}_0^n\,dV - \int_V \frac{\boldsymbol{P}^{st}}{\rho_0}\boldsymbol{\nabla}_0 N_a\,dV; \tag{87a}$$

$$\sum_b M_{ab}\frac{\left(\boldsymbol{\Sigma}_{\boldsymbol{F}}^{b,int}-\boldsymbol{\Sigma}_{\boldsymbol{F}}^{b,n}\right)}{\Delta t} = \int_V N_a\left[W_{\boldsymbol{FF}}^n + W_{\boldsymbol{F}J}^n\otimes\boldsymbol{H}_{\boldsymbol{\Sigma}}^n\right]:\boldsymbol{\nabla}_0\boldsymbol{v}^n\,dV; \tag{87b}$$

$$\sum_b M_{ab}\frac{\left(\boldsymbol{\Sigma}_{\boldsymbol{H}}^{b,int}-\boldsymbol{\Sigma}_{\boldsymbol{H}}^{b,n}\right)}{\Delta t} = \int_V N_a\left[W_{\boldsymbol{HH}}^n\times\boldsymbol{F}_{\boldsymbol{\Sigma}}^n + W_{\boldsymbol{H}J}^n\otimes\boldsymbol{H}_{\boldsymbol{\Sigma}}^n\right]:\boldsymbol{\nabla}_0\boldsymbol{v}^n\,dV; \tag{87c}$$

$$\sum_b M_{ab}\frac{\left(\hat{\Sigma}_J^{b,int}-\hat{\Sigma}_J^{b,n}\right)}{\Delta t} = \int_V N_a\left[W_{J\boldsymbol{F}}^n + W_{J\boldsymbol{H}}^n\times\boldsymbol{F}_{\boldsymbol{\Sigma}}^n + \gamma^n\boldsymbol{H}_{\boldsymbol{\Sigma}}^n\right]:\boldsymbol{\nabla}_0\boldsymbol{v}^n\,dV. \tag{87d}$$

Here, the stabilised first Piola-Kirchhoff stress tensor and the correspoding time rate and time integrated stabilisations have already been defined in (80) and (57). As in Section 5.2.1, the pressure correction renders a similar expression to (70) and (71), but replacing $\boldsymbol{H}^n$ with $\boldsymbol{H}_{\boldsymbol{\Sigma}}^n$, namely:

$$\sum_b\left[M_{ab}^{vol}+\frac{\Delta t^2}{\rho_0}\mathcal{K}_{ab}\right]\left(\frac{\Delta p}{\Delta t}\right) = \int_{\partial V} N_a\boldsymbol{v}^B\cdot\boldsymbol{H}_{\boldsymbol{\Sigma}}^n\boldsymbol{N}\,dA - \int_V \boldsymbol{v}^{st}\cdot(\boldsymbol{H}_{\boldsymbol{\Sigma}}^n\boldsymbol{\nabla}_0 N_a)\,dV. \tag{88}$$

The mass matrix contribution M_{ab}^{vol}, the viscosity matrix contribution $\mathcal{K}_{ab}$ and the stabilised velocity $\boldsymbol{v}^{st}$ are defined as

$$M_{ab}^{vol} := \int_V \frac{1}{\kappa}N_a N_b\,dV; \tag{89a}$$

$$\mathcal{K}_{ab} := \int_V (\boldsymbol{H}_{\boldsymbol{\Sigma}}^n\boldsymbol{\nabla}_0 N_a)\cdot(\boldsymbol{H}_{\boldsymbol{\Sigma}}^n\boldsymbol{\nabla}_0 N_b)\,dV; \tag{89b}$$

$$\boldsymbol{v}^{st} := \boldsymbol{v}^{int} + \tau_{\boldsymbol{v}}\boldsymbol{\mathcal{R}}_{\boldsymbol{v}^{int}}, \tag{89c}$$

respectively. To update the entropy set $\boldsymbol{\mathcal{V}}^{n+1}$, it is essential to first update the velocity field using the standard Bubnov-Galerkin formulation

$$\sum_b M_{ab}\frac{\left(\boldsymbol{v}_b^{n+1}-\boldsymbol{v}_b^{int}\right)}{\Delta t}=\int_V \frac{N_a}{\rho_0}\mathrm{DIV}(\boldsymbol{H}_{\boldsymbol{\Sigma}}^n\Delta p)\,dV, \tag{90}$$

followed by

$$\sum_b M_{ab}\frac{(\boldsymbol{\Sigma}_{\boldsymbol{F}}^{n+1}-\boldsymbol{\Sigma}_{\boldsymbol{F}}^{int})}{\Delta t}=\int_V N_a W_{\boldsymbol{F}J}^n\left(\boldsymbol{H}_{\boldsymbol{\Sigma}}^n:\boldsymbol{\nabla}_0\Delta\boldsymbol{v}\right)\,dV; \tag{91a}$$

$$\sum_b M_{ab}\frac{(\boldsymbol{\Sigma}_{\boldsymbol{H}}^{n+1}-\boldsymbol{\Sigma}_{\boldsymbol{H}}^{int})}{\Delta t}=\int_V N_a W_{\boldsymbol{H}J}^n\left(\boldsymbol{H}_{\boldsymbol{\Sigma}}^n:\boldsymbol{\nabla}_0\Delta\boldsymbol{v}\right)\,dV; \tag{91b}$$

$$\sum_b M_{ab}\frac{(\hat{\Sigma}_J^{n+1}-\hat{\Sigma}_J^{int})}{\Delta t}=-\int_V N_a\left(W_{J\boldsymbol{F}}^n+W_{J\boldsymbol{H}}^n\boldsymbol{\times}\boldsymbol{F}_{\boldsymbol{\Sigma}}^n+\gamma^n\boldsymbol{H}_{\boldsymbol{\Sigma}}^n\right):\boldsymbol{\nabla}_0\Delta\boldsymbol{v}\,dV. \tag{91c}$$

As mentioned at the end of Section 5.1, the algorithm is finally evolved in time via a Total Variation Diminishing Runge-Kutta time integrator with a time step limit controlled, in this case, by the shear wave speed c_s (47).

7. Newton Raphson iterative technique

In the case of the entropy-based formulation (see Section 6), the strain measures $\{\boldsymbol{F}_{\boldsymbol{\Sigma}},\boldsymbol{H}_{\boldsymbol{\Sigma}},J_{\boldsymbol{\Sigma}}\}$ have to be obtained by means of reversed constitutive laws in terms of the stresses $\{\boldsymbol{\Sigma}_{\boldsymbol{F}},\boldsymbol{\Sigma}_{\boldsymbol{H}},\hat{\Sigma}_J,p\}$. This, in general, leads to the solution of nonlinear equations which might require to employ a Newton-Raphson iterative process in conjunction with the appropriate tangent operator $[\mathbb{H}_W]$ (either (10) or (21)).

For a nearly incompressible polyconvex model (16), expression (19) enables the explicit computation of the Jacobian in terms of the pressure p as follows:

$$J_{\boldsymbol{\Sigma}}=\frac{p}{\kappa}+1. \tag{92}$$

It is now possible to directly evaluate the deformation gradient field $\boldsymbol{F}_{\boldsymbol{\Sigma}}$ by substituting the above expression of $J_{\boldsymbol{\Sigma}}$ into (17a) as:

$$\boldsymbol{F}_{\boldsymbol{\Sigma}}=\frac{1}{2\varsigma}J_{\boldsymbol{\Sigma}}^{2/3}\boldsymbol{\Sigma}_{\boldsymbol{F}}. \tag{93}$$

However, the evaluation of the area map strain measure $\boldsymbol{H}_{\boldsymbol{\Sigma}}$ requires the solution of the nonlinear equation (17b) via a k-iterative Newton-Raphson scheme, which can be formulated as:

$$W^k_{\boldsymbol{HH}} : \Delta \boldsymbol{H} = \boldsymbol{\Sigma}^k_{\boldsymbol{H}} - 3\xi J^{-2}_{\boldsymbol{\Sigma}} (\boldsymbol{H}^k_{\boldsymbol{\Sigma}} : \boldsymbol{H}^k_{\boldsymbol{\Sigma}})^{1/2} \boldsymbol{H}^k_{\boldsymbol{\Sigma}}; \quad \boldsymbol{H}^{k+1}_{\boldsymbol{\Sigma}} = \boldsymbol{H}^k_{\boldsymbol{\Sigma}} + \Delta \boldsymbol{H}, \tag{94}$$

where $W_{\boldsymbol{HH}}$ is already defined in (22). This equation is solved at a quadrature point level and requires of very few iterations to achieve machine accuracy convergence. It is interesting to point out that in the particular case of using the compressible polyconvex model (11), due to its simplicity, the set of strains can be explicitly computed from the corresponding stresses [20], without the need to solve a nonlinear equation.

8. Numerical examples

8.1. Low dispersion cube

The main aim of this example is to assess the convergence behaviour of the polyconvex entropy-based PG methodology in three dimensions[8] [1, 2, 38]. A unit cube (1 m $\times$ 1 m $\times$ 1 m) has symmetric boundary conditions (i.e. roller supports) applied on the faces $X_1 = X_2 = X_3 = 0$ and skew-symmetric boundary conditions on the rest of the boundary surfaces $X_1 = X_2 = X_3 = 1$ m. For small deformations, the analytical displacement field (and hence velocity and stress at any time t) can be described by a closed-form expression as

$$\boldsymbol{u}(\boldsymbol{X}, t) = U_0 \cos\left(\frac{\sqrt{3}}{2} c_d \pi t\right) \begin{bmatrix} A \sin\left(\frac{\pi X_1}{2}\right) \cos\left(\frac{\pi X_2}{2}\right) \cos\left(\frac{\pi X_3}{2}\right) \\ B \cos\left(\frac{\pi X_1}{2}\right) \sin\left(\frac{\pi X_2}{2}\right) \cos\left(\frac{\pi X_3}{2}\right) \\ C \cos\left(\frac{\pi X_1}{2}\right) \cos\left(\frac{\pi X_2}{2}\right) \sin\left(\frac{\pi X_3}{2}\right) \end{bmatrix}; \; c_d = \sqrt{\frac{\mu}{\rho_0}}. \tag{95}$$

Parameters $\{A, B, C\}$ are arbitrary constants such that $A + B + C = 0$, ensuring no contribution from volumetric deformation. For values of U_0 below 0.001 m, the solution can be considered to be linear and the closed-form solution holds. In this particular case, a polyconvex compressible neo-Hookean model is chosen such that Young's modulus $E = 0.017$ GPa, density

[8] A two dimensional version of this particular example has been carried out in References [5, 37].

$\rho_0 = 1.1$ Mg/m^3, Poisson's ratio $\nu = 0.3$, $\alpha = \frac{\mu}{2}$ and $\beta = 0$. We set the solution parameters as $A = B = 1$, $C = -2$ and $U_0 = 5 \times 10^{-4}$ m in linear regime.

The cube is initially loaded with a known deformation gradient field $\boldsymbol{F}$ calculated using the relationship of $\boldsymbol{F} \equiv \boldsymbol{I} + \boldsymbol{\nabla}_0 \boldsymbol{u}$ (by computing a material gradient of (95) at $t = 0$) without any initial velocity. This would then lead to the calculation of its determinant $J \equiv \det(\boldsymbol{\nabla}_0 \boldsymbol{x})$. Thus, initial conditions for the entropy stresses $\{\boldsymbol{\Sigma}_{\boldsymbol{F}}, \Sigma_J\}$ can be obtained via expression (13). Figure 1 shows the deformed states of the cube (i.e. shear stresses contour plot) as it evolves in time. Global convergence error analysis (i.e. L^1 and L^2 induced norm[9]) for velocity and stress on a sequence of grids at time $t = 2 \times 10^{-3}$ s are examined in Figure 2. As expected, each of the diagrams tends to asymptotic quadratic convergence for velocity and stress of the $\boldsymbol{v}$-$\boldsymbol{\Sigma}_{\boldsymbol{F}}$-$\Sigma_J$ compressible entropy formulation (82) when linear interpolating functions are used. Notice that $\boldsymbol{\Sigma}_{\boldsymbol{H}}$ is redundant since a neo-Hookean model with $\beta = 0$ is used. For completeness, we simulate the exact same problem using the classical hexahedral B-bar elements, resulting in a reduced order of convergence for the stresses (see Figure 3).

8.2. 3D L-shaped block

This benchmark problem has been presented in [1, 38] to assess the ability of the algorithm to preserve angular momentum. We consider the motion of a three-dimensional L-shaped block subjected to initial impulse traction boundary conditions at two of its sides described as follows (see Figure 4)

$$\boldsymbol{F}_1(t) = -\boldsymbol{F}_2(t) = \begin{cases} t\boldsymbol{\eta}_0, & 0 \leq t < 2.5 \\ (5-t)\boldsymbol{\eta}_0, & 2.5 \leq t < 5 \\ 0, & t \geq 5 \end{cases} \tag{96}$$

where $\boldsymbol{\eta}_0 = [150, 300, 450]^T$. The material response is governed by a polyconvex compressible neo-Hookean model where its physical properties are Young's modulus $E = 50046$ Pa, density $\rho_0 = 1$ Mg/m^3, Poisson's ratio $\nu = 0.3$ and material parameters $\alpha = \frac{\mu}{2}$ and $\beta = 0$ (i.e. $\boldsymbol{\Sigma}_{\boldsymbol{H}}$ is redundant in this case). Figure 5 presents the momentum evolution of the system

[9] L^1 and L^2 induced norm of a $m \times n$ matrix $\boldsymbol{A}$ are defined in the usual fashion as: $\|\boldsymbol{\mathcal{A}}\|_{L^1} = \max_{1 \leq j \leq n} \sum_{i=1}^{m} |a_{ij}|$ and $\|\boldsymbol{\mathcal{A}}\|_{L^2} = \left[\lambda_{\max}(\boldsymbol{A}^T \boldsymbol{A})\right]^{1/2}$.

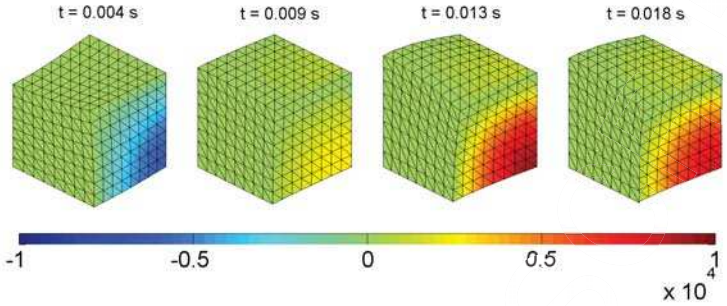

(a) Shear stress P_{12}

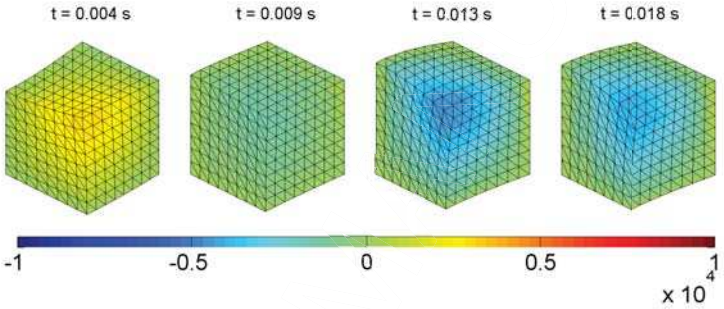

(b) Shear stress P_{13}

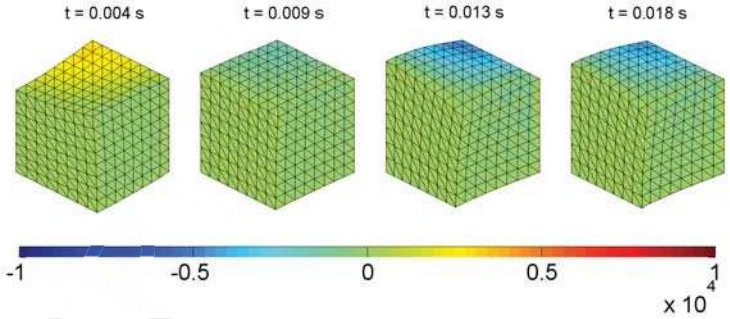

(c) Shear stress P_{23}

Figure 1: Low Dispersion Cube: Sequence of deformed shapes for (a) P_{12} shear stress; (b) P_{13} shear stress; and (c) P_{23} shear stress. Results obtained with $U_0 = 5 \times 10^{-4}$ m, $A = B = 1$ and $C = -2$. A polyconvex compressible neo-Hookean constitutive model is used such that Young's modulus $E = 0.017$ GPa, density $\rho_0 = 1.1$ Mg/m^3, $\alpha = \frac{\mu}{2}$, $\beta = 0$, Poisson's ratio $\nu = 0.3$ and $\alpha_{CFL} = 0.3$. Discretisation of $8 \times 8 \times 8 \times 6$ linear tetrahedral elements. Stabilising parameters: $\tau = \Delta t$, $\tau_{\boldsymbol{v}} = 0.2\Delta t$, $\zeta_J = 0.5$, $\zeta = 0$. Lumped mass contribution. Solution plotted with displacement scaled 200 times.

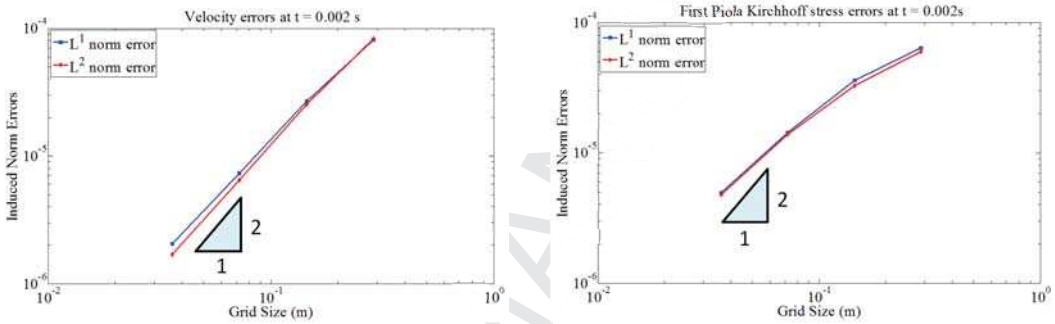

(a) (b)

Figure 2: Low Dispersion Cube: Induced L^1 and L^2 norm convergence errors obtained with $U_0 = 5 \times 10^{-4}$ m, $A = B = 1$ and $C = -2$ using compressible entropy $\boldsymbol{v}$-$\boldsymbol{\Sigma_F}$-Σ_J formulation for (a) Normed velocity field $\|\frac{\boldsymbol{v}-\boldsymbol{v}_{\text{exact}}}{c_{max}}\|_{L^{1,2}}$; and (b) Normed first Piola Kirchhoff stress $\|\frac{\boldsymbol{P}-\boldsymbol{P}_{\text{exact}}}{\mu}\|_{L^{1,2}}$. A polyconvex compressible neo-Hookean constitutive model is used such that Young's modulus $E = 0.017$ GPa, density $\rho_0 = 1.1$ Mg/m^3, $\alpha = \frac{\mu}{2}$, $\beta = 0$, Poisson's ratio $\nu = 0.3$ and $\alpha_{CFL} = 0.3$. Stabilising parameters: $\tau = \Delta t$, $\tau_{\boldsymbol{v}} = 0.2\Delta t$, $\zeta_J = 0.5$, $\zeta = 0$. Lumped mass contribution.

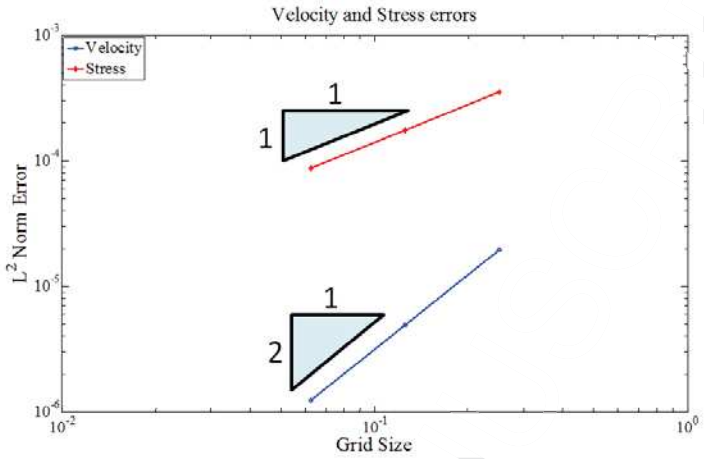

(a)

Figure 3: Low Dispersion Cube: L^2 norm convergence errors (for a generic component of the velocity vector and the stress tensor) obtained with $U_0 = 5 \times 10^{-4}$ m, $A = B = 1$ and $C = -2$ using the classical hexahedral B-bar methodology for velocity and stresses. A polyconvex nearly incompressible neo-Hookean constitutive model is used such that Young's modulus $E = 0.017$ GPa, density $\rho_0 = 1.1$ Mg/m^3, $\alpha = \frac{\mu}{2}$, $\beta = 0$ and Poisson's ratio $\nu = 0.3$.

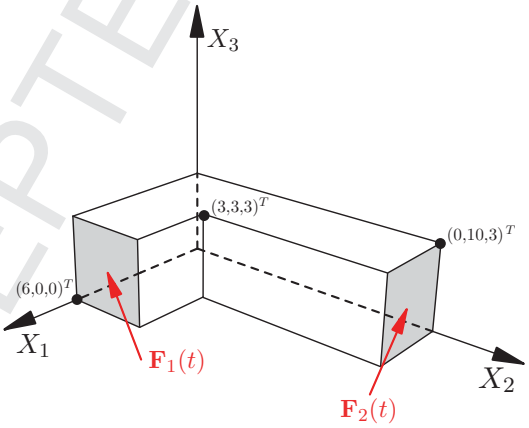

Figure 4: L-shaped block configuration

calculated with the nonlinear explicit $\boldsymbol{v}$-$\boldsymbol{\Sigma_F}$-Σ_J PG entropy formulation. A sequence of deformed states, together with the Frobenius norm of the velocity field, simulated using entropy- and conservation-based PG formulations is illustrated in Figure 6. Both methodologies produce practically identical deformed shapes. Figure 7 shows a series of snapshots in terms of pressure resolution without introducing any spurious modes.

8.3. 3D short column

A three dimensional column [1, 2, 38, 55] clamped on its bottom face ($X_3 = 0$) is presented in this numerical example (see Figure 8). An initial linear variation in velocity field $\boldsymbol{v}^0 = (V_0 X_3/L, 0, 0)^T$ is given (where $V_0 = 10$ m/s and $L = 6$m) and the column is left oscillating in time, leading to large strain oscillatory motion. The objective is to assess the performance of the proposed entropy-based PG methodologies (i.e. explicit $\boldsymbol{v}$-$\boldsymbol{\Sigma_F}$-$\boldsymbol{\Sigma_H}$-$\hat{\Sigma}_J$-p algorithm ((77) and (81)) and fractional step $\boldsymbol{v}$-$\boldsymbol{\Sigma_F}$-$\boldsymbol{\Sigma_H}$-$\hat{\Sigma}_J$-p formulation ((87) and (91))) in nearly and truly incompressible bending dominated scenarios, benchmarked against the $\boldsymbol{p}$-$\boldsymbol{F}$-$\boldsymbol{H}$-J explicit conservation-based PG formulation ((59) and (60)) and fractional step conservation-based formulation ((69) and (72)). A polyconvex nearly incompressible Mooney-Rivlin model (16) is employed such that Young's modulus $E = 0.017$ GPa, density $\rho_0 = 1.1$ Mg/m^3 and material parameters $\varsigma = \xi = \frac{\mu}{2+3\sqrt{3}}$.

We first examine the effectiveness of the proposed entropy-based schemes using Poisson's ratio $\nu = 0.45$. Figure 9 and Figure 10 clearly show that both entropy- and conservation-based mixed PG methodologies produced similar (and excellent) locking-free behaviour without spurious hydrostatic oscillations. For quantitative comparison purposes, the time history of both the horizontal displacement at point $[1, 1, 6]$ and the P_{22} component of stresses at point $[1/3, 1/3, 3]$ are monitored in Figure 11. Mesh refinement analysis is also shown in Figure 12. For truly incompressible solids where the Poisson's ratio is now $\nu = 0.5$, the explicit formulation cannot be employed due to the incompressibility constraint $\kappa = \infty$. Such limitation is removed by employing the fractional step PG entropy-based mixed methodologies in which the time step depends solely on the shear wave speed (47) (see Figure 13).

8.4. 3D Tensile Cube

The objective of this three dimensional tensile cube problem is to demonstrate the performance of the entropy-based PG formulations when a tetrahedral mesh is used in compressible and truly incompressible regimes. A

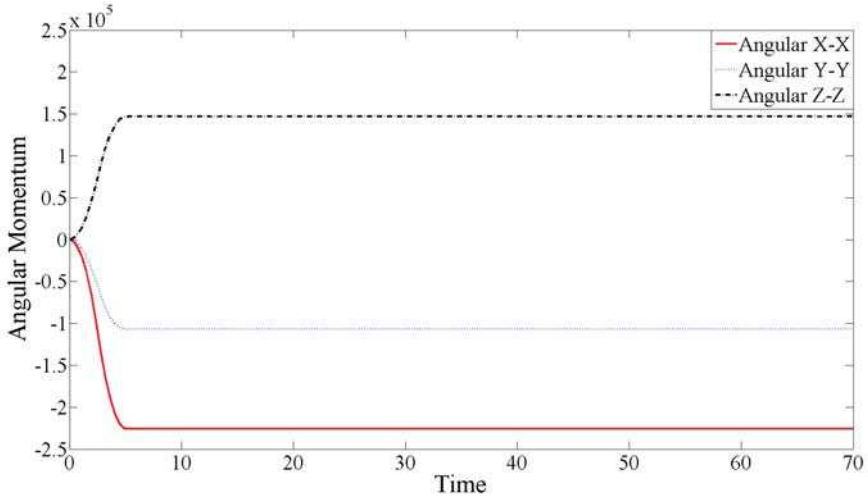

(a) Angular Momentum

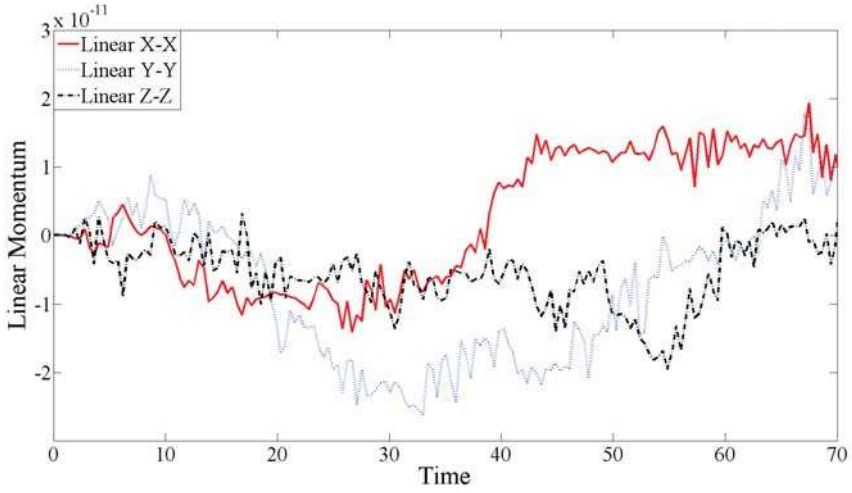

(b) Linear Momentum

Figure 5: L-shaped Block: Results obtained with an impulse traction boundary conditions (96) at two of its sides using explicit $\boldsymbol{v}$-$\boldsymbol{\Sigma_F}$-Σ_J PG formulation: (a) Angular momentum; and (b) Linear momentum. This example is run with the polyconvex compressible neo-Hookean constitutive model and material properties are such that Young's modulus $E = 50046$ Pa, density $\rho_0 = 1$ Mg/m^3, Poisson's ratio $\nu = 0.3$, $\alpha_{CFL} = 0.3$, $\alpha = \frac{\mu}{2}$ and $\beta = 0$. Stabilising parameters: $\tau = \Delta t$, $\tau_{\boldsymbol{v}} = 0.2\Delta t$ and $\zeta_J = 0.5$, $\zeta = 0$. Lumped mass contribution.

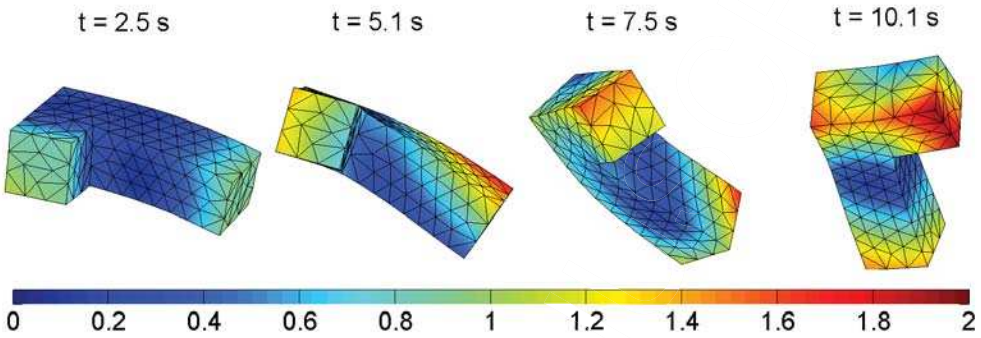

(a) Explicit $\boldsymbol{v}$-$\boldsymbol{\Sigma_F}$-Σ_J PG formulation

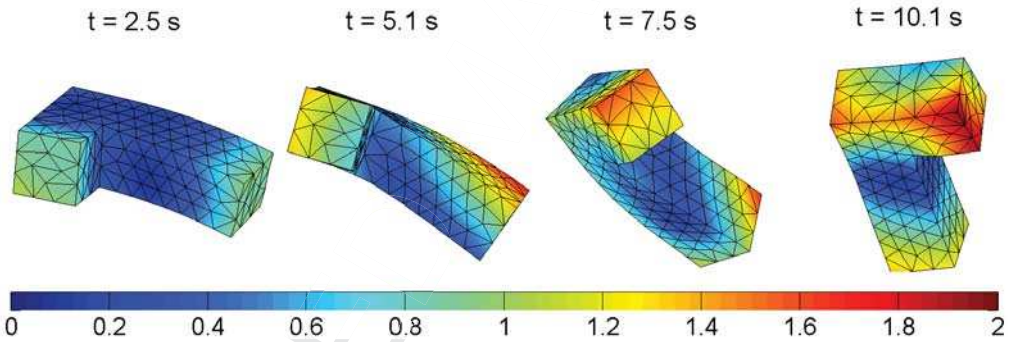

(b) Explicit $\boldsymbol{p}$-$\boldsymbol{F}$-$\boldsymbol{H}$-J PG formulation [1]

Figure 6: L-shaped Block: Results (i.e. Frobenius norm of velocity field) obtained with an impulse traction boundary conditions (96) at two of its sides using (a) Explicit entropy PG formulation ($\tau = \Delta t$, $\tau_{\boldsymbol{v}} = 0.2\Delta t$, $\zeta_J = 0.5$, $\zeta = 0$); and (b) Explicit conservation PG formulation ($\tau = \Delta t$, $\tau_{\boldsymbol{p}} = 0.2\Delta t$, $\zeta_J = 0.5$, $\zeta = 0$). This example is run with the polyconvex compressible neo-Hookean constitutive model and material properties are such that Young's modulus $E = 50046$ Pa, density $\rho_0 = 1$ Mg/m^3, $\alpha = \frac{\mu}{2}$, $\beta = 0$, Poisson's ratio $\nu = 0.3$ and $\alpha_{CFL} = 0.3$. Lumped mass contribution.

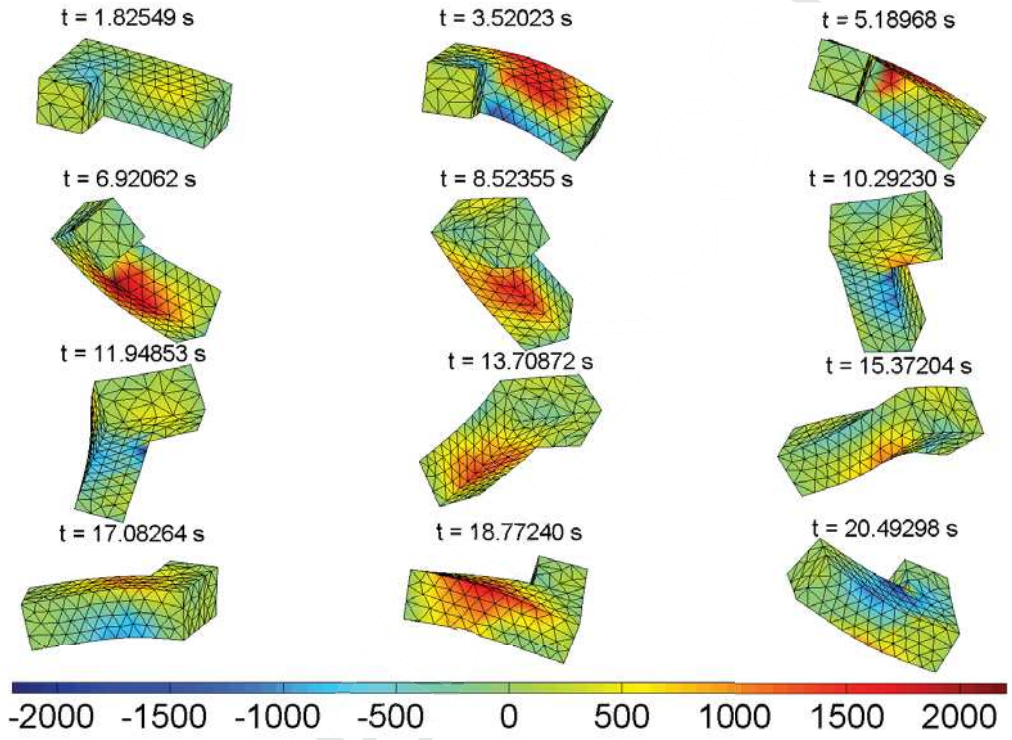

Figure 7: L-shaped Block: Results (i.e. pressure contour plot) obtained with an impulse traction boundary conditions (96) at two of its sides using explicit compressible $\boldsymbol{v}$-$\boldsymbol{\Sigma_F}$-Σ_J PG formulation. This example is run with the compressible polyconvex neo-Hookean constitutive model and material properties are such that Young's modulus $E = 50046$Pa, density $\rho_0 = 1$Mg/m^3, Poisson's ratio $\nu = 0.3$, $\alpha_{CFL} = 0.3$, $\alpha = \frac{\mu}{2}$ and $\beta = 0$. Stabilising parameters: $\tau = \Delta t$, $\tau_{\boldsymbol{v}} = 0.2\Delta t$ and $\zeta_J = 0.5$, $\zeta = 0$. Lumped mass contribution.

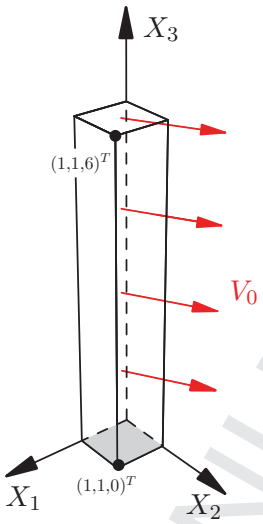

Figure 8: Thick column configuration

unit block clamped at the bottom (traction-free conditions for the rest of the boundaries) is subjected to a sinusoidal variation in initial velocity field $\boldsymbol{v}^0 = \left[0, 0, v_0 \sin\left(\frac{\Pi X_3}{2L}\right)\right]^T$ (where $v_0 = 500$ m/s) which is compatible with the boundary. A nearly incompressible polyconvex Mooney-Rivlin constitutive model is employed where the Young's modulus $E = 21$ GPa, density $\rho_0 = 7$ Mg/m^3, Poisson's ratio $\nu = 0.3$ and material parameters $\varsigma = \xi = \frac{\mu}{2+3\sqrt{3}}$. For comparison purposes, an ample spectrum of alternative numerical strategies, including explicit conservation-based PG, explicit entropy-based PG, fractional step conservation-based PG and fractioal step entropy-based PG, is employed in order to assess the interior pressure distribution. Figure 14 shows a sequence of deformed states for the interior of a tensile cube (a quarter of the whole domain is removed for visualisation purposes) simulated using explicit entropy-based $\boldsymbol{v}$-$\boldsymbol{\Sigma_F}$-$\boldsymbol{\Sigma_H}$-$\hat{\Sigma}_J$-p PG and explicit conservation-based $\boldsymbol{p}$-$\boldsymbol{F}$-$\boldsymbol{H}$-J PG. It can be clearly seen that these algorithms produce similar deformation behaviours and eliminate the appearance of non-physical mechanisms similar to hourglassing. The same problem is now assessed by scaling up the value of Poisson's ratio $\nu = 0.5$. Observe that the fractional step entropy- and conservation-based PG enhanced formulations can be used without any difficulties within truly incompressible regime (see Figure 15).

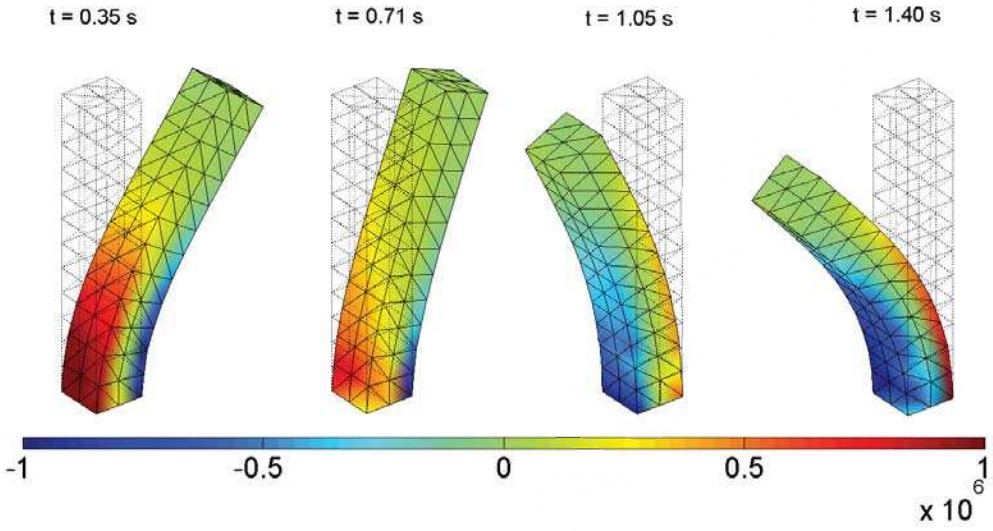

(a) Explicit entropy-based $\boldsymbol{v}$-$\boldsymbol{\Sigma_F}$-$\boldsymbol{\Sigma_H}$-$\hat{\Sigma}_J$-p PG formulation

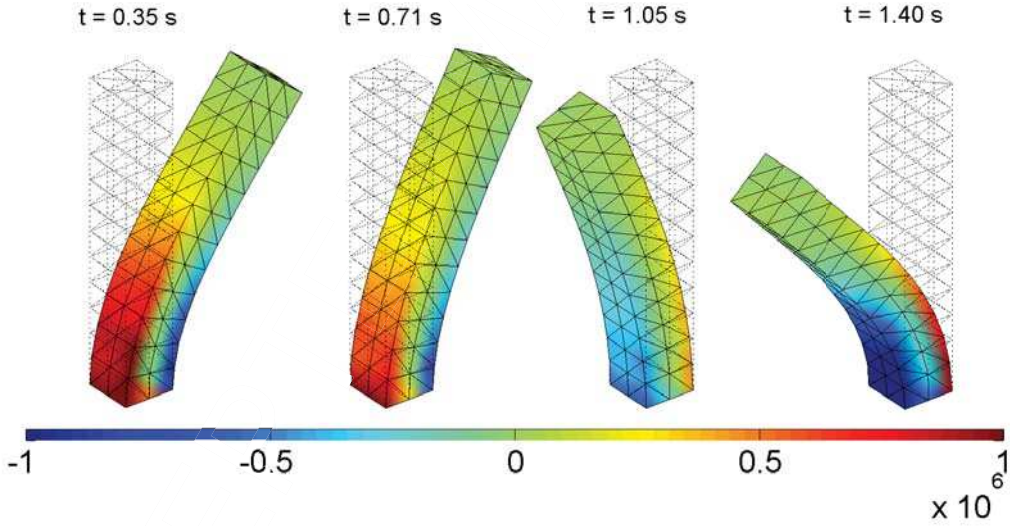

(b) Explicit conservation-based $\boldsymbol{p}$-$\boldsymbol{F}$-$\boldsymbol{H}$-J PG formulation

Figure 9: Bending Column: Sequence of deformed shapes (pressure contour plot) using: (a) Explicit entropy-based $\boldsymbol{v}$-$\boldsymbol{\Sigma_F}$-$\boldsymbol{\Sigma_H}$-$\hat{\Sigma}_J$-p PG formulation ($\tau_{\boldsymbol{v}} = 0.05\Delta t, \zeta_J = 0.05$); and (b) Explicit $\boldsymbol{p}$-$\boldsymbol{F}$-$\boldsymbol{H}$-J PG conservation-based formulation ($\tau_{\boldsymbol{p}} = 0.05\Delta t$ $\zeta_J = 0.5\frac{\mu}{\kappa}$). Results obtained with a linear variation in velocity field $\boldsymbol{v}^0 = (V_0 X_3/L, 0, 0)^T$ where $V_0 = 10$ m/s and $L = 6$m. The nearly incompressible polyconvex Mooney-Rivlin constitutive model is used such that Young's modulus $E = 0.017$ GPa, density $\rho_0 = 1.1$ Mg/m^3, $\varsigma = \xi = \frac{\mu}{2+3\sqrt{3}}$, Poisson's ratio $\nu = 0.45$ and $\alpha_{CFL} = 0.3$. Discretisation of $2 \times 2 \times 12 \times 6$ tetrahedral elements. Stabilising parameters: $\tau = \Delta t$, $\zeta = 0$. Lumped mass contribution.

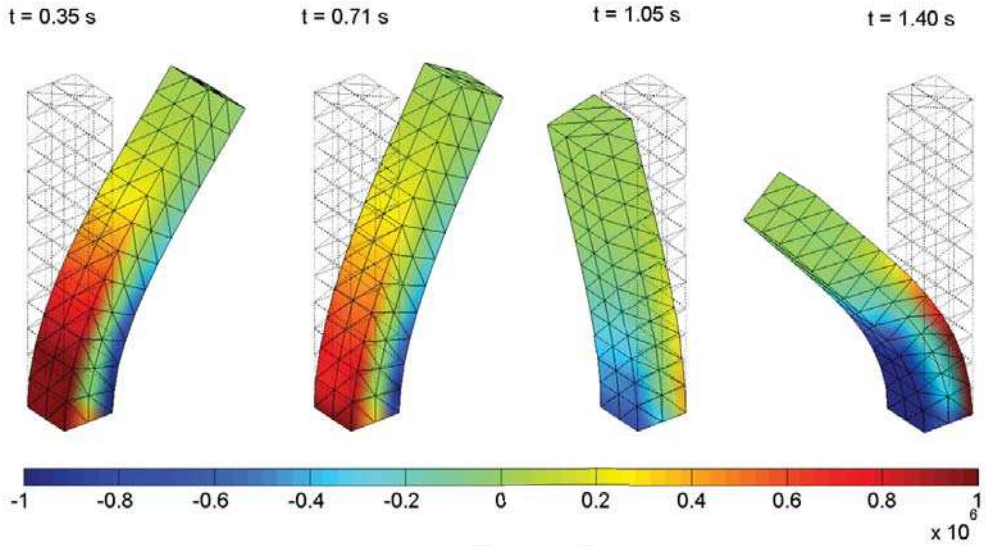

(a) Fractional step entropy-based PG formulation

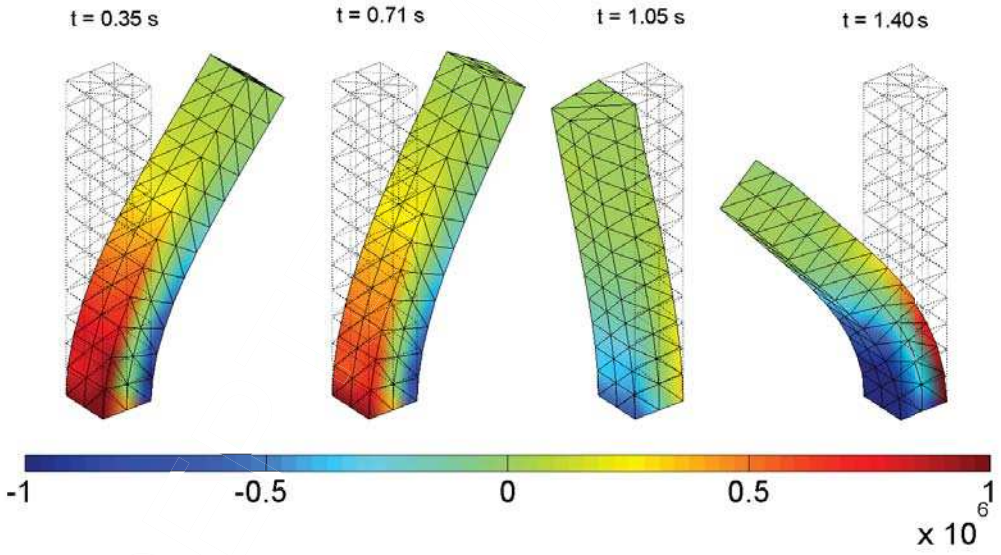

(b) Fractional step conservation-based PG formulation

Figure 10: Bending Column: Sequence of deformed shapes (pressure contour plot) using (a) Nonlinear entropy-based fractional step PG formulation ($\tau_{\boldsymbol{v}} = 0.05\Delta t$); and (b) Nonlinear fractional step conservation-based PG formulation ($\tau_{\boldsymbol{p}} = 0.05\Delta t$). Results obtained with a linear variation in velocity field $\boldsymbol{v}^0 = (V_0 X_3/L, 0, 0)^T$ where $V_0 = 10$ m/s and $L = 6$m. The nearly incompressible polyconvex Mooney-Rivlin constitutive model is used such that Young's modulus $E = 0.017$ GPa, density $\rho_0 = 1.1$ Mg/m^3, $\varsigma = \xi = \frac{\mu}{2+3\sqrt{3}}$, Poisson's ratio $\nu = 0.45$ and $\alpha_{CFL} = 0.3$. Discretisation of $2 \times 2 \times 12 \times 6$ tetrahedral elements. Lumped mass contribution. Stabilising parameters: $\tau = \Delta t$, $\zeta_J = 0.05$, $\zeta = 0$.

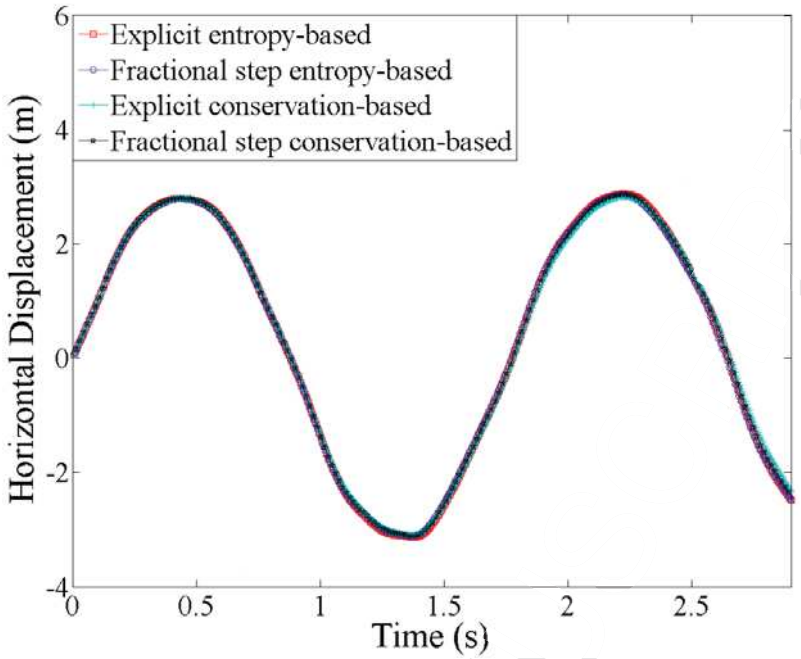

(a) Time history of horizontal displacement

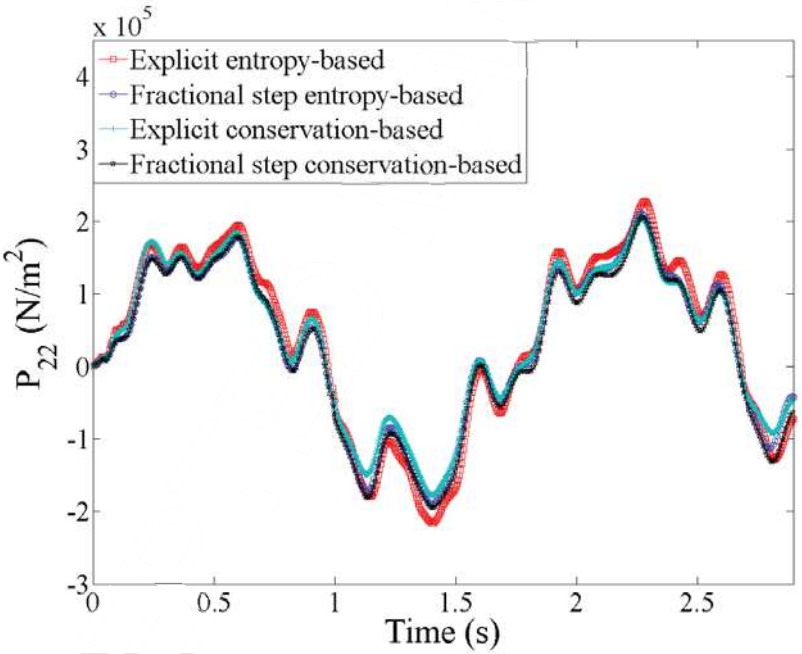

(b) Time history of P_{22}

Figure 11: Bending Column: Time history of (a) Horizontal displacement at $[1, 1, 6]$; and (b) P_{22} at $[1/3, 1/3, 3]$ simulated using four different strategies, namely: Explicit entropy-based ($\tau_{\boldsymbol{v}} = 0.05\Delta t$, $\zeta_J = 0.05$), Fractional step entropy-based ($\tau_{\boldsymbol{v}} = 0.05\Delta t$, $\zeta_J = 0.15$), Explicit conservation-based ($\tau_{\boldsymbol{p}} = 0.2\Delta t$, $\zeta_J = 0.5$) and Fractional step conservation-based ($\tau_{\boldsymbol{p}} = 0.05\Delta t$, $\zeta_J = 0.15$). Results obtained with a linear variation in velocity field $\boldsymbol{v}^0 = (V_0 X_3/L, 0, 0)^T$ where $V_0 = 10$ m/s and $L = 6$m. The nearly incompressible polyconvex Mooney-Rivlin constitutive model is used such that Young's modulus $E = 0.017$ GPa, density $\rho_0 = 1.1$ Mg/m^3, $\varsigma = \xi = \frac{\mu}{2+3\sqrt{3}}$, Poisson's ratio $\nu = 0.45$ and $\alpha_{CFL} = 0.3$. Discretisation of $3 \times 3 \times 18 \times 6$ tetrahedral elements. Lumped mass contribution. Stabilising parameters: $\tau = \Delta t$ and $\zeta = 0$.

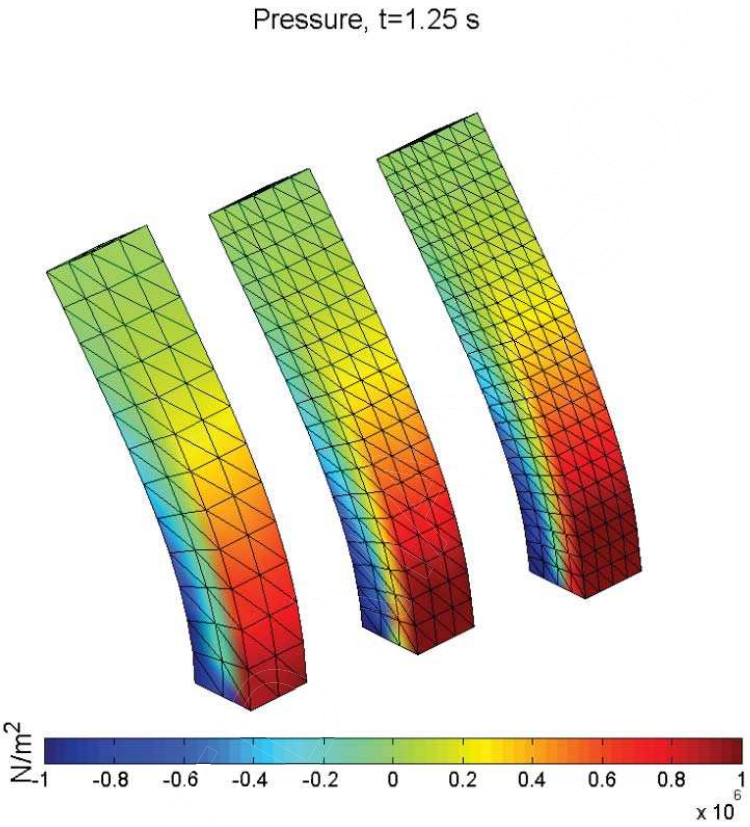

Figure 12: Bending Column: Mesh refinement analysis for three different types of meshes (namely $2\times2\times12\times6$, $3\times3\times18\times6$ and $4\times4\times24\times6$) simulated using explicit conservation-based formulation. Results obtained with a linear variation in velocity field $\boldsymbol{v}^0 = (V_0 X_3/L, 0, 0)^T$ where $V_0 = 10$ m/s and $L = 6$m. The nearly incompressible polyconvex Mooney-Rivlin constitutive model is used such that Young's modulus $E = 0.017$ GPa, density $\rho_0 = 1.1$ Mg/m^3, $\varsigma = \xi = \frac{\mu}{2+3\sqrt{3}}$, Poisson's ratio $\nu = 0.45$ and $\alpha_{CFL} = 0.3$. Lumped mass contribution. Stabilising parameters: $\tau = \Delta t$, $\tau_{\boldsymbol{p}} = 0.2\Delta t$, $\zeta_J = 0.5$ and $\zeta = 0$.

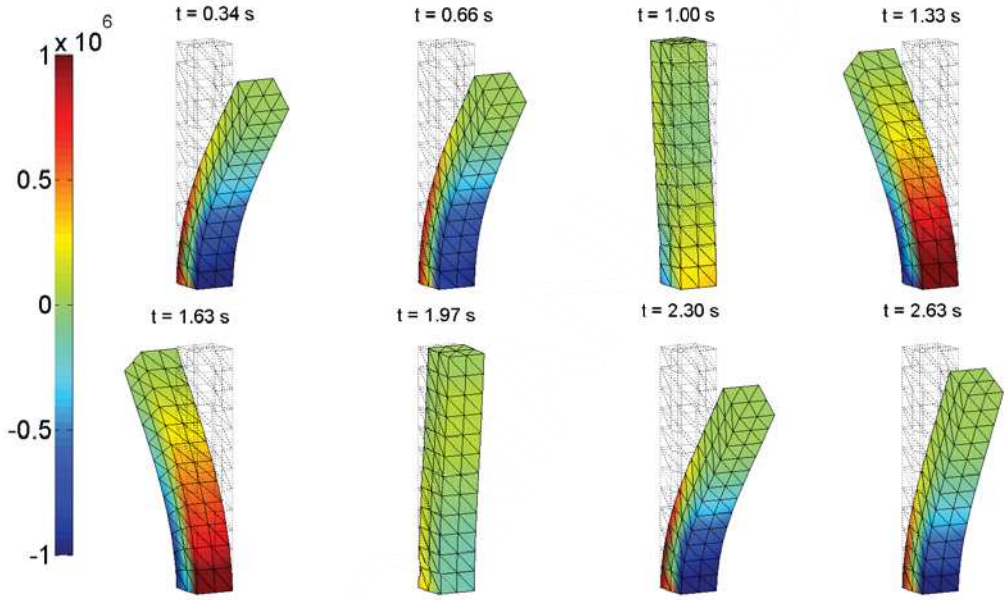

(a) Fractional step entropy-based PG formulation

Figure 13: Bending Column: Sequence of deformed shapes (pressure contour plot) using fractional step entropy-based PG. Results obtained with a linear variation in velocity field $\boldsymbol{v}^0 = (V_0 X_3/L, 0, 0)^T$ where $V_0 = 10$ m/s and $L = 6$m. Incompressible polyconvex Mooney-Rivlin constitutive model is used such that Young's modulus $E = 0.017$ GPa, density $\rho_0 = 1.1$ Mg/m^3, $\varsigma = \xi = \frac{\mu}{2+3\sqrt{3}}$, Poisson's ratio $\nu = 0.5$ and $\alpha_{CFL} = 0.3$. Discretisation of $2 \times 2 \times 12 \times 6$ tetrahedral elements. Stabilising parameters: $\tau = 0.5\Delta t$, $\tau_{\boldsymbol{v}} = 0.2\Delta t$, $\zeta_J = 0.5$, $\zeta = 0$. Lumped mass contribution.

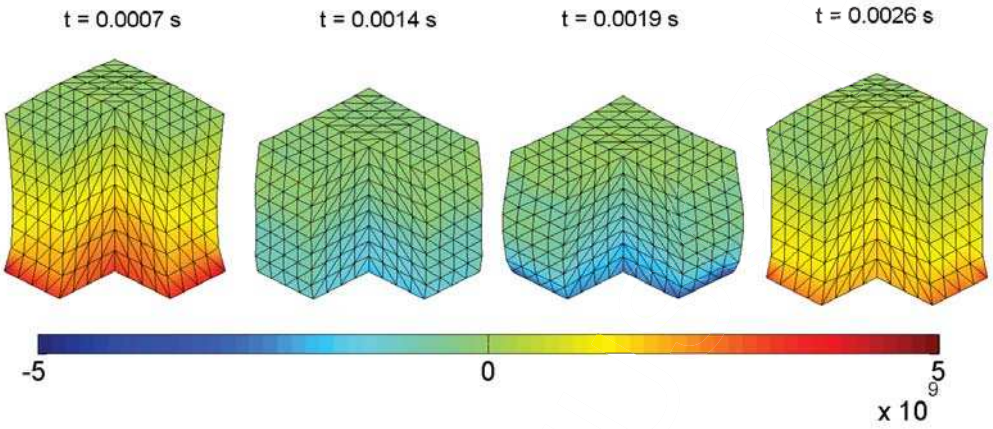

(a) Explicit $\boldsymbol{v}$-$\boldsymbol{\Sigma_F}$-$\boldsymbol{\Sigma_H}$-$\hat{\Sigma}_J$-p PG formulation

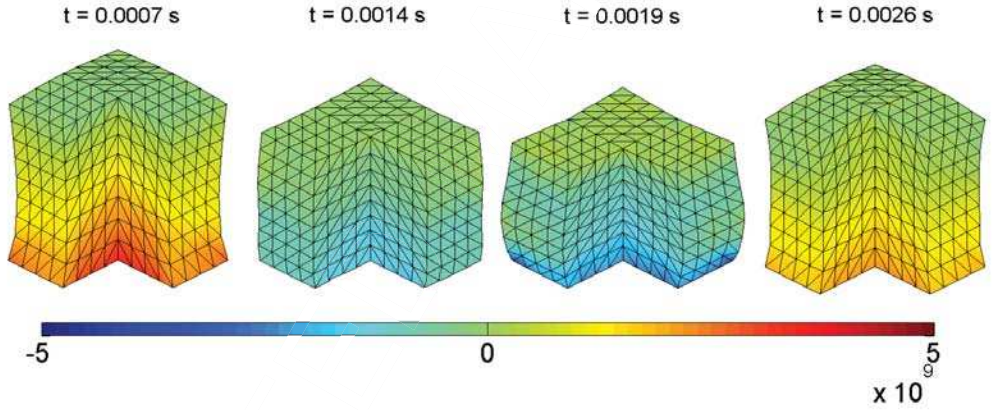

(b) Explicit $\boldsymbol{p}$-$\boldsymbol{F}$-$\boldsymbol{H}$-J PG formulation

Figure 14: Tensile Cube: A sequence of deformed shapes for the interior of a tensile cube (pressure contour plot) using (a) Explicit $\boldsymbol{v}$-$\boldsymbol{\Sigma_F}$-$\boldsymbol{\Sigma_H}$-$\hat{\Sigma}_J$-p PG formulation ($\tau_{\boldsymbol{v}} = 0.1\Delta t$); and (b) Explicit $\boldsymbol{p}$-$\boldsymbol{F}$-$\boldsymbol{H}$-J PG formulation ($\tau_{\boldsymbol{p}} = 0.1\Delta t$). Results obtained with a sinusoidal variation in initial velocity field $\boldsymbol{v}^0 = \left[0, 0, v_0 \sin\left(\frac{\Pi X_3}{2L}\right)\right]^T$ where $v_0 = 500$ m/s. A nearly incompressible polyconvex neo-Hookean constitutive model is used such that Young's modulus $E = 21$ GPa, density $\rho_0 = 7$ Mg/m^3, $\varsigma = \frac{\mu}{2}$, $\xi = 0$, Poisson's ratio $\nu = 0.3$ and $\alpha_{CFL} = 0.3$. Discretisation of $8 \times 8 \times 8 \times 6$ tetrahedral elements. Stabilising parameters: $\tau = \Delta t$, $\zeta_J = 0.5$, $\zeta = 0.1$. Lumped mass contribution.

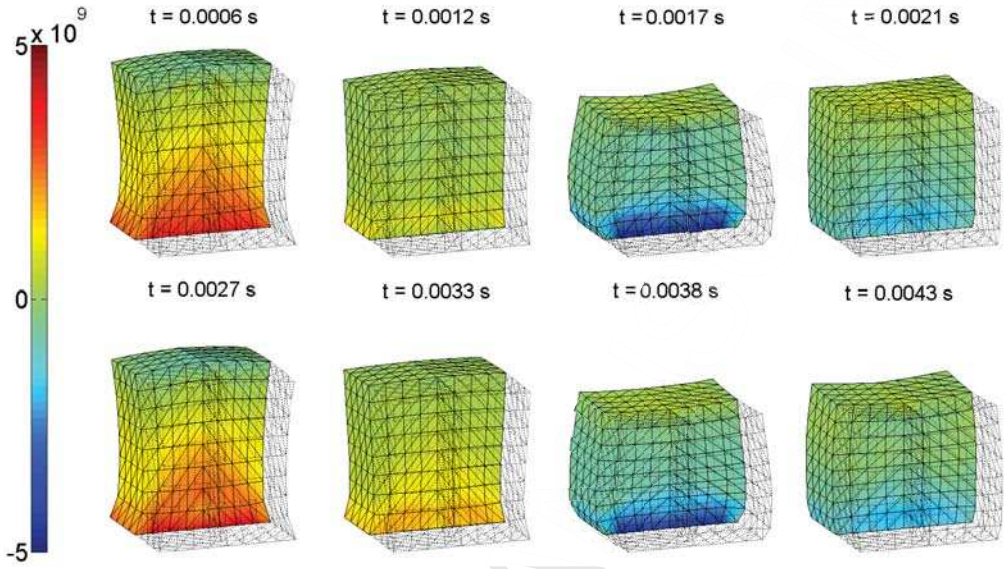

(a) Fractional step entropy-based PG formulation

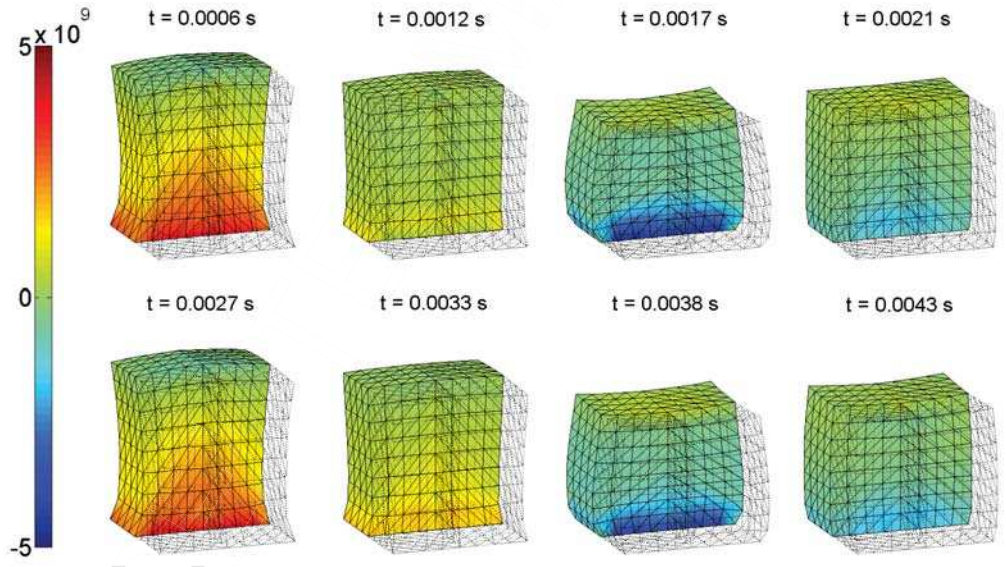

(b) Fractional step conservation-based PG formulation

Figure 15: Tensile Cube: A sequence of cross-sectional deformed shapes (pressure contour plot) using (a) Fractional step entropy-based PG ($\tau_{\boldsymbol{v}} = 0.1\Delta t$); and (b) Fractional step conservation-based PG ($\tau_{\boldsymbol{p}} = 0.1\Delta t$). Results obtained with a sinusoidal variation in initial velocity field $\boldsymbol{v}^0 = \left[0, 0, v_0 \sin\left(\frac{\Pi X_3}{2L}\right)\right]^T$ where $v_0 = 500$ m/s. A fully Incompressible Mooney-Rivlin constitutive model is used such that Young's modulus $E = 21$ GPa, density $\rho_0 = 7$ Mg/m^3, $\varsigma = \xi = \frac{\mu}{2+3\sqrt{3}}$, Poisson's ratio $\nu = 0.5$ and $\alpha_{CFL} = 0.3$. Discretisation of $8 \times 8 \times 8 \times 6$ tetrahedral elements. Stabilising parameters: $\tau = \Delta t$, $\zeta_J = 0.5$, $\zeta = 0.1$. Lumped mass contribution.

8.5. 3D Taylor impact bar

The classical benchmarking example [2] demonstrates the impact of a cylindrical copper bar, of initial radius $r_0 = 0.0032$ m and length $L_0 = 0.0324$ m, against a rigid wall (see Figure 16). The bar is made of a fully incompressible polyconvex Mooney-Rivlin constitutive model, by means of Young's modulus $E = 117$ GPa, density $\rho_0 = 8930$ kg/m^3, Poisson's ratio $\nu = 0.5$ and parameters $\varsigma = \xi = \frac{\mu}{2+3\sqrt{3}}$, and is dropped with a constant velocity $V_0 = 1000$ m/s. The primary interest of this problem is to show the importance of the incorporation of the parameter $\tau_{\boldsymbol{v}}$ (70) into the pressure evolution $\dot{p}$ of the fractional-step PG entropy methodology. Observe that the pressure resolution is clearly freed from non-physical pressure checkerboard modes by introducing the velocity correction $\boldsymbol{v}^{st}$ (70) (see Figure 17).

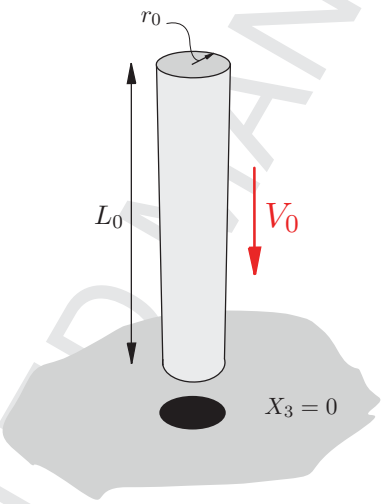

Figure 16: Classical benchmark impact bar configuration

8.6. 3D Twisting column

To assess the applicability and robustness of the stabilised entropy-based PG mixed formulation in extreme nonlinear deformations, a twisting column clamped on its bottom face ($X_3 = 0$) is presented [1, 2, 20] (see Figure 18). This problem is particularly challenging as it involves a large number of deformation modes. An initial sinusoidal rotational velocity field relative to

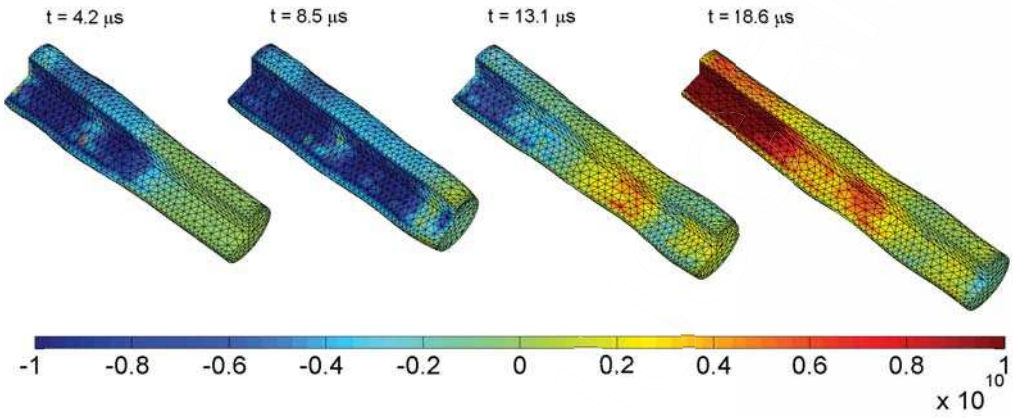

(a) Spurious pressure modes

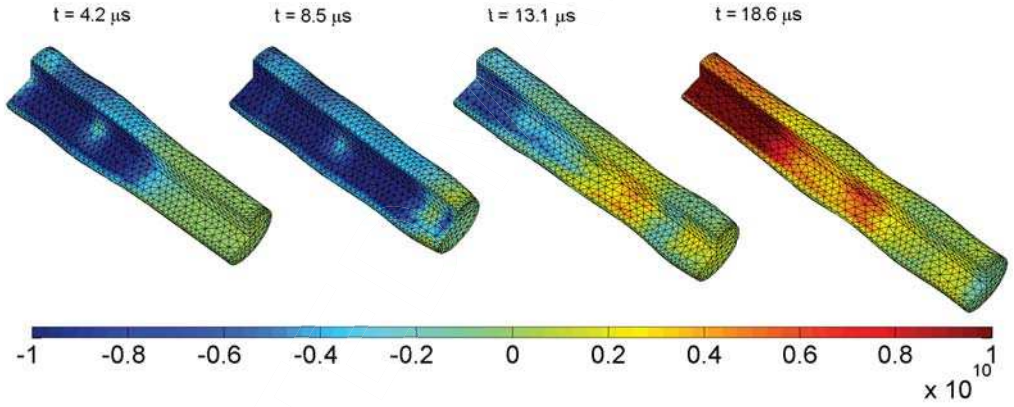

(b) Smooth pressure resolution

Figure 17: Classical Taylor impact bar: Sequence of deformed shapes (pressure contour plot) using a nonlinear fractional-step PG formulation: (a) $\tau_{\boldsymbol{v}} = 0$; and (b) $\tau_{\boldsymbol{v}} = 0.2\Delta t$. Results obtained with a constant initial velocity $V_0 = 1000$m/s. This example is run with the polyconvex fully incompressible Mooney-Rivlin constitutive model and material properties are such that Young's modulus $E = 117$ GPa, density $\rho_0 = 8930$ kg/m^3, $\varsigma = \xi = \frac{\mu}{2+3\sqrt{3}}$, Poisson's ratio $\nu = 0.5$ and $\alpha_{CFL} = 0.3$. Stabilising parameters: $\tau = \Delta t$, $\zeta_J = 0.5$, $\zeta = 0.2$. Lumped mass contribution.

the origin is given by

$$\boldsymbol{v}^0(\boldsymbol{X}) = \boldsymbol{\omega} \times \boldsymbol{X}; \qquad \boldsymbol{\omega} = \left[0, 0, \Omega \sin\left(\frac{\Pi X_3}{2L}\right)\right]^T \tag{97}$$

where $\Omega = 100$ rad/s. Its objective is to examine the effectiveness of both the fractional step $\boldsymbol{v}$-$\boldsymbol{\Sigma_F}$-$\boldsymbol{\Sigma_H}$-$\hat{\Sigma}_J$-p PG entropy-based methodology and the fractional-step $\boldsymbol{p}$-$\boldsymbol{F}$-$\boldsymbol{H}$-J PG conservation-based formulation. This problem is modelled by using a nearly incompressible polyconvex Mooney-Rivlin constitutive model where Young's modulus $E = 0.017$ GPa, material density $\rho_0 = 1.1$ Mg/m^3, material parameters $\varsigma = \xi = \frac{\mu}{2+3\sqrt{3}}$ and Poisson's ratio $\nu = 0.495$.

For benchmarking purposes, we simulate the exact same problem using two alternative implicit based techniques, namely the classical B-bar hexahedral formulation [11] and the recently introduced [20] Hu-Washizu type seven field $\{\boldsymbol{x}, \boldsymbol{F}, \boldsymbol{H}, J, \boldsymbol{\Sigma_F}, \boldsymbol{\Sigma_H}, \Sigma_J\}$ mixed tetrahedral formulation [20]. The latter corresponds to the following selection of functional spaces for a tetrahedral mesh: continuous quadratic interpolation of the displacement field (geometry) $\boldsymbol{x}$, piecewise linear interpolation of the strain and stress fields $\boldsymbol{F}$, $\boldsymbol{H}$, $\boldsymbol{\Sigma_F}$ and $\boldsymbol{\Sigma_H}$, and piecewise constant interpolation of the Jacobian J and its associated stress conjugate Σ_J[10]. In addition, as shown in Reference [14], a classical $\mathcal{P}_1/\mathcal{P}_1$ mixed Galerkin hexahedral formulation is presented to emphasise the spurious modes appearing when no stabilisation technique is employed.

From the time discretisation standpoint, a generalised-α method is employed [9] with a built-in numerical damping coefficient $\rho_\infty = 0.85$ in order to dissipate high frequency oscillations.

Both the fractional-step PG entropy- and the conservation-based implementation render very similar results (locking-free deformed shapes that are freed from low-energy modes) to those of the implicit Hu-Washizu variational multi-field formulation and the classical B-bar formulation with hexahedral elements. As expected, it can be observed that the classical $\mathcal{P}_1/\mathcal{P}_1$ mixed hexahedral formulation exhibits spurious hydrostatic oscillations (see Figure 21).

[10]This selection of functional spaces ensures the satisfaction of the Ladyzenskaya-Babuška-Brezzi (LBB) constraint [10] and hence, removes the need to employ numerical stabilisation.

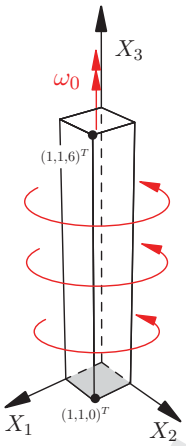

Figure 18: Highly nonlinear twisting column

9. Conclusions

In Part I of this series, Bonet *et al.* [1] introduced a new computational framework for the analysis of large strain isothermal fast solid dynamics. This Part II paper expands this formulation to the range of nearly incompressible and truly incompressible materials in the context of polyconvexity [46]. The consideration of an extended set of unknowns $\boldsymbol{p}$-$\boldsymbol{F}$-$\boldsymbol{H}$-J and the use of polyconvex energy functionals has enabled the definition of generalised convex entropy functions and associated entropy fluxes, where two variants of the same formulation have been presented, namely, conservation-based $\boldsymbol{p}$-$\boldsymbol{F}$-$\boldsymbol{H}$-J and entropy-based $\boldsymbol{v}$-$\boldsymbol{\Sigma}_{\boldsymbol{F}}$-$\boldsymbol{\Sigma}_{\boldsymbol{F}}$-$\Sigma_J$. In addition, the adoption of polyconvexity as a mathematical requirement [46, 47] guarantees both stability of the scheme and the existence of real wave speeds.

It has been shown that both conservation-based and entropy-based formulations overcome locking difficulties and non-physical hydrostatic fluctuations, providing a good balance between accuracy and speed of computation. Moreover, both implementations provide practically identical results. In terms of computational efficiency, an adapted Petrov-Galerkin fractional step [2] methodology has been formulated when dealing with very large wave speeds.

A comprehensive set of numerical examples has been presented, in order to benchmark the results obtained against those of alternative numerical

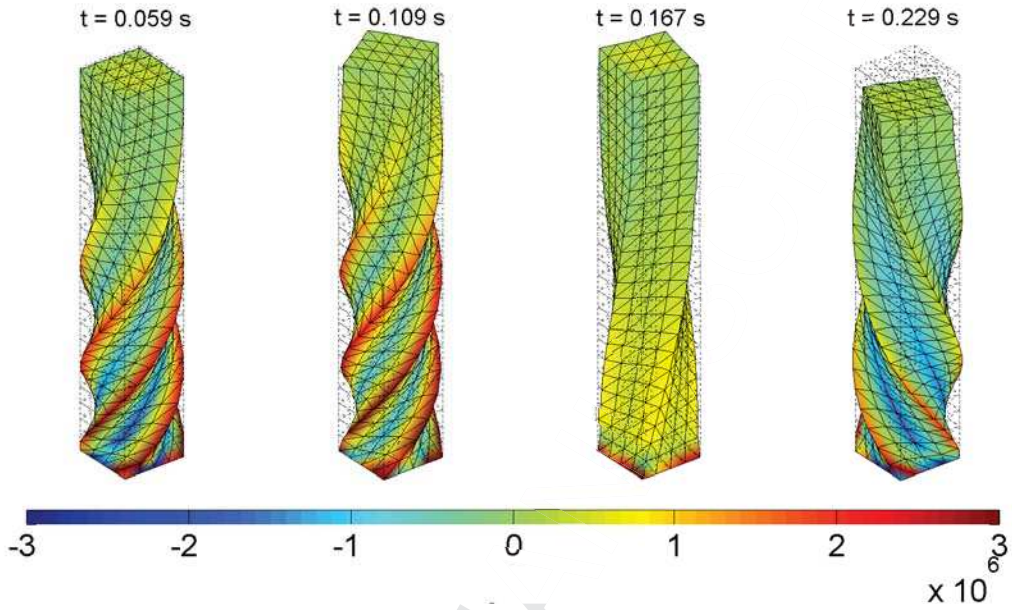

(a) HuWashizu type variational mixed formulation

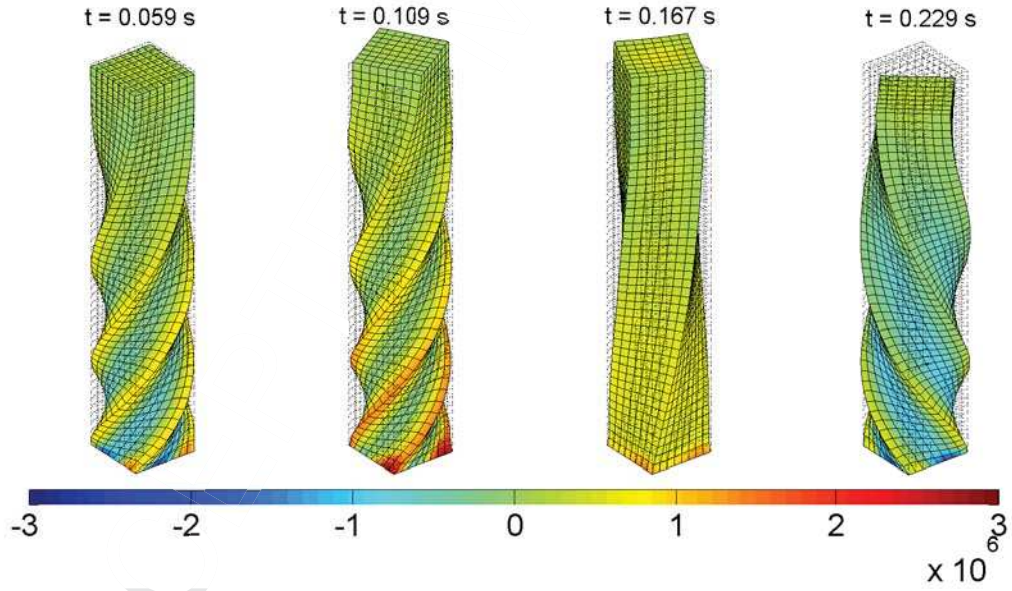

(b) Classical B-bar hexahedral formulation

Figure 19: Twisting Column: Sequence of deformed shapes (pressure contour plot) using (a) Implicit HuWashizu type variational mixed formulation; and (b) Classical $\boldsymbol{v}$-p formulation. Results obtained with a initial sinusoidal rotational velocity $\Omega = 100$ rad/s. A nearly incompressible polyconvex Mooney-Rivlin constitutive model is used such that Young's modulus $E = 0.017$ GPa, density $\rho_0 = 1.1$ Mg/m^3, $\varsigma = \xi = \frac{\mu}{2+3\sqrt{3}}$, Poisson's ratio $\nu = 0.495$ and $\rho_\infty = 0.85$.

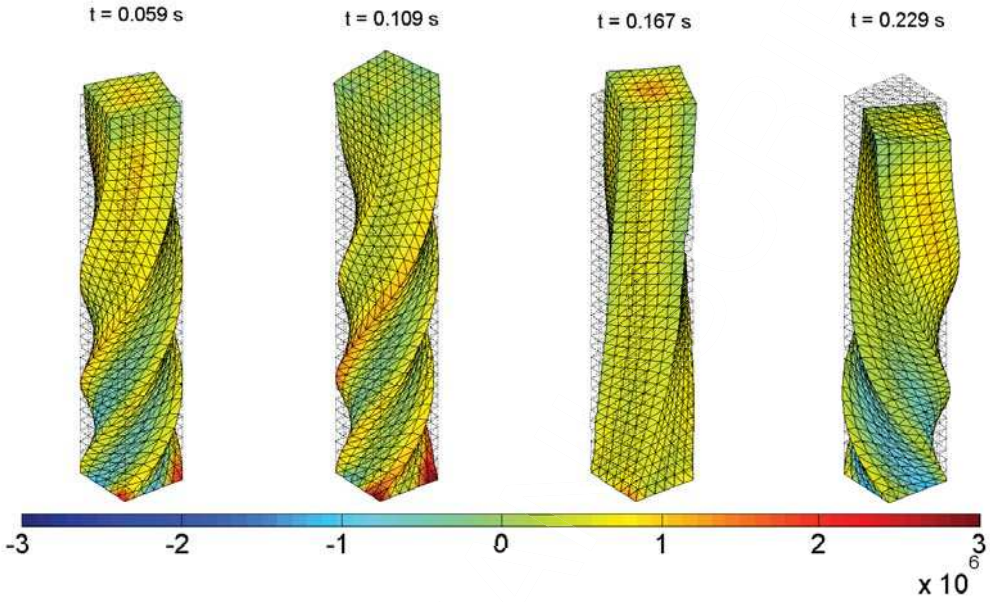

(a) Fractional step entropy-based PG formulation

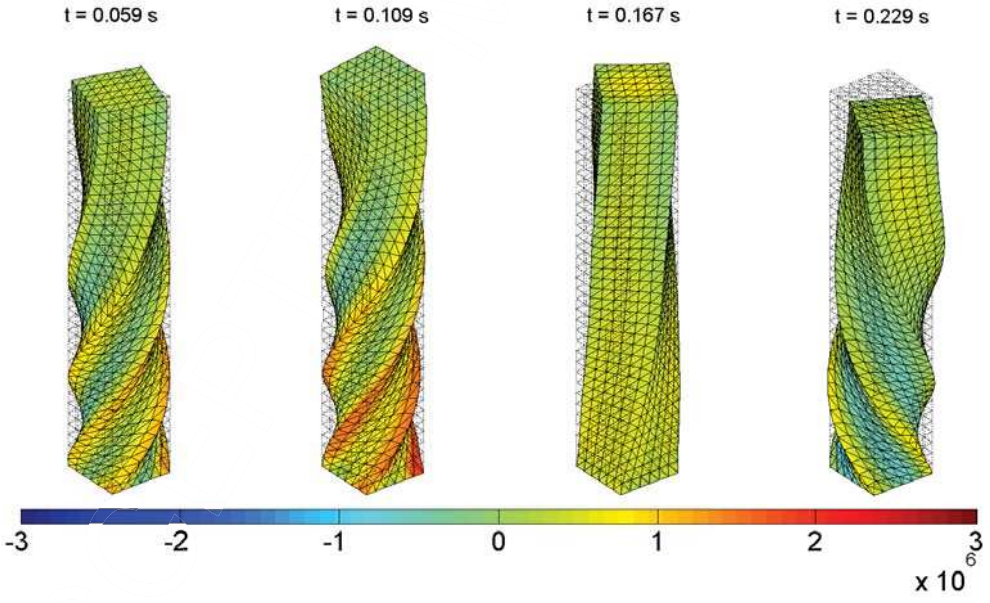

(b) Fractional step conservation-based PG formulation

Figure 20: Twisting Column: Sequence of deformed shapes (pressure contour plot) using (a) Fractional step entropy-based PG formulation ($\tau_{\boldsymbol{v}} = 0.2\Delta t$); and (b) Fractional step conservation-based PG formulation ($\tau_{\boldsymbol{p}} = 0.2\Delta t$). Results obtained with a initial sinusoidal rotational velocity $\Omega = 100$ rad/s. A nearly incompressible polyconvex Mooney-Rivlin constitutive model is used such that Young's modulus $E = 0.017$ GPa, density $\rho_0 = 1.1$ Mg/m^3, $\varsigma = \xi = \frac{\mu}{2+3\sqrt{3}}$, Poisson's ratio $\nu = 0.495$ and CFL $\alpha_{CFL} = 0.3$. Stabilising parameters: $\tau = \Delta t$, $\zeta_J = 0.5$, $\zeta = 0.2$. Lumped mass contribution.

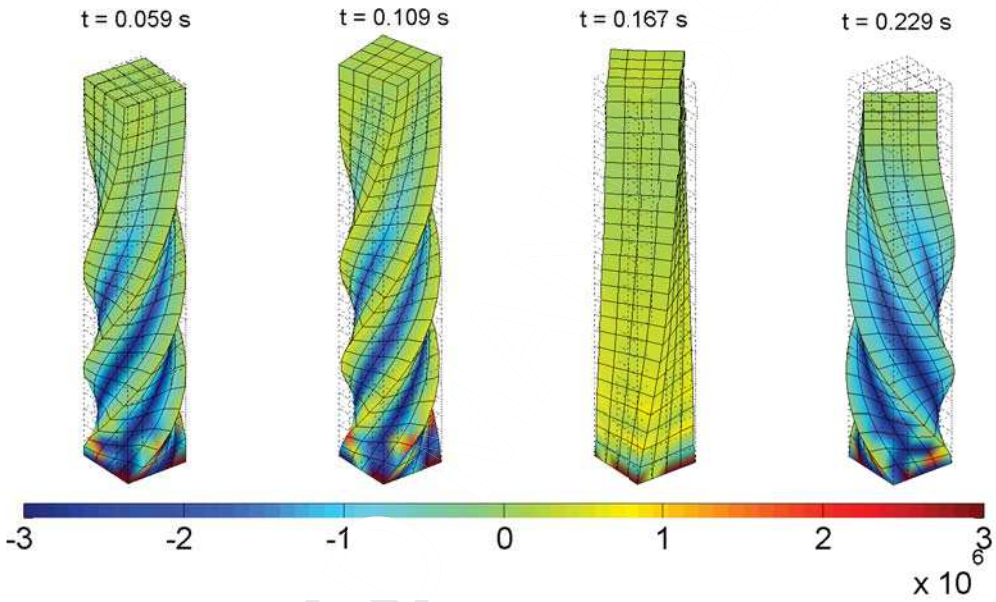

(a) Classical $\mathcal{P}_1/\mathcal{P}_1$ mixed Galerkin without stabilisation

Figure 21: Twisting Column: Sequence of deformed shapes (pressure contour plot) using classical $\mathcal{P}_1/\mathcal{P}_1$ mixed Galerkin without stabilisation. Results obtained with a initial sinusoidal rotational velocity $\Omega = 100$ rad/s. A nearly incompressible polyconvex Mooney-Rivlin constitutive model is used such that Young's modulus $E = 0.017$ GPa, density $\rho_0 = 1.1$ Mg/m^3, $\varsigma = \xi = \frac{\mu}{2+3\sqrt{3}}$, Poisson's ratio $\nu = 0.495$ and $\rho_\infty = 0.85$.

strategies, including implicit finite element based discretisations. Both velocities and stresses (volumetric and deviatoric) display the same (second order) rate of convergence when using linear finite elements, usually preferred in commercial codes.

The consideration of thermal and inelastic effects within the current computational framework is the next step of our work.

Acknowledgements

The authors gratefully acknowledge the financial support provided by the Sêr Cymru National Research Network for Advanced Engineering and Materials, United Kingdom. The first author would like to acknowledge the financial support received through "The Leverhulme Prize" awarded by The Leverhulme Trust, United Kingdom.

References

[1] J. Bonet, A. J. Gil, C. H. Lee, M. Aguirre, R. Ortigosa, A first order hyperbolic framework for large strain computational solid dynamics. Part I: Total Lagrangian isothermal elasticity, Computer Methods in Applied Mechanics and Engineering 283 (2015) 689–732.

[2] A. J. Gil, C. H. Lee, J. Bonet, M. Aguirre, A stabilised Petrov-Galerkin formulation for linear tetrahedral elements in compressible, nearly incompressible and truly incompressible fast dynamics, Computer Methods in Applied Mechanics and Engineering 276 (2014) 659–690.

[3] D. J. Benson, Computational methods in Lagrangian and Eulerian hydrocodes, Computer Methods in Applied Mechanics and Engineering 99 (1992) 235–394.

[4] D. P. Flanagan, T. Belytschko, A uniform strain hexahedron and quadrilateral with orthogonal hourglass control, International Journal for Numerical Methods in Engineering 17 (1981) 679–706.

[5] C. H. Lee, A. J. Gil, J. Bonet, Development of a stabilised Petrov-Galerkin formulation for conservation laws in Lagrangian fast solid dynamics, Computer Methods in Applied Mechanics and Engineering 268 (2014) 40–64.

[6] C. R. Dohrmann, M. W. Heinstein, J. Jung, S. W. Key, W. R. Witkowski, Node-based uniform strain elements for three-node triangular and four-node tetrahedral meshes, International Journal for Numerical Methods in Engineering 47 (2000) 1549–1568.

[7] J. Bonet, H. Marriott, O. Hassan, An averaged nodal deformation gradient linear tetrahedral element for large strain explicit dynamic applications, Communications in Numerical Methods in Engineering 17 (2001) 551–561.

[8] M. W. Gee, C. R. Dohrmann, S. W. Key, W. A. Wall, A uniform nodal strain tetrahedron with isochoric stabilization, International Journal for Numerical Methods in Engineering 78 (2009) 429–443.

[9] J. Chung, G. M. Hulbert, A time integration algorithm for structural dynamics with improved numerical dissipation: The generalized α method, Journal of Applied Mechanics 60 (1993) 371–375.

[10] T. J. R. Hughes, The finite element method: Linear static and dynamic finite element analysis, Dover Publications, 2000.

[11] T. J. R. Hughes, Generalization of selective integration procedures to anisotropic and nonlinear media, International Journal for Numerical Methods in Engineering 15 (1980) 1413–1418.

[12] J. Bonet, R. D. Wood, Nonlinear continuum mechanics for finite element analysis, Cambridge University Press, second edition, 2008.

[13] J. Donea, A. Huerta, Finite element methods for flow problems, Wiley and Sons, 2004.

[14] G. Scovazzi, B. Carnes, X. Zeng, S. Rossi, A simple, stable, and accurate tetrahedral finite element for transient, nearly and fully incompressible solid dynamics: A dynamic variational multiscale approach, International Journal for Numerical Methods in Engineering (2015). DOI: 10.1002/nme.5138.

[15] A. J. Gil, P. D. Ledger, A coupled *hp*-finite element scheme for the solution of two-dimensional electrostrictive materials, International Journal for Numerical Methods in Engineering 91 (2012) 1158–1183.

[16] D. Jin, P. D. Ledger, A. J. Gil, An *hp*-fem framework for the simulation of electrostrictive and magnetostrictive materials, Computers and Structures 133 (2014) 131–148.

[17] T. Elguedj, Y. Bazilevs, V. M. Calo, T. J. R. Hughes, $\bar{B}$ and $\bar{F}$ projection methods for nearly incompressible linear and nonlinear elasticity and plasticity using higher-order NURBS elements, Computer Methods in Applied Mechanics and Engineering 197 (2008) 2732–2762.

[18] T. J. R. Hughes, L. P. Franca, M. Balestra, A new finite element formulation for computational fluid dynamics: V. Circumventing the Babuška-Brezzi condition: a stable Petrov-Galerkin formulation of the Stokes problem accommodating equal-order interpolations, Computer Methods in Applied Mechanics and Engineering 59 (1986) 85–99.

[19] F. Auricchio, L. B. da Veiga, C. Lovadina, A. Reali, R. L. Taylor, P. Wriggers, Approximation of incompressible large deformation elastic problems: Some unresolved issues, Computational Mechanics (2013) 1–15.

[20] J. Bonet, A. J. Gil, R. Ortigosa, A computational framework for polyconvex large strain elasticity, Computer Methods in Applied Mechanics and Engineering 283 (2015) 1061–1094.

[21] J. C. Simo, R. L. Taylor, K. S. Pister, Variational and projection methods for the volume constraint in finite deformation elasto-plasticity, Computer Methods in Applied Mechanics and Engineering 51 (1985) 177–208.

[22] E. A. de Souza Neto, D. Peric, M. Dutko, D. R. J. Owen, Design of simple low order finite elements for large strain analysis of nearly incompressible solids, International Journal of Solids and Structures 33 (1996) 3277–3296.

[23] M. A. Puso, A highly efficient enhanced assumed strain physically stabilized hexahedral element, International Journal for Numerical Methods in Engineering 49 (2000) 1029–1064.

[24] J. Bonet, A. J. Burton, A simple average nodal pressure tetrahedral element for incompressible and nearly incompressible dynamic explicit

applications, Communications in Numerical Methods in Engineering 14 (1998) 437–449.

[25] Y. Onishi, K. Amaya, A locking-free selective smoothed finite element method using tetrahedral and triangular elements with adaptive mesh rezoning for large deformation problems, International Journal for Numerical Methods in Engineering 99 (2014) 354–371.

[26] M. A. Puso, J. Solberg, A stabilized nodally integrated tetrahedral, International Journal for Numerical Methods in Engineering 67 (2006) 841–867.

[27] O. C. Zienkiewicz, J. Rojek, R. L. Taylor, M. Pastor, Triangles and tetrahedra in explicit dynamic codes for solids, International Journal for Numerical Methods in Engineering 43 (1998) 565–583.

[28] J. Bonet, H. Marriott, O. Hassan, Stability and comparison of different linear tetrahedral formulations for nearly incompressible explicit dynamic applications, International Journal for Numerical Methods in Engineering 50 (2001) 119–133.

[29] G. Scovazzi, Stabilized shock hydrodynamics: II. Design and physical interpretation of the SUPG operator for Lagrangian computations, Computer Methods in Applied Mechanics and Engineering 196 (2007) 967–978.

[30] G. Scovazzi, A discourse on Galilean invariance, SUPG stabilization, and the variational multiscale framework, Computer Methods in Applied Mechanics and Engineering 196 (2007) 1108–1132.

[31] G. Scovazzi, Galilean invariance and stabilized methods for compressible flows, International Journal for Numerical Methods in Fluids 54 (2007) 757–778.

[32] G. Scovazzi, Lagrangian shock hydrodynamics on tetrahedral meshes: A stable and accurate variational multiscale approach, Journal of Computational Physics 231 (2012) 8029–8069.

[33] G. Scovazzi, M. A. Christon, T. J. R. Hughes, J. N. Shadid, Stabilized shock hydrodynamics: I. A Lagrangian method, Computer Methods in Applied Mechanics and Engineering 196 (2007) 923–966.

[34] G. Scovazzi, E. Love, A generalized view on Galilean invariance in stabilized compressible flow computations, International Journal for Numerical Methods in Fluids 64 (2010) 1065–1083.

[35] G. Scovazzi, E. Love, M. J. Shashkov, A multi-scale Q1/P0 approach to Lagrangian shock hydrodynamics, Computer Methods in Applied Mechanics and Engineering 197 (2008) 1056–1079.

[36] G. Scovazzi, J. N. Shadid, E. Love, W. J. Rider, A conservative nodal variational multiscale method for Lagrangian shock hydrodynamics, Computer Methods in Applied Mechanics and Engineering 199 (2010) 3059–3100.

[37] C. H. Lee, A. J. Gil, J. Bonet, Development of a cell centred upwind finite volume algorithm for a new conservation law formulation in structural dynamics, Computers and Structures 118 (2013) 13–38.

[38] M. Aguirre, A. J. Gil, J. Bonet, A. A. Carreño, A vertex centred finite volume Jameson-Schmidt-Turkel (JST) algorithm for a mixed conservation formulation in solid dynamics, Journal of Computational Physics 259 (2014) 672–699.

[39] I. A. Karim, C. H. Lee, A. J. Gil, J. Bonet, A two-step Taylor Galerkin formulation for fast dynamics, Engineering Computations 31 (2014) 366–387.

[40] G. Kluth, B. Després, Discretization of hyperelasticity on unstructured mesh with a cell-centered Lagrangian scheme, Journal of Computational Physics 229 (2010) 9092–9118.

[41] A. J. Gil, J. Bonet, J. Silla, O. Hassan, A Discrete Geometric Conservation Law (DGCL) for a cell vertex finite-volume algorithm on moving domains, International Journal for Numerical Methods in Biomedical Engineering 26 (2010) 770 – 779.

[42] P. D. Thomas, C. K. Lombard, Geometric conservation law and its application to flow computations on moving grids, The American Institute of Aeronautics and Astronautics (AIAA) 10 (1979) 1030 – 1037.

[43] N. C. Nguyen, J. Peraire, Hybridizable Discontinuous Galerkin methods for partial differential equations in continuum mechanics, Journal of Computational Physics 231 (2012) 5955–5988.

[44] M. Aguirre, A. J. Gil, J. Bonet, C. H. Lee, An upwind vertex centred finite volume solver for Lagrangian solid dynamics, Journal of Computational Physics 300 (2015) 387–422.

[45] A. J. Chorin, Numerical solution of the Navier-Stokes equations, Mathematics of Computation 22 (1968) 745–762.

[46] J. M. Ball, Convexity conditions and existence theorems in nonlinear elasticity, Archive for Rational Mechanics and Analysis 63 (1976) 337–403.

[47] J. Schröder, P. Neff, Invariant formulation of hyperelastic transverse isotropy based on polyconvex free energy functions, International Journal of Solids and Structures 40 (2003) 401–445.

[48] T. J. R. Hughes, L. P. Franca, M. Mallet, A new finite element formulation for computational fluid dynamics: I. Symmetric forms of the compressible Euler and Navier-Stokes equations and the second law of thermodynamics, Computer Methods in Applied Mechanics and Engineering 54 (1986) 223–234.

[49] R. de Boer, Vektor- und Tensorrechnung für Ingenieure, Springer-Verlag, 1982.

[50] J. Bonet, A. J. Gil, R. Ortigosa, On a tensor cross product based formulation of large strain solid mechanics, Journal of the Mechanics and Physics of Solids (2015). Accepted.

[51] J. Schröder, P. Wriggers, D. Balzani, A new mixed finite element based on different approximations of the minors of deformation tensors, Computer Methods in Applied Mechanics and Engineering 200 (2011) 3583–3600.

[52] T. J. R. Hughes, Multiscale phenomena: Green's functions, the Dirichlet-to-Neumann formulation, subgrid scale models, bubbles and the origins of stabilized methods, Computer Methods in Applied Mechanics and Engineering 127 (1995) 387–401.

[53] C. W. Shu, Efficient implementation of essentially non-oscillatory shock capturing schemes, Journal of Computational Physics 77 (1988) 439–471.

[54] A. N. Brooks, T. J. R. Hughes, Streamline upwind/Petrov-Galerkin formulations for convection dominated flows with particular emphasis on the incompressible Navier-Stokes equations, Computer Methods in Applied Mechanics and Engineering 32 (1982) 199–259.

[55] S. K. Lahiri, J. Bonet, J. Peraire, A variationally consistent mesh adaptation method for triangular elements in explicit Lagrangian dynamics, International Journal for Numerical Methods in Engineering 82 (2010) 1073–1113.